

Supplementary Material for:  
Catastrophic caldera-forming pyroclastic eruptions and climate perturbations: the result of tectonic and magmatic controls on the Paleocene-Eocene Kilchrist Caldera, Isle of Skye, NW Scotland

Simon M. Drake\*<sup>α</sup>,  David J. Brown<sup>β</sup>,  Andrew D. Beard<sup>α</sup>, Padej Kumlersakul<sup>α</sup>,  
David J. Thompson<sup>α</sup>,  Charlotte L. Bays<sup>α</sup>,  Ian L. Millar<sup>γ</sup>, and  Kathryn M. Goodenough<sup>δ</sup>

<sup>α</sup> School of Earth and Planetary Sciences, Birkbeck College, University of London, Malet St, London, WC1E 7HX, UK.

<sup>β</sup> School of Geographical and Earth Sciences, University of Glasgow, Lilybank Gardens, Glasgow, G12 8QQ, UK.

<sup>γ</sup> British Geological Survey, Natural Environment Research Council, Keyworth, Nottingham, NG12 5GC, UK.

<sup>δ</sup> British Geological Survey, Research Avenue South, Edinburgh, EH14 4AP, UK.

This Supplementary Material accompanies the article: Drake, S. M., Brown, D., Beard, A., Kumlersakul, P., Thompson, D., Bays, C., Millar, I. and Goodenough, K. (2022) “Catastrophic caldera-forming eruptions and climate perturbations: the result of tectonic and magmatic controls on the Paleocene-Eocene Kilchrist Caldera, Isle of Skye, NW Scotland”, *Volcanica*, 5(2), pp. 397–432. doi: <https://doi.org/10.30909/vol.05.02.397432>.

Drake et al. [2022] should be cited if this material is used independently of the article.

Table S1: Grid reference of figures and sample numbers

Rock type/feature	Figure number in paper/ supplementary file	Grid reference/ log/ height (in metres)	Sample number
Paleosol	Figure 4A	NG 59635 20663, Log 16, 290 m	SD/51
Amygdaloidal basalt	Figure 4B, <b>Figure S1B</b>	NG 59625 20664, Log 16, 320 m	
Tholeiitic basalt	Figure 4C	NG 96142 20690, Log 16, 355 m	SD/58
Fall deposit	Figure 4D	NG 59640 20645, Log 16, 295 m	SD/52
Hawaiite	<b>Figure S1A</b>	NG 58107 23851, Log 15, 5 m	
sT- cooling joints	Figure 5A	NG 59999 20876, Log 9, 3 m	SD/217
sT (XP)	Figure 5B	NG 59999 20876, Log 9, 2 m	SD/217a
mLTacc	Figure 5C	NG 58238 22102, Log 4, 21 m	
mLT acc scan (XP)	Figure 5D	NG 58238 22102, Log 4, 21 m	SD/5d
mLT acc scan (PPL)	<b>Figure S2A</b>	NG 58238 22102, Log 4, 21 m	SD/5d
sT- underside cooling joints	<b>Figure S2B</b>	NG 59999 20876, Log 9, 3 m	SD/217
sT thin section (XP)	<b>Figure S2C</b>	NG 59999 20876, Log 9, 3 m	
sT thin section (PPL)	<b>Figure S2D</b>	NG 59999 20876, Log 9, 3 m	
mLTacc	<b>Figure S2E</b>	NG 58230 22095, Log 4, 8 m	
mLTacc	<b>Figure S2F</b>	NG 58230 22095, Log 4, 8 m	
mLT acc EMP image	<b>Figure S2G</b>	NG 58238 22102, Log 4, 21 m	SD/5d
mLTacc- oblate	<b>Figure S2H</b>	NG 58238 22102, Log 4, 21 m	
mBr containing quartzite block	Figure 6A	NG 59992 20854, Log 9, 9 m	
mLT	Figure 6B	NG 59574 20917, Log 16, 630 m	SD/76
mLT (XP) resorbed quartz	Figure 6C	NG 60673 20643, Log 13, 19 m	SD/226a
mBr/mLTi faulted contact	Figure 6D	NG 59583 20818, Log 16, 500m	
mLT type III enclave	Figure 6E	NG59805 20997, Log 18, 220 m	SD/89
mBr clast supported (thin section XP)	<b>Figure S3A</b>	NG 59677 20417, Log 16, 25 m	SD/33
mBr clast supported	<b>Figure S3B</b>	NG 59677 20417, Log 16, 25 m	SD/33
dsLT	<b>Figure S4A</b>	NG 59802 20301	
mLT	<b>Figure S4B</b>	NG 59676 21028, Log 10, 40 m	SD/219
mLT- thin section calcite	<b>Figure S5A</b>	NG 59682 20508, Log 16, 142 m	SD/36
mLT (XP) disequilibrium-fan spherulite	<b>Figure S5B</b>	NG 60673 20643, Log 13,18 m	SD/226
mLT (XP) disequilibrium- alk fspa	<b>Figure S5C</b>	NG 60673 20643, Log 13,18 m	SD/226
mLT (XP) basaltic lapilli	<b>Figure S5D</b>	NG 59676 21028, Log 10, 40 m	SD/219
mLTi containing type III enclaves	Figure 7A	NG 59619 20757, Log 16, 447 m	
mLTi fiamme/cooling joints	Figure 7B	NG 59620 20756, Log 16, 440 m	
mLTi matrix	Figure 7C	NG 59355 21087, Log 18, 292 m	SD/93
mLTi containing type III enclaves	Figure 7D	NG 59619 20754, Log 16, 442 m	
mLTe eutaxitic fabric	Figure 7E	NG 59424 20980, Log 14, 305 m	
mLTe (PPL)	Figure 7F	NG 59565 20901, Log 16, 610 m	SD74
mLTi type II enclave	<b>Figure S6A</b>	NG 59625 20773, Log 16,445m	SD/64
mLTi melt globule	<b>Figure S6B</b>	NG 59692 21051, Log 10, 62m	SD/219a
mLTi swallow tail fiamme	<b>Figure S6C</b>	NG 59625 20773, Log 16, 445 m	SD/64
mLTi mechanically fractured fiamme	<b>Figure S6D</b>	NG 59625 20773, Log 16, 445 m	SD/64
mLTi containing fiamme	<b>Figure S6E</b>	NG 59625 20773, Log 16, 445 m	SD/64
mLTi Type III enclave	<b>Figure S6F</b>	NG 59603 20795, Log 16, 476m	SD/66
mLTi containing fiamme/enclaves	<b>Figure S6G</b>	NG 59625 20773, Log 16, 445 m	SD/64
mLTi (56.14 ± 0.19 Ma)	Figure 17C, D	NG 59618 20783 (Log 16 445m)	SD ANS1
mLT lava-like	Figure 8A	NG 59345 21145, Log 18, 318 m	SD/83
mLT lava-like (XP)	Figure 8B	NG 59345 21145, Log 18, 318 m	SD/83
mLT lava-like parataxitic fabric (PPL)	Figure 8C	NG 59346 21146, Log 18, 316 m	SD/82

Table S1 [cont.]: Grid reference of figures and sample numbers

Rock type/feature	Figure number in paper/ supplementary file	Grid reference/ log/ height (in metres)	Sample number
Tuff filling fissure- Allt Coire Forsaidth	Figure 8D	NG 6026821232	
Tuff filling fissure	Figure 8E	NG 59623 20840	
Tuff filling fissure	Figure 8F	NG 59623 20840	
mLTe- eutaxitic fabric	Figure S7A	NG 58094 23560, Log 8, 5 m	SD/216
mLTe- eutaxitic/swallow tails	Figure S7B	NG 58094 23560, Log 8, 5 m	SD/216
mLTe- rotated lapilli	Figure S7C	NG 60307 21223, Log 12, 47 m	
Mafic enclaves in mLTe	Figure S7D	NG 59659 20985, Log 10, 5 m	
mLTe cooling joints	Figure S7E	NG 58226 22093, Log 4, 3m	
mLTe (PPL)	Figure S7F	NG 59355 20997, Log 18, 242 m	SD/85
mLTe (PPL)	Figure S7G	NG 59355 21155, Log 18, 315 m	SD86
mLTe- type II enclaves	Figure S7H	NG 58094 23560, Log 8, 5 m	SD/216
mLT lava-like- recumbent folding	Figure S8A	NG 59346 21146, Log 18, 316 m	SD/82
mLT lava-like- parataxitic fabric	Figure S8B	NG 59346 21146, Log 18, 316 m	SD/82
mLT lava-like- recumbent folding	Figure S8C	NG 59346 21146, Log 18, 316 m	SD/82
mLT lava-like- type II enclaves	Figure S8C	NG 59346 21146, Log 18, 316 m	SD/82
mLT lava like micro-folding (PPL)	Figure S9A	NG 57994 23274, Log 7, 15 m	SD/210
mLT lava-like parataxitic fabric (XP)	Figure S9B	NG 59346 21146, Log 18, 316 m	SD/82
mLT lava like micro hinge (PPL)	Figure S9C	NG 57994 23274, Log 7, 15 m	SD/210
mLT lava like micro hinge (XP)	Figure S9D	NG 57994 23274, Log 7, 15 m	SD/210
mLT lava-like	Figure S10A	NG 60180 21230	
Fissure filled tuff in dyke	Figure S10B	NG 62154 23527	AB/1A
Spherules in fissure filled rhyolitic tuff	Figure S10C	NG 62154 23527	AB/1B
mLT lava-like	Figure S10D	NG 61803 23119	
Tuff filling fissure	Figure S10E	NG 59589 20965	
Grading within mBr	Figure 9A	NG 54301 25012	SD/B2
Granite lithic lapilli inclusion in basic dyke ( $56.45 \pm 0.15$ Ma)	Figure 9B/ Figure 17A, B	NG 54301 25012	SD BS/01
sT	Figure 9C	NG 54301 24908	SD/B4
mLTacc	Figure 9D	NG 54325 24866	
dsLT	Figure 9E	NG 54328 24646	
mLT matrix to clast supported	Figure 9F	NG 54308 24994	SD/B3
mBr- gabbro blocks	Figure 9G	NG 54345 24591	
Granitic inclusions in dyke	Figure 10A	NG 63191 20477	SD/252 SD/BS01
Granitic inclusion clusters in dyke	Figure 10B	NG 63191 20477	SD/252 SD/BS01

Table S2: Abbreviations for lithologies used on Kilchrist map (Figure 3) and logged sections (Logs A, Logs B) after (and modified from) Branney and Kokelaar [1992, 2002].

Ignimbrites	Lithology
mLT	Massive lapilli tuff
dsLT	Diffuse stratified lapilli tuff
mBr	Massive breccia
dsIB	Diffuse stratified lithic breccia
mLTacc	Massive lapilli tuff accretionary lapilli bearing
mLTi	Massive lapilli tuff incipiently welded
mLT <sub>e</sub>	Massive lapilli tuff with eutaxitic fabric
mLT lava-like	Massive lapilli tuff lava-like
sT	Stratified tuff
Extrusives	
bas	Basalt
mug	Mugearite
haw	Hawaiite
Intrusives	
Tuff	Tuff filling fissures
Brecciated tuff	Brecciated tuff within fissure
Rhy	Rhyolitic dyke
KH	Kilchrist hybrid, mixed magma intrusive
Others	
paleo	Paleosol
pep	Peperite
ash lay	Ash layer

## 1 SAMPLING AND METHODS

Mapping at Kilchrist was conducted over two field seasons with particular emphasis placed on detailed logging (Figures S3 and S4) in order to correlate lithofacies and establish an eruption history. Thin section analysis was conducted on both polarising microscope and electron microprobe.

Major element mineral analyses were obtained using a Jeol JXA8100 Superprobe (WDS) with an Oxford Instruments AZtec system (EDS) at Birkbeck College, University of London. EDS analysis was carried out using an accelerating voltage of 15 kV, current of 1  $\mu$ A, and a beam diameter of 1  $\mu$ m. with an acquisition time for 20 seconds. A proxy to bulk elemental whole rock analysis, was determined by multiple area (100  $\times$  40  $\mu$ m) scan analysis of representative matrix, carefully avoiding lithic lapilli in the case of ignimbrites, and phenocrysts in the case of lava. Analyses were calibrated against standards of natural silicates, oxides and Specpure metals with the data corrected using a ZAF program.

## 2 KVF LITHOFACIES (ADDITIONAL NOTES IN CONJUNCTION WITH SECTION 4 MAIN TEXT)

### Basic lavas (Tholeiite, Hawaiiite, Mugearite)

Tholeiitic basalts and highly subordinate hawaiiites and mugearites comprise the basic lavas at Kilchrist. Volumetrically, basic lavas are the dominant rock type in the study area, and may be cut by sporadic,  $\leq 0.5$  m-thick, NNW–NW-trending dykes of the regional Paleocene swarm. Lava stratigraphy is best observed in Allt nan Suidheachan (Log 16) where four shallowly inclined flows crop out over 90 m along the stream bed. The dip of these lavas is  $\leq 10^\circ$  towards the SSE which suggests a maximum true total thickness of  $\sim 8$  m. Each flow is capped by either a paleosol, or tuff layer and at the base of the uppermost lava, peperite is recorded.

In the west of the study area around Creagan Dubh both hawaiiites (Figure S1A) and mugearites form the prominent crags. However, whilst contact relationships between lava types at Creagan Dubh are absent, the lowermost hawaiiite flows are  $\sim 50$  % thicker than overlying mugearite flows. The mugearite is aphanitic, blocky, and cut by irregular joints. Elsewhere cross cutting relationships between basalt, ignimbrite and intrusive igneous rocks are numerous, and lava flows are frequently intercalated with ignimbrite lithofacies for example mLT and mBr around Allt Nan Suidheachan, (Log 16, Logs B). It is not possible to correlate lava flows in the south with flows at either Creagan Dubh (Log 15, Logs A) or NW of Loch Cill Chriosd to establish any temporal relationship. Chemically, tholeiite lavas at both Kilchrist and Creagan Dubh are akin to the Skye Main Lava Series [Bell and Williamson 1994]. Such lavas plot in the same geochemical fields as mafic enclaves contained within mLT (Figure S11). The inter-lava flow tuff layers are interpreted as fall deposits which were produced in eruptions that occurred between emplacement of lavas.

Basalt may be aphanitic, amygdaloidal or porphyritic, and is commonly highly altered and brecciated. Zeolites occur towards the top and bases of individual tholeiitic flows (Figure S1B). The majority are oblate towards the top of flows, and

larger and less rounded, towards flow bases. EMP analysis shows tholeiitic olivine basalt is the most common basic lava at Kilchrist and typically contains altered augite and forsterite, turbid calcium rich feldspars, and chloritised clinopyroxene with calcite reaction rims. Fayalite frequently has  $\leq 30$   $\mu$ m thick ferro-richterite reaction rims. Clino-pyroxenes are commonly twinned and possess resorbed margins. The youngest lavas in the south and west of the study area are hawaiiites and are exposed in Allt nan Suidheachan (Log 16, Logs B) and Creagan Dubh (Log 15, Logs A). They lack amygdales, possess abundant olivine phenocrysts (Fo<sub>78-55</sub>), labradorite (An<sub>55-61</sub>), chloritized clinopyroxene, and sporadic magnetite. In thin section mugearite contains andesine-labradorite (An<sub>30-55</sub>) phenocrysts and has a flow aligned groundmass.

### Paleosols, ash horizons, peperite

Paleosols are fossil lateritic soils that form by *in situ* weathering, oxidation and leaching of extrusive eruptive products (principally basalt) under warm, wet, conditions [Bell and Harris 1986; Bell et al. 1996; Emeleus et al. 1996]. The presence of paleosols indicates that flows were not continuous and that hiatuses were long enough for primitive soils to form on flow tops. Two paleosols and a laminated tuff layer crop out intercalated between tholeiite lava flows in Allt nan Suidheachan in the south of the mapping area (Log 16 290–296 m, Logs B). The paleosols are  $\leq 5$  cm thick, dark red, fine-grained, fissile and grade down over  $\leq 10$  cm into underlying flows and there is a reduction in colour intensity with depth. Conversely the tuff layer retains a deep red colour throughout its profile, is fine grained, laminated, fissile and has a sharp contact with underlying lava. In thin section the tuff layer contains euhedral augite, quartz, plagioclase, and heterogeneous lithic fragments. Such features could not have been produced in a primitive soil. Under EMP backscatter former glass shards, and axiolitic devitrification of frequently broken bubble wall margins are evident within the tuff layer. The layer is composed of highly oxidized, altered glass, within an altered granular matrix, containing mafic lithic fragments, anhedral oligoclase, and quartz. The SiO<sub>2</sub> matrix content is 24.97 % whilst FeO is 32.95 %. Groundmass phases include K-feldspar, zircon, and sporadic chrome spinel with magnetite rims ( $\leq 25$   $\mu$ m thick). Basaltic and granitic fragments with embayed margins are present in the groundmass. Rare, localised, peperite is present as a  $\leq 20$  cm thick layer at the base of the uppermost tholeiitic lava in Allt nan Suidheachan (log 16, 335m, Figure S4, NG 59625 20664). Here lobate mafic clots  $\leq 4$  cm in length are surrounded by  $\leq 70$  % ash-granular matrix which is highly friable. Clots may either be completely isolated within the matrix, or clustered together in a jigsaw-fit separated by matrix. Slight normal grading of mafic clots [Brown and Bell 2007] is evident within the layer. The presence of peperite provides evidence that paleosurfaces were locally covered with unconsolidated, likely wet, sediment and that lava interacted with these [White et al. 2000]. Grading indicates that settling of larger mafic clasts within the sediment occurred during peperite formation [Brown and Bell 2007].



Figure S1: Field characteristics of KVF lavas. [A] Blocky hawaiite lava at Creagan Dubh (Log 15, 5m height, [Logs A](#)). [B] Laterally discontinuous zeolite rich regions within amygdaloidal basalt. Frequently such regions grade into aphanitic fractured basalt (Log 16, 320 m height, [Logs B](#)).

### Stratified tuff (sT)

Rhyolitic stratified tuffs (sT) are rare in the study area and only found in one stream section (Log 9, [Logs B](#)). This unit is ~3.5 m thick, columnar jointed and laterally extensive for ~20 m ([Figure S2B](#)). It is juxtaposed on the east bank with both mBr and mLT in a faulted contact. Columnar joints which pervade the unit, are variably 4–5 sided, spaced  $\leq 30$  cm apart, and plunge 60→040 ([Figure S5B](#)). At macroscale alternating fine grained, melanocratic and leucocratic laminations  $\leq 1$  mm thick are orientated at  $\sim 90^\circ$  to these columns. The rock has a matrix content of  $\geq 95\%$ , and contains sporadic arkosic sandstone lithic fragments  $\leq 8$  mm diameter. Such lithics are frequently draped with ash ([Figure S2C, D](#)).

Stratified tuff matrix is rhyolitic, and comprises quartz, K-feldspar, albite, titanite, chlorite, and sporadic allanite, and zircon crystals. The leucocratic laminations comprise normally graded domains ( $\leq 70$   $\mu\text{m}$  thick) of quartz and alkali feldspar which alternate with thinner ungraded ( $\leq 10$   $\mu\text{m}$  thick), melanocratic domains of chloritized quartz, magnetite and ilmenite. Changes in chemistry are reflected between these alternating laminations, and opaque minerals and chlorite are the principal minerals in melanocratic layers, and only found sporadically in leucocratic layers. Cross-stratification within leucocratic laminations ([Figure S2A](#)) is evident within several layers together with evidence of loading, syn-sedimentary faulting, and normal ash grading.

The fine-grained laminations and ash drapes within sT indicate deposition were generated via direct fall-out from eruption ash clouds. Ash was necessarily hot, due to the presence of contractional cooling joints, which were probably developed as a result of rapid burial that accounted for minimal heat loss. Such contractional cooling joints within sT have previously been reported from Taupo, New Zealand ([Wilson and Walker 1985](#)). Loading and cross stratification within sT indicates sub-aqueous reworking took place following depo-

sition and probably accounts for the unit preservation. Brittle offset of layers was probably induced by volcano-tectonic induced faulting which was contemporaneous with eruptions.

### Accretionary lapilli bearing mLT (mLTacc)

Ash aggregate-bearing units fringe the Eastern Red Hill granites laterally over 1.5 km (logs 1, 4, 6, 8, [Logs A](#)), range in thickness from 80 cm to 3 m, and contain accretionary lapilli together with sporadic cored accretionary lapilli. The most complete ash aggregate-bearing section contains two units of matrix-supported mLTacc (Log 4, 9, and 23 m, [Logs A](#)). Both units have a fine-grained, crystal-poor, vitroclastic matrix ( $\geq 90\%$ ), which contains concentric (spherical to sub-spherical) accretionary lapilli, with normally graded, multiple laminae ([Figure SF/2c-d](#)). At outcrop fabric within mLTacc is highlighted by sub-parallel linear trails of cored rounded accretionary lapilli, and oblate accretionary lapilli. The lower mLTacc unit (Log 4, [Logs A](#)) is approximately 2.5 m thick, and contains  $\leq 5\%$  rounded to sub-rounded ([Figure S2F](#)) accretionary lapilli ( $\leq 15$  mm diameter) *sensu* [Thordarson \[2004\]](#). Within individual accretionary lapilli, laminae are normally graded from core to rim ([Figure S2G](#)) and whilst the majority in the upper unit (Log 4, [Logs A](#)) are highly spherical, a few are oblate ([Figure S2H](#)). Conversely the upper unit contains numerous broken, angular accretionary lapilli fragments, together with  $\sim 5\%$  cored accretionary lapilli that have up to 4 parallel- sub parallel concentric layers, and an armoured outer layer ( $\leq 1$  mm thick). Pellets as described by [Brown et al. \[2010\]](#) are not evident within the study area. Chemically mLTacc matrix varies from basaltic andesite to dacite (?), is fine-grained, contains broken glass shards, and small basaltic (labradorite-bytownite, magnetite and chlorite-after clinopyroxene) and granitic (albite, quartz, k-feldspar, rutile, and ilmenite) lithic fragments ( $\leq 50$ – $130$   $\mu\text{m}$ ). Matrix phases may comprise K-feldspar, quartz, clinopyroxene, Ca-plagioclase,

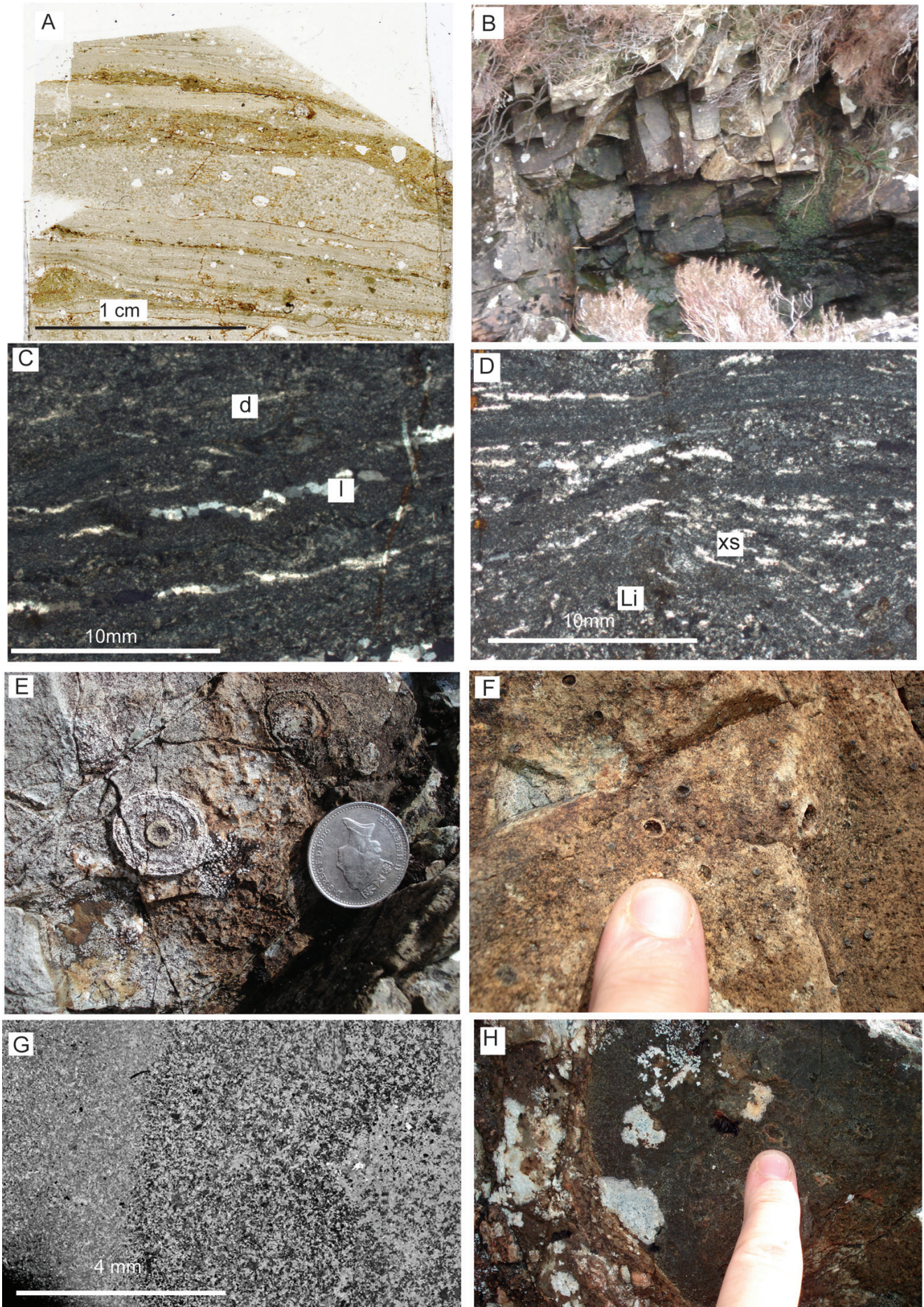


Figure S2: (Previous page) Field and petrographic characteristics of stratified tuff (sT) and accretionary lapilli bearing massive lapilli tuff (mLTacc). [A] PPL scan of sT from Cnoc nan Uan. Subtle changes in ash chemistry are reflected in layer colouration. Melanocratic layers are richer in magnetite, ilmenite and titanite and have been chloritized. [B] Underside of steeply plunging columnar cooling joints within sT on the west bank of Cnoc nan Uan (Log 9, 3 m height, **Logs B**). [C] XP image of slide in [D] showing sporadic quartz-rich sandstone lithic lapilli (L) with fabric draped around it. To the upper right of the lithic lapilli, quartz rich domains are truncated below an upper layer of laterally continuous quartz crystals. This cross-stratification (xs) provides compelling way-up evidence (to top of photomicrograph), and may indicate re-working, in a sub-aqueous environment. [D] PPL image showing sporadic quartz-rich sandstone lithic lapilli (L) with fabric draped around it. To the upper right of the lithic lapilli, quartz rich domains are truncated below an upper layer of laterally continuous quartz crystals. This cross-stratification (xs) provides compelling way-up evidence (to top of photomicrograph), and may indicate re-working, in a sub-aqueous environment. [E] Accretionary lapilli (Log 4, 8 m height, **Logs A**) comprising weathered out core and concentric laminations within a silicic, matrix rich, mLTacc. [F] Accretionary lapilli laminations are graded from chloritised cores to finer grained, marginal rims. [G] EMP stitched image of an individual lapilli (core to right), with lapillus laminae grading normally towards left of image. (Log 4, 23 m height, **Logs A**). Note the sharp nature of individual concentric laminations. [H] Oblate accretionary lapilli which have been syn-post depositionally deformed in a soft state during PDC transportation.

oligoclase, zircon, chrome, spinel, rutile, epidote, and biotite and ~75 % of samples are chemically more evolved from core to rim.

It is envisaged that ash pellets acting as nucleation points, grew into accretionary lapilli by rapid coalescence of wet ash within warm turbulent up drafted plumes. The growing accretionary lapilli then reached a critical density, and fell into underlying PDCs, where they continued to grow, and accrete, during transportation. Such a scenario is similar to that envisaged to have produced mLTacc deposits in the 273 ka Poris ignimbrite, Tenerife [Brown et al. 2010]. At Kilchrist, both mLTacc units are very fine grained, and highly matrix supported, which suggests they were deposited from cool moist currents [Branney and Kokelaar 1992]. Normally graded laminations within individual lapilli, probably reflect cohesive variations within the generating ash clouds [Moore and Peck 1962], or changes in available moisture content within the thermally stratified transporting PDC. The presence of oblate accretionary lapilli indicates that parts of transporting PDCs contained enough moisture to promote syn-post depositional soft-state deformation.

#### Massive breccia (mBr) and diffuse-stratified lithic breccia (dslBr)

Massive breccia (mBr) covers a lateral extent of ~2.5 km, and commonly forms the steep crags south of Beinn Dearg Bheag, west of Cnoc Nam Forsaidh, and on Meall Coire Forsaidh and frequently succeeds mLT gradationally, both vertically and laterally, over distances of 1–5 m. mBr units typically possess erosive bases (Logs 18, 16,10,15, 5, **Figure S4**), and range in thickness from 1–20 m, apart from units around Meall Coire Forsaidh which range from 35–60 m in thickness. In this study we differentiate between mBr containing small blocks (64–256 mm) and mBr containing large blocks (256 mm). Matrix supported mBr may possess a localised incipient welding fabric, evidenced by slight imbrication patterns of lithic lapilli, and streaked out pumices with length: width ratios of <5:1. Compositionally blocks are heterolithic and may be fractured (**Figure S3B**) comprising arkosic sandstone, amygdaloidal and aphanitic basalt, quartzite, calcare-

ous sandstone, dolostone, mLTi, mLTe, mLT lava-like, and mBr. Blocks reach a maximum size of ~1 m × 60 cm in mBr and may be angular to sub-angular or sub-rounded. mBr units commonly exhibit lithic grading patterns, i.e. ungraded, graded or reverse graded (**Figure S3B**). Reverse graded mBr is the most common breccia lithofacies. Exfoliation and thermal spalling of blocks (log 16, 50 m height, **Logs B**) is a common feature of reverse graded mBr. Frequently rounded blocks have exfoliated thermally spalled rims pervasive to a depth of ~1.5 cm with fine-grained ash present between individual layers. Columnar cooling joints (15 cm–1.1 m diameter) are common within mBr with a block population <17 cm diameter. Such columns may be either poorly developed (1–3 sided), or well developed (5–6 sided). Column development is not apparent in mBr that contains blocks >17 cm diameter. Matrix supported mBr may contain sporadic gas-escape structures including lithophysae and elutriation pipes (e.g. Log 15, 200 m height, **Logs A**). Lithophysal cavities may be oblate to amorphous, and in places fringed with marginal epidote. Localised imbrication of blocks within breccia is evident near the contact with Meall Dearg Bheag and on steep crags composed of breccia for example Meall Coire Forsaidh. Such imbrication is a useful indicator of both flow direction and way-up. Massive breccia may be juxtaposed with other ignimbrites across fault planes. For example, matrix supported mBr in Allt nan Suidheachan (Log 16, 500 m, **Logs B**) is faulted against incipiently welded mLTi and a ≤10 cm thick layer of angular mLTi fault gouge is evident at the fault plane.

Matrix within mBr is typically dacite-rhyolitic in composition (**Figure S12**) and contains former vitric chloritised bubble wall shards, sub-rounded quartz crystals, K-feldspar, albite, chlorite, zircon, epidote, titanite, and sporadic allanite, pyrite, and calcite. Frequently, matrix appears isotropic due to glass replacement by very fine-grained chlorite. Matrix lithics may be highly variable (e.g. granitic lapilli, basalt, mLT, mLTi, mLT lava-like). Mechanical fracture of matrix lithic lapilli is common at both macro-scale and in thin section. Within the matrix sporadic, aphanitic type II mafic enclaves [Troll et al. 2004] are strongly deformed around lithic fragments. Such mafic enclaves lack chilled margins. The numerous heat-derived features within mBr (contractional cooling

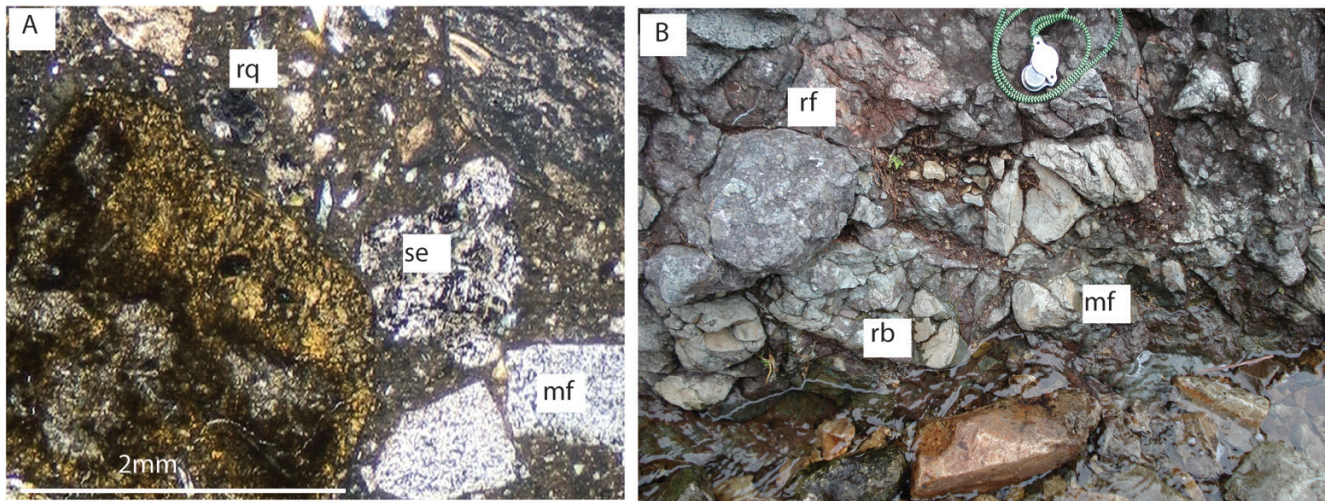


Figure S3: Field and petrographic characteristics of massive breccia (mBr). [A] Photomicrograph of mBr (log 16, 25 m, **Logs B**) showing planar mechanical fracture (mf) of quartzite lithic lapilli (bottom right-hand corner). Unwelded glass shards in top right-hand corner and a lobate margined silicic enclave (se) in mid-ground, are in close proximity to a rounded quartz crystal (rq). XP field of view 2 mm. [B] Heterolithic blocks within clast-supported, reverse graded mBr containing blocks of rounded red arkosic sandstone with radial fractures (rf), rounded blocks (rb), mechanical fracture (mf) of angular quartzite (right and below hand lens for scale—5 cm length), sub-rounded blocks of aphanitic basalt and reddish arkosic sandstone (Log 16, 50 m height, **Logs B**).

joints, lithophysae, thermal spalling of blocks, together with inter-layer ash, provide compelling evidence of genesis within ‘hot’ high particle concentration PDCs. Conditions at aggrading depositional flow boundaries were dominated by fluid-escape processes [Branney and Kokelaar 2002], where temporal and spatial changes in supply and filtering of components took place. Mechanically fractured, and faceted blocks within mBr, indicate block collision and abrasion during transportation. Sporadic alignment of lapilli within mBr matrix, together with slight deformation of matrix around lithic lapilli suggests transporting PDCs were turbulent. The graded nature of mBr deposits indicates eruptions were non steady state, and periodically waxed and waned in terms of vent energy output, and therefore had capacity to transport different sizes of block. Electron Micro-Probe area scans of mBr matrix samples indicates considerable chemical heterogeneity exists within individual mBr units and that matrix may be chemically variable over samples  $\leq 1$  m apart. This suggests deposition of mBr probably took place via incremental progressive aggradation [Branney and Kokelaar 1992] within ‘hot’ PDCs. The presence of mafic enclaves within mBr matrix indicate basic melt fractions were periodically incorporated into highly silicic PDCs [Sparks et al. 1977; Eichelberger 1980; Folch and Martí 1998].

Diffuse stratification of lithic blocks largely comprised of quartzite, mLT-lava like, and basalt crop out around the upper reaches of log 16 (**Logs B**, NG 59488 21333). Diffusely stratified lithic-breccia (dslBr) may contain a bi-modal block population where lithics comprised of mBr and mLTi are block sized, and basalt blocks are generally smaller (around NG 59325 21324). In close proximity small blocks of mLTi and mLT lava-like have been deformed plastically which suggests they were incorporated into PDCs in a molten–semi molten state. Diffusely stratified lithic breccias are highly localised,

frequently die out laterally over several metres into mLT, and generally crop out in stage 4 KVF units (discussed in main text).

#### Massive lapilli tuff (mLT) and diffuse-stratified lapilli tuff (dslT)

Silicic mLT is the most abundant type of ignimbrite within the study area, and is typically 30–95 % matrix supported, cropping out as  $\leq 10$  m thick, laterally impersistent units, which frequently interdigitate with other ignimbrite lithofacies. Most mLT is preceded or succeeded by mBr, with gradational contacts taking place over 10s of cm. mLT lapilli populations are heterolithic with ungraded mLT being most common (**Figure S4B**), followed by reverse graded, and highly subordinate normally graded mLT. Units display complex grading patterns. Most mLT units are poorly sorted, matrix-supported,  $< 10$  m thick, non-stratified, and crop out as laterally discontinuous units. Their matrix varies from coarse to granular, is highly variable in colour (mid- to light-grey, to dark green, chlorite-epidote altered), and contains ubiquitous sub - rounded quartz crystals  $\leq 2$  mm diameter. Most lapilli are highly angular to sub angular, and the dominant clast types are arkosic sandstone and quartzite. Subordinate clast types are amygdaloidal basalt, dolostone, mLT, mLT<sub>e</sub>, mLT lava-like, and mBr. Normally graded mLT frequently contain sporadic outsized angular blocks (Log 3, **Figure S3**). Within the most complete logged section (Log 16, **Logs B**) basalt (aphantic, porphyritic, and amygdaloidal) is the most abundant lapilli type within mLT, together with arkosic sandstone.

At the macroscale ‘heat’ derived features such as lithophysae, contractional cooling joints, and thermal spalling are common features within mLT. Sporadic, ellipsoid to lenticular shaped, hollow lithophysae  $\leq 5 \times 3$  cm, are evident around Creagan Dubh (Log 15, 212 m height, **Logs A**) throughout unit

profiles. Contractional cooling joints are also common within mLT (Log 13 at 12 m height, log 10 at 30 and 75m height and log 6 at 25 m height; **Logs B**), and are often poorly developed, with columns spaced  $\leq 30$  cm apart. The majority of columnar joints are planar-slightly curved, and spaced  $\leq 15$  cm apart. mLT units at Kilchrist are highly variable both chemically and petrographically, and predominantly matrix supported. Matrix may be vitric or fine- medium grained, and variably basaltic-basaltic andesite-rhyolitic-trachytic in chemistry (**Figure S12**). mLT units are heterolithic with respect to lithics, and may contain sub-rounded to sub-angular basalt, arkosic sandstone, quartzite, calcareous sandstone, pumice, mLT, mLTi, mLT<sub>e</sub>, and mBr lapilli which are commonly chloritised. Sub angular to sub-rounded matrix lithic fragments (60–250  $\mu\text{m}$  size fraction) are common, and are granitic (K-feldspar, quartz and chlorite or K-feldspar, titanite, quartz and Ca-rich epidote), to basaltic (labradorite, chlorite, allanite, rutile, calcite, and opaques) in affinity.

Ubiquitous sub-rounded quartz crystals  $\leq 2$  mm diameter, type III mafic enclaves, type II enclaves, alkali feldspars with fritted margins (**Figure S5C**) and marginal chlorite, and fan spherulites (**Figure S5B**) are common within matrix. Resorbed quartz crystals and mafic enclaves occur throughout matrix supported mLT units and are frequently chloritised with chilled margins. They may be either very fine-grained, or possess  $\leq 40$  % randomly orientated feldspar laths, and have highly irregular lobate margins. Undeformed silicic bubble wall glass shards (**Figure S5D**) may be apparent within lapilli pressure shadows and often former glass is devitrified, and amorphous. Calcite is present within numerous samples as both groundmass crystals (**Figure S5A**), and as late-stage cross cutting vein infill. Frequently quartz crystals located in pressure shadows between lithic lapilli have  $120^\circ$  triple junctions.

The absence of volcanic bombs, and the presence of cooling joints, lithophysae, and thermal spalling of lapilli, argues for transportation and deposition within 'hot' PDCs. Conditions within PDCs fluctuated throughout eruption duration, (evidenced by grading profiles of lapilli) and fluid escape-dominated processes operated at flow boundary zones within aggrading PDCs. Ungraded mLT deposits indicate steady state eruptions, together with sustained PDC deposition, and constant eruption plume heights. Reverse graded mLT was also deposited at a fluid-escape dominated depositional flow boundary zone [**Branney and Kokelaar 2002**], where temporal and spatial changes in supply and filtering of current components took place. Increasing lapilli size within reverse graded profiles, likely reflect increases in vent/conduit mass flux, together with changes in size and height of eruption columns during sustained eruptions [**Branney and Kokelaar 2002**]. Mechanical fracture of lapilli indicate collision of lithics took place in high concentration PDCs. Such collisions were probably enhanced by seismic rupturing [**Smith et al. 2010**]. Normally graded mLT (coarse tail grading of lithic lapilli) were probably deposited in conditions of waning mass flux/current flow, where PDCs were unable to transport the size of lithic lapilli that mBr depositing PDCs carried. Conversely normally graded lithic profiles probably reflect decreasing availability of lithics for scavenging, due to the paleo-surface being rapidly

buried by aggrading PDCs, or may be due to selective filtering [**Branney and Kokelaar 2002**]. Spalled lithic lapilli within mLT matrix are rare features, and indicate cooling and reheating of lithics took place during transportation in host PDCs.

Diffuse stratified lapilli tuff (dsLT) crops out sporadically throughout, and within, the extent of the southern inner ring fault, and typically comprises millimetre to decimetre layering of coarse ash, to granule sized matrix. Within individual outcrops stratification whilst parallel, may thicken, or rarely splay into mLT. Individual dsLT units are overwhelmingly laterally discontinuous over distances of  $\leq 5$  m, and vertically may pass into mBr or mLT, either gradationally over distances  $\leq 1$  m, or sharply. Angular to sub-rounded lithic lapilli may form laterally discontinuous parallel to sub-parallel alignment between stratified matrix (around NG 59802 20301). Units of dsLT may also be variably reverse to normally graded (**Figure S4A**), with respect to lithic lapilli. Individual lithic lapilli within dsLT are frequently mechanically fractured, and sporadic sub-rounded to rounded lapilli may have outer margins with curvilinear spalled like fractures.

The lateral gradation of dsLT into mLT over a few metres indicates that particle concentrations, and shear gradients within the flow boundary zone of aggrading PDCs, varied between fluid escape dominated to traction dominated. Diffuse stratification is interpreted as indicating subtle unsteadiness within the flow-boundary zone of sustained depositing PDCs [**Branney and Kokelaar 2002**]. Such unsteadiness has been attributed to either successive surges in fluctuating sustained currents, frictional effects within granular flow-dominated flow boundary zones, or, periodic turbulent eddies [**Branney and Kokelaar 2002**].

#### Massive lapilli tuff, incipiently welded (mLTi)

mLTi crops out both south and west of the Eastern Red Hills laterally over  $\sim 400$  m south of Beinn Dearg Bheag (Log 10, 16–18, **Logs B**), and  $\sim 1$  km west of Beinn Dearg Mhor (Log 1 and 15, **Logs A**). These units are frequently laterally discontinuous over distances of  $\leq 5$  m, and grade into mLT, mBr, mLT<sub>e</sub>, or mLT lava-like. In the west units are much thinner, less numerous, and contact relationships between mLTi and adjacent lithologies both laterally or vertically, are frequently absent due to lack of exposure. Where present, contacts are either gradational, undulatory, or sharp and erosive. mLTi units frequently contain cooling joints (SF6c) which may be poorly-well developed, with individual columns spaced between 5–60 cm. mLTi varies in matrix content ( $\leq 80$  %), lithic type, fabric intensity, and grading profiles. Lapilli may comprise sub-angular to sub-rounded basalt, quartzite, arkose, or mLT<sub>e</sub>. Fiamme ( $\leq 15$  cm in length) are common in matrix and frequently have swallow tails (**Figure S6E, G**). Parallel to sub-parallel alignment of reverse graded fiamme is common (Log 16, 445m height, **Logs B**). Increase in fiamme length to width ratio (from  $\sim 3:1$  to  $>10:1$ ) over distances of  $\leq 2$  m is often accompanied by a subtle reverse grading of both lithic lapilli (**Logs 1, 15, 16, Logs A, Logs B**, and type III mafic enclaves. mLTi groundmass is rhyolitic (**Figure S12**), and contains deformed bubble wall shards, sporadic resorbed crystal phases, and angular to sub-angular fragments of quartz rich

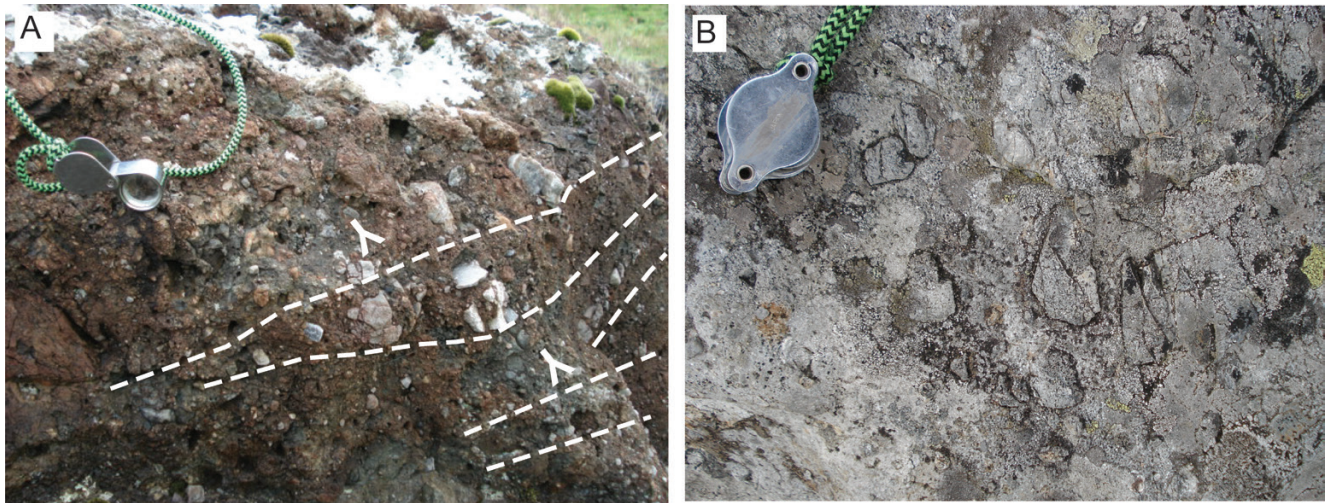


Figure S4: Field characteristics of diffuse stratified lapilli tuff (dsLT). [A] Reverse graded to normal graded dsLT (NG 59802 20301) containing mechanically fractured sub-rounded arkose lapilli. Hatched white lines indicate a very weak stratification. The unit youngs (Y) to top left of photo. [B] Ungraded mLT containing mechanically fractured sub-rounded arkosic lithic lapilli (Log 10, 40 m height, Figure S4).

lithic lapilli. Ubiquitous sub-rounded matrix quartz crystals  $\leq 550 \mu\text{m}$ , have embayed margins mantled by Fe-rich chlorite, and are frequently mechanically fractured. Matrix quartz and K-feldspar, are frequently inter-grown with chloritized pumices. mLTi matrix displays a pronounced incipient fabric (Figure S6A) and may contain recrystallised silicate melt globules (Figure S6B), varietal allanite and pyrite, together with accessory polycrase, xenotime, and dendritic zircon. Incipient welding of matrix fabric is evidenced by glass shards ( $\leq 2 \mu\text{m}$  across) which have been deflected around lithic lapilli (Figure S6A). Deformation of this glass occurred as a result of syn-post-depositional shear and loading, which forced shards into a preferred orientation [Branney and Kokelaar 2002]. However, glass shards next to lithic lapilli are often situated within pressure shadows and are less deformed. Outside of pressure shadows fiamme are commonly mechanically fractured and sheared (Figure S6D). Different states of welding intensity, indicated by varying intensity of shard deformation, are often apparent within the same thin section. Type III mafic enclaves  $\leq 400 \mu\text{m}$  across, are common within the matrix (Figure S6F). They possess lobate margins, and may or may not have chilled margins. Where evident, chilled margins are  $\leq 30 \mu\text{m}$  thick. Matrix fabric is frequently deformed around enclaves which indicates enclaves were rigid when entrained within PDCs (Figure S6F). The poor sorting and absence of tractional stratification within mLTi units suggest that deposition took place within high-concentration, fluid-escape dominated, depositional flow boundary zones of ‘hot’ PDCs [Branney and Kokelaar 2002]. Reverse grading of fiamme, and lithic lapilli, suggests vent mass flux was non-steady state, and periodically increased in intensity. Repeating cycles of mLTi and mLTe (evident over distances of  $\sim 10\text{s}$  of metres) suggests that fluctuations in both conduit energy levels, and eruption plume heights varied temporally. Reverse grading of mLTi units towards the top of Logs 17 and 18 (Logs B) suggests flux levels increased towards the latter stages of mLTi producing erup-

tions. Within these units, reverse grading of mafic blebs also suggests increased tapping of sub-surface mafic melt, and enhanced magma mingling took place towards the latter stages of those eruptions.

#### Massive lapilli tuff with eutaxitic fabric (mLTe)

Field identification of mLTe is frequently hampered by lack of evident microfabric, which is only later apparent in thin section. This problem is well known in ancient volcanic terrains, and has recently been highlighted at the Sgurr of Eigg [Brown and Bell 2013]. However, mLTe with pronounced eutaxitic fabric (Figure S7A, B) crops out to the south and west of Beinn Dearg Bheag (Logs 10,13,14,16,17,18, Logs B) and west of Beinn Dearg Mhor (Logs 1,2,6,7,15, Logs A). Individual mLTe units may range from 1–40 m in thickness, but the vast majority are  $< 4$  m thick. There are two notable exceptions. Firstly, a 30 m-thick continuous mLTe unit capped by mLT with a highly erosive base, crops out in the west (Log 7, Logs A). Secondly in the south (Logs 16, 18, Logs B) repeating cycles of mLTi and mLTe, crop out in both tributaries of the upper reaches of Allt nan Suidheachan (Logs 16, 18, Logs B). Some of the mLTe units are  $\leq 25$  m thick, (between 730–755 m). In log 16 these repeating mLTi and mLTe cycles have a lateral extent of 55 m, and in log 18 some 197 m. In both of these logged sections alternating deposits of mLTi and mLTe are capped by mBr. Cooling joints are common within mLTe units (Figure S7E), with individual columns spaced 0.6–1.5 m apart, and typically plunging at angles  $\leq 15^\circ$ . Weathered surfaces are frequently white in colour, whilst fresh rock is commonly black or dark grey. Matrix is fine grained to glassy, and in content  $\leq 90$  %. Matrix welding states may be highly variable. Where matrix is intensely welded, lithic lapilli may show evidence of rotation during PDC transportation (Figure S7C). Lithic lapilli within matrix may comprise amygdaloidal basalt, aphanitic basalt, mLT, mLTe, mLT lava-like, arkosic sandstone, or quartzite. Eutaxitic matrix fabric is

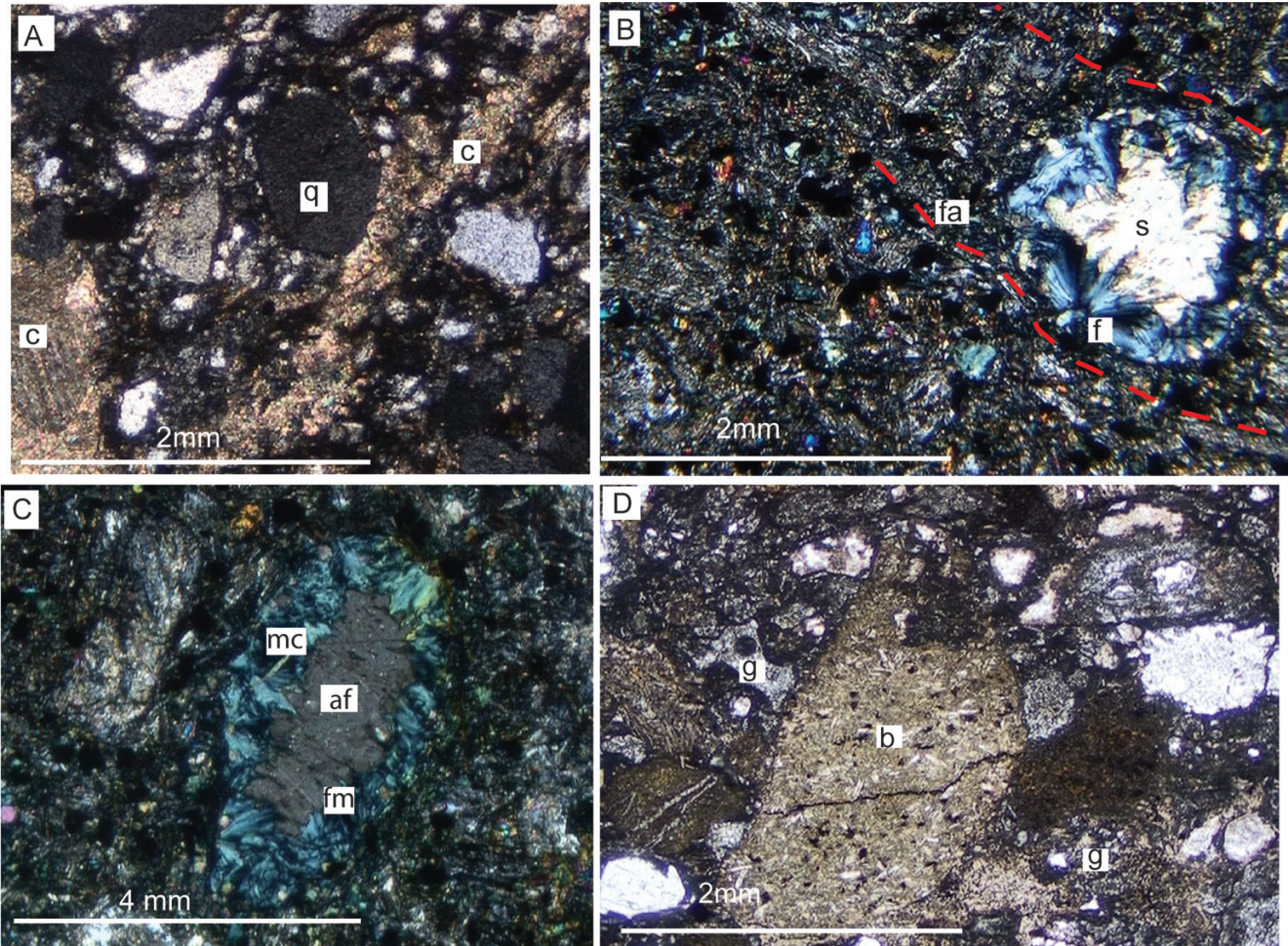


Figure S5: Petrographic characteristics of mLT. [A] Ubiquitous calcite (c) occurs both as sub-rounded lithic lapilli (bottom left), and interstitially as laterally discontinuous bands, evident to the right of a sub-rounded quartz (q) crystal, XP. (Log 16 142 m height, **Logs B**). [B] XP image of a fan spherulite (s) [after **Lofgren 1974**] within mLT matrix. Spherulite is composed of quartz fibres (f) radiating from a single point. Nucleation and growth started on the margins of a former gas cavity (lithophysae). Distorted matrix fabric (fa) suggests lithophysae growth was syn-post depositional. Secondary quartz (s) infills the lithophysae (Log 13, 18 m height, **Logs B**). Type III rounded matrix mafic enclave (me), with highly irregular lobate margins (lm) see (Log 18, 220 m height, **Logs B**). [C] XP image of alkali feldspar crystal (af) with fritted margins (fm) fringed by marginal chlorite (mc) within matrix supported mLT (Log 13, 18 m height, **Logs B**). XP image of alkali feldspar crystal (af) with fritted margins (fm) fringed by marginal chlorite (mc) within matrix supported mLT (Log 13, 18 m height, **Logs B**). [D] XP image of clast supported mLT containing fine grained, sub-rounded, basaltic lithic lapilli (b) and undeformed glass shards (g). A bubble wall shard is evident to top left of the basaltic lapilli (Log 10, 40 m height, **Logs B**). XP image of a fan spherulite (s) (after **Lofgren, 1974**) within mLT matrix. Spherulite is composed of quartz fibres (f) radiating from a single point. Distorted matrix fabric (fa) suggests lithophysae growth was syn-post depositional. Secondary quartz (s) infills the lithophysae (Log 13, 18 m height, **Logs B**).

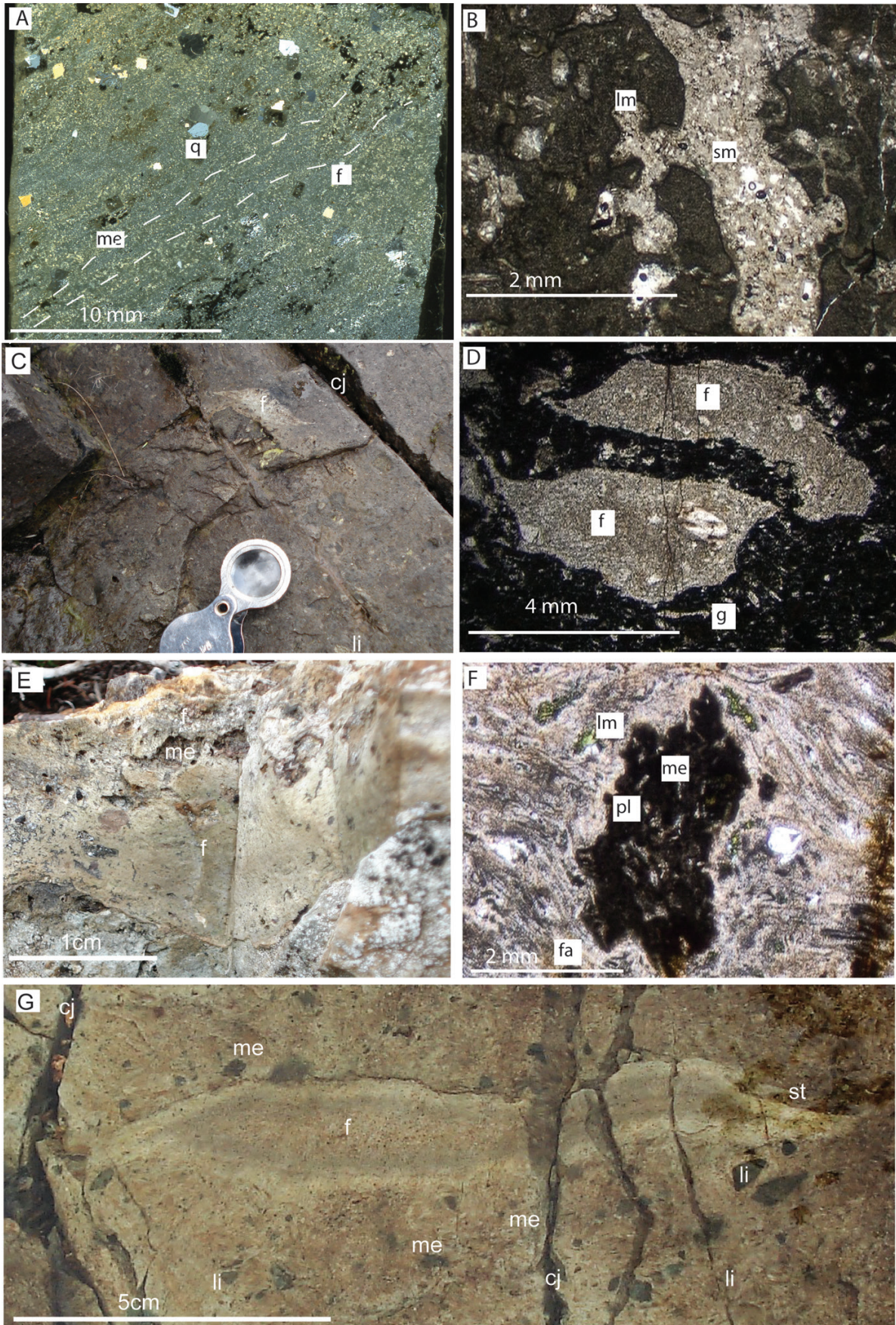


Figure S6: (Caption next page)

Figure S6: (Previous page) Field and thin section characteristics of incipient welded massive lapilli tuff (mLTi). [A] XP Scan of mLTi from Log 16, 445 m height, (Logs B). White hatched lines indicate incipient fabric (f), secondary quartz crystals (q) have overgrown this fabric, which contains type II mafic enclaves (me). [B] silicic melt (sm) globule with lobate margins (lm) above fiamme in [E] XP, (Log 10, 62 m height, Logs B). [C] Close up of cooling joints (cj) in [C] within mLTi showing fiamme (f) and sub-rounded lithic lapilli (li) (Log 16, 445 m height, Logs B). [D] XP photomicrograph of fiamme (f) which has recrystallised to micro-crystalline quartz within a glass (g) matrix. The fabric has been deflected around the fiamme, which itself has been mechanically fractured. (Log 16, 445 m, Logs B). [E] Type II mafic enclave (me) closely associated with swallow tailed fiamme (f) within mLTi. (Log 16, 445 m height, Logs B). [F] A type III mafic enclave (me) with highly irregular lobate margin (lm) and plagioclase laths (pl), within mLTi matrix which has a strong fabric (fa) deflected around the enclave, PPL (Log 16, 476m height, Logs B). [G] Matrix rich mLTi containing fiamme (f), with chloritized core, and swallow tail (st), with a length to width ratio of  $\leq 10:1$ . Individual fiamme are  $\leq 15$  cm in length, (Log 16, 445 m height, Logs B). Note ubiquitous Type II and III mafic enclaves (me), and columnar cooling joints (cj) which are perpendicular to an incipient left-right orientated fabric. Basaltic lithic lapilli (Li) lack lobate margins.

typically deformed around type II and III mafic enclaves (Figure S7G, H). Such enclaves have highly irregular margins, are frequently chloritised, and comprise  $\leq 5$  % of matrix content. In hand specimen some enclaves are very fine-grained, whilst others possess up to 20 % randomly orientated feldspar crystals, and possess 1–2 mm thick chilled margins.

All mLTi matrix is rhyolitic in composition (Figure S12), extremely fine-grained and commonly contains dominant quartz  $>55$  %. Other matrix phases are alkali feldspar, chlorite, Fe-rich chlorite and accessory allanite and zircon. Rounded quartz, embayed quartz and type II (Figure S7D) and III mafic enclaves are common within matrix. Skeletal allanite frequently occurs as overgrowths around unrounded mechanically fractured matrix quartz. Former glass shards have frequently re-crystallised to quartz, and are mechanically fractured. Often such mechanically fractured quartz has ( $\leq 25$   $\mu\text{m}$  thick) palagonitised rims. Palagonite rimmed quartz within mLTi deposits has been recorded elsewhere [Ross and Smith 1961; Riehle 1973; Riehle et al. 1995; Freundt 1999]. Cuspate matrix fiamme are frequently streaked out into a pronounced fabric and deformed around matrix lithics (Figure S7F–H). Matrix lithics are commonly  $\leq 4$  mm diameter, sub-angular to sub-rounded, and may comprise granite, aphanitic basalt, amygdaloidal basalt, or arkosic sandstone. Un-deformed bubble wall glass shards are visible within pressure shadows adjacent to lithic lapilli. Away from pressure shadows fiamme are streaked out with length:width ratios of  $\geq 20:1$ . Within thin section both evidence of vitroclastic textures may be destroyed and welding intensity may increase within mLTi samples over distances of  $<1$  mm.

Deposition of mLTi units took place from high-concentration, fluid-escape dominated, depositional flow boundary zones of ‘hot’ PDCs as indicated by poor sorting and absence of tractional stratification [Branney and Kokejar 2002]. Temperatures within mLTi producing PDCs were likely to have been  $>600$  °C, because welding of rhyolite has been shown experimentally to commence above this temperature [Bierwith 1982]. Syn-post depositional shearing and compaction, was accompanied by glass shard agglutination, whilst stress free areas existed in pressure shadows around lithic lapilli, where glass shards were largely undeformed. Localised shear stress varied considerably in intensity over very short distances, since eutaxitic and parataxitic fabric commonly oc-

cur together in the same thin section. Heat is needed to promote welding, and it is envisaged that air ingestion into eruption columns was therefore minimal, and PDCs were generated via low-fountaining fissure events. The presence of ubiquitous chlorite indicates that fluids and halogens were present during and after the deposition from PDCs [Duffield and Dalrymple 1990]. Type II and type III mafic enclaves within the matrix, indicate mafic melt was being introduced into rhyolitic PDCs throughout eruptions.

#### Lava like ignimbrite (mLT lava-like)

mLT lava like ignimbrites crop out west of Beinn Dearg Mhor (log 7, Logs A) and south of Beinn Dearg Bheag (log 12, 13, and 16, Logs B), as laterally discontinuous units, 1.8–6 m thick, capped by either mLT or mBr. Upper contacts are sharp and erosive whilst lower contacts are gradational over distances  $\leq 30$  cm. In log 7 mBr grades vertically into mLT lava-like over  $\leq 0.5$  m and in log 16 mLTi grades into mLT lava-like over  $\leq 20$  cm vertically. Similarly, mLT lava-like may grade laterally into mLTi or mLTi over distances  $\leq 2$  m (log16, 615–620 m height, Logs B).

In hand specimen mLT lava-like is flow banded, vitrophyric, and contains  $\leq 5$  % angular lithic lapilli  $\leq 30$  mm diameter. An orange weathered rind pervades  $\leq 2$  mm whilst fresh rock is frequently white in colour. Banding is on a sub-mm scale (Figure S8A, B), and comprises contorted leucocratic and melanocratic layers, often forming recumbent folds (Figure S8A, C), antiform- synform pairs, or ptygmatic folds. An intense parataxitic fabric is frequently deflected around lithic lapilli, and amorphous, chloritised, type II mafic inclusions (Figure S8D). Rare lithophysae ( $\leq 3$  cm long) are present in the matrix, and vary in form from lenticular, amorphous to oblate. mLT lava-like is highly matrix rich ( $\leq 95$  %), extremely fine grained, and rhyolitic in composition (Figure S12). The main matrix phases are quartz and alkali feldspars, with highly subordinate plagioclase, rutile, chlorite, zircon and monazite. A very strong sub-linear parataxitic fabric pervades the matrix, which is composed of alternating leucocratic and melanocratic layers.

Leucocratic layers are composed of  $\mu\text{m}$  thick laminations of quartz, alkali feldspar and rare monazite. Melanocratic layers are highly chloritised, and contain allanite, titanite, and

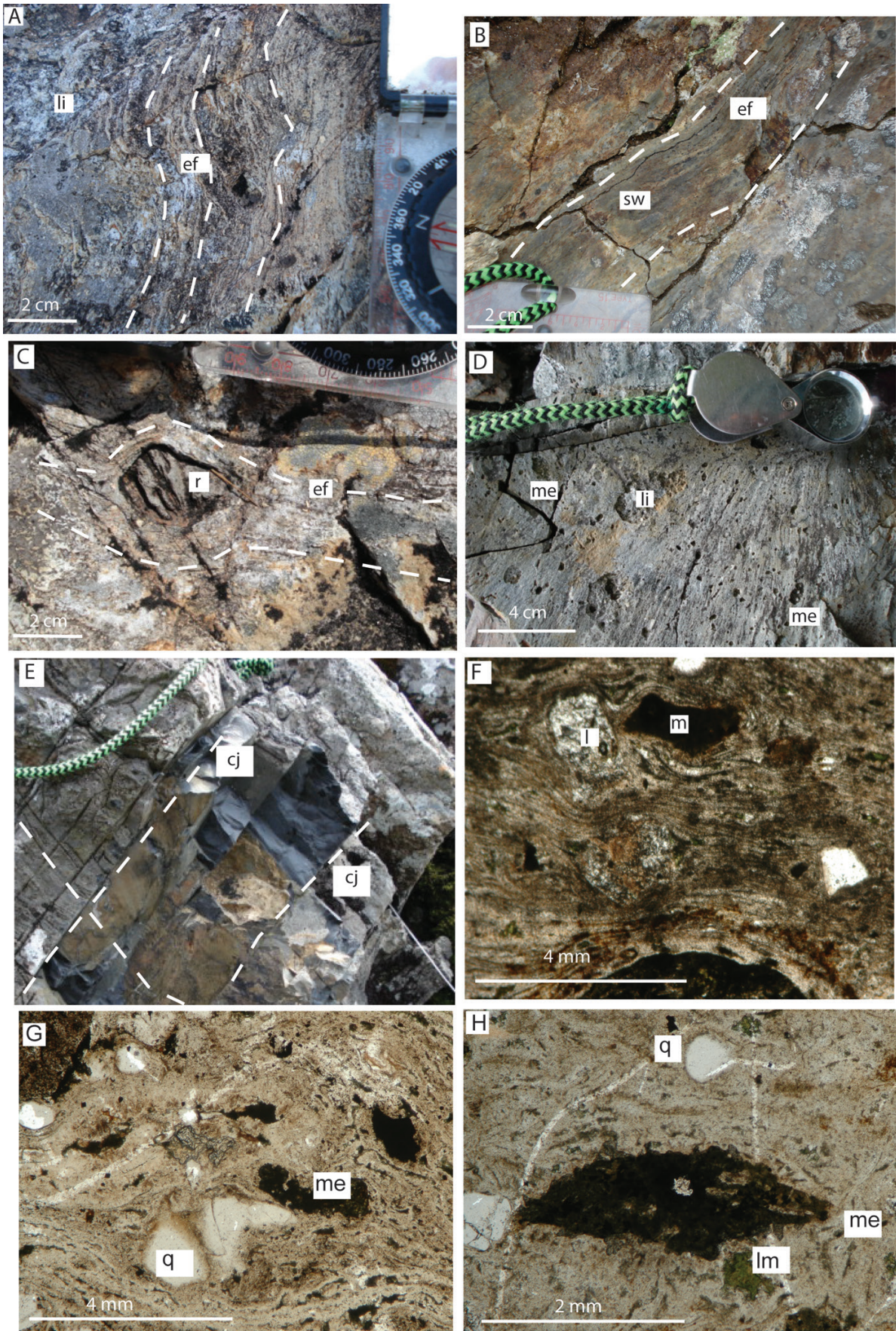


Figure S7: (Caption next page)

Figure S7: (Previous page) Field and petrographic characteristics of massive lapilli tuff with eutaxitic fabric (mLT<sub>e</sub>). [A] Intensely welded eutaxitic fabric (ef) delineated by hatched white lines deflected around angular rhyolitic lithic lapilli (li)  $\leq 1$ cm (Log 8, 5 m height, **Logs A**). Intensely welded eutaxitic fabric (ef) delineated by hatched white lines deflected around angular rhyolitic lithic lapilli (li)  $\leq 1$ cm (Log 8, 5 m height, **Logs A**). [B] Same locality where matrix often appears glassy and black. Eutaxitic fabric (ef) is evident top right to bottom left. Fiamme are highly streaked, and virtually closed swallow tails (sw) are evident. [C] lithic lapilli of mLT<sub>i</sub> incorporated within mLT<sub>e</sub> (Log 12, 47 m height, **Logs B**). Note how external eutaxitic fabric (ef) is strongly deflected around rhyolitic mLT<sub>i</sub> lithic lapilli (r). [D] Type II mafic enclaves (me) and angular chloritized lapilli (li) recorded in Log 10, 5 m height, (**Logs B**). [E] nature of the angular relationship between columnar cooling joints (cj), and eutaxitic fabric (ef) in [D]), which is orientated approximately perpendicular to columnar jointing. Matrix is highly silicic and frequently glassy. Note strong parallel/eutaxitic fabric (bottom right) evident within the white weathered surface. [F] PPL photomicrograph of pronounced eutaxitic fabric within mLT<sub>e</sub> (Log 18, 242 m height, **Logs B**) containing mafic clast (m), butted up against rotated lithic lapilli (l). Note the presence of cusped fiamme which have been deflected above and below the mafic clast. Eutaxitic fabric (white hatched lines) orientated parallel to chloritised fiamme (f). Note fiamme are reverse graded from bottom to top of photograph (Log 14, 305 m height, **Logs B**). [G] PPL photomicrograph of mLT<sub>e</sub> from Log 18, 315 m height, (**Logs B**). The highly contorted matrix fabric is deflected around angular quartz crystals (q) and ubiquitous streaked out, lobate, type II mafic enclaves (me). [H] PPL photomicrograph of rounded quartz (q), and type II mafic enclave (me) with lobate margin (lm), within a partially chloritised silicic matrix. The enclave clearly post-dates top to bottom trending quartz veins, (Log 8, 5 m height, **Logs A**).

fan spherulites of quartz [Lofgren 1974]. Spherulites are concentrated at the outer margins of melanocratic layers. Matrix layers have been strongly deformed into a parataxitic fabric [Pioli and Rosi 2005] around crystals, and lithic lapilli (Figure S9B–D). Matrix fabric consists of parallel to rectangular shaped domains which are laterally discontinuous on a micron scale. Compressional features such as en-echelon micro scale ‘piggy back’ thrust slices occur sporadically throughout mLT lava-like matrix. Extensional features are also evident for example boudinaging of quartz rich parataxitic fabric in the hinge regions of micro-scale antiforms. Elsewhere, antiforms and antiform-synform pairs are common within matrix.

Lithic lapilli within mLT lava-like comprise sub-angular fragments of micro-granite, rhyolite, and sub-rounded basalt. Quench features such as matrix spherulites are very common and may radiate out from a single point source or fringe parataxitic fabric margins in trails. Spherulite cores comprise strain free quartz crystals, with margins frequently interlocking at 120° triple junctions. Spherulite cores are surrounded by radiating fibres of K-feldspar, themselves mantled by quartz. Lithophysae and axiolites are subordinate volumetrically to spherulites within matrix. Spherulites are frequently orientated parallel to parataxitic fabric, and spherulitic rich domains are located between leucocratic or melanocratic domains. They are either radial, or lithophysal spherical structures [Lofgren 1974; Breitzkreuz 2013]. Within mLT lava-like matrix fan spherulites are volumetrically subordinate to spherical spherulites. External fabric is frequently deformed around both type II and III mafic enclaves. Individual enclaves may contain plagioclase that is either aligned in a sub-parallel orientation, or randomly orientated. mLT lava-like was deposited incrementally during very hot ( $\leq 1000$  °C) quasi-single sustained eruptions, from very low, fissure fed fountaining columns [Branney and Kokelaar 1992; 2002]. Macroscale evidence of extremely ‘hot’  $\sim 1100$  °C [Andrews and Branney 2011] emplacement of mLT lava-like deposits is evidenced by the flow banded vitrophyric texture, spherulitic rich domains, and lithophysae. During transportation within PDCs the amount of heat present, topographic gradient, and viscosity, were suf-

ficient to promote rheomorphic flow. This resulted in intense folding (i.e. pygmatic, recumbent, antiform-synform pairs) and faulting which is evident both at macro and micro-scale (Figure S9A). The post depositional brittle state of mLT lava-like is evidenced by the presence of en-echelon micro faults which were probably caused after the deposit cooled, and passed through the glass transition zone.

Fissures containing rhyolitic tuff are often in close proximity (10  $\leq$  40 m) to lava like ignimbrite (logs 12 and 16, **Logs B**). However, such fissures are not always evident near mLT lava-like deposits (e.g. log 7 and log 13, **Logs A**, **Logs B**). During eruptions lava-like ignimbrite producing PDCs were syn-post-depositionally welded and agglutinated on paleo-topography, before cooling through the glass brittle–ductile transition zone [Freundt 1999; Russell et al. 2003]. The very close proximity of fissure fed tuff to outcrops of mLT lava-like and their very similar chemistry (Figures S12 and S13) strongly suggests PDCs were fed from fissures.

The presence of ubiquitous mafic blebs within mLT lava-like matrix indicates magma-mingling took place extensively between rhyolitic, and mafic-rich melt bodies, throughout mLT lava-like producing eruptions. Since the margins of mafic blebs are lobate, and external fabric is deflected around them, a pronounced temperature difference must have existed between host rhyolite, and introduced pulses of mafic melt, during incorporation into PDCs.

#### Tuff filling fissures (TFF)

Within logs 11,12, and 17 (**Logs B**) fissure filled tuff  $\pm$  brecciated tuff crops out along NW–NNW trending linear outcrops. The most extensive of these fissures is 380 m long, links Logs 11 and 17 then broadly parallels the east bank of Allt nan Suidheachan. The fissure resembles a dyke, but lacks either chilled margins, or cooling joints. The fissure is offset and ranges in thickness from  $\leq 5$  cm–4 m. Tuff contained within the fissure is fine grained, weathers white, has an intense near vertically orientated fabric, and contains sheath folds whose axes are sub-parallel to the pervasive fabric. They appear as

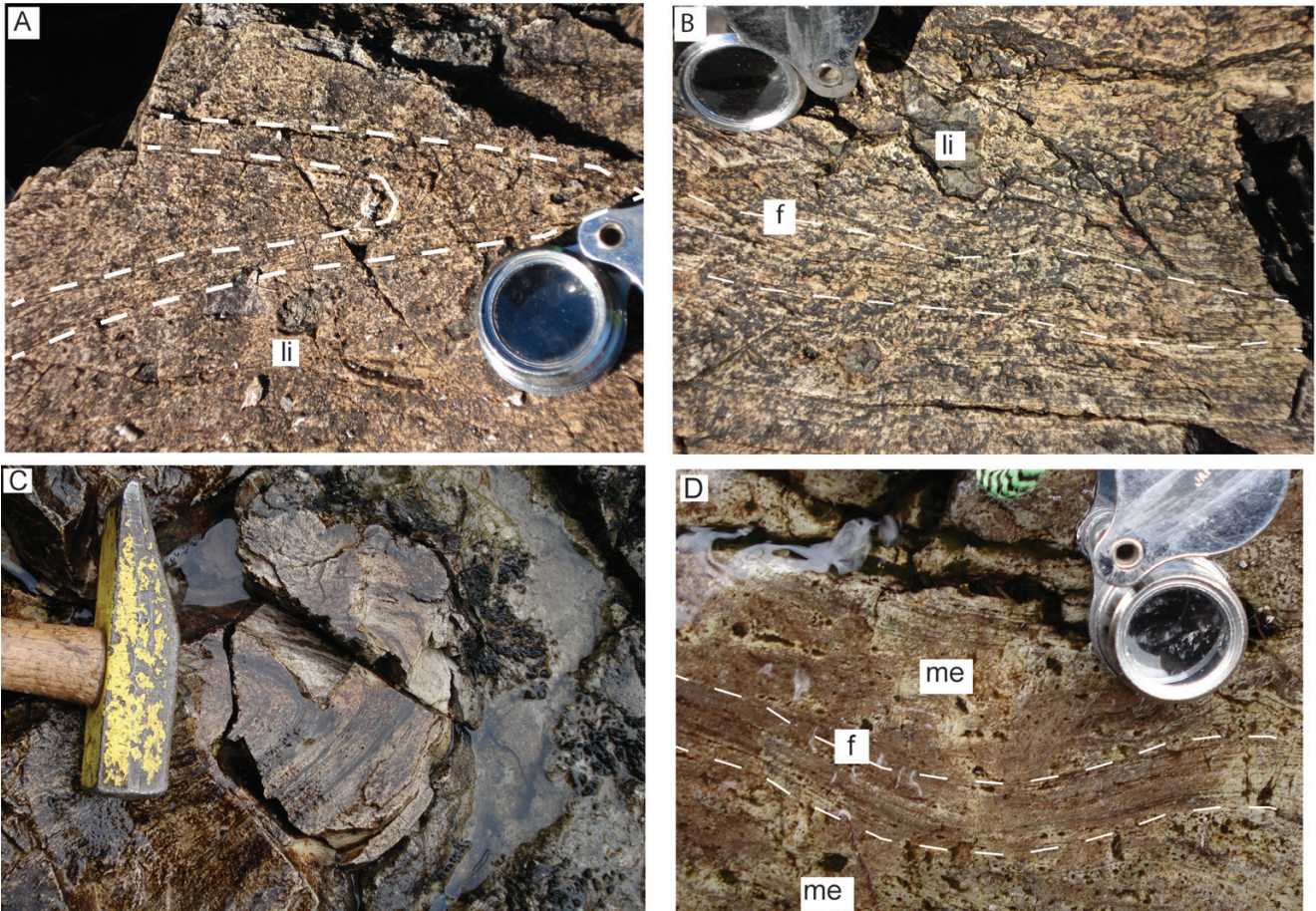


Figure S8: Field and petrographic characteristics of lava-like massive lapilli tuff (mLT lava-like). [A] Intensely folded lava-like ignimbrite, contains angular rhyolitic tuff (li) lapilli  $\leq 1$  cm in length. [B] mLT lava-like, (Log 18, 316 m height, **Logs B**) a flow banded vitrophyre, with intense planar parataxitic fabric (pf). The matrix is deflected around sporadic rhyolitic tuff lapilli (li), towards both top and bottom of image. [C] mLT lava-like, (Log 18, 318 m height, **Logs B**) which has been rheomorphosed into a recumbent antiform. Hammer head is 17 cm long. [D] Type II mafic enclaves (me) within mLT lava-like ignimbrite with intense fabric (f), (Log 18, 316 m height, **Logs B**).

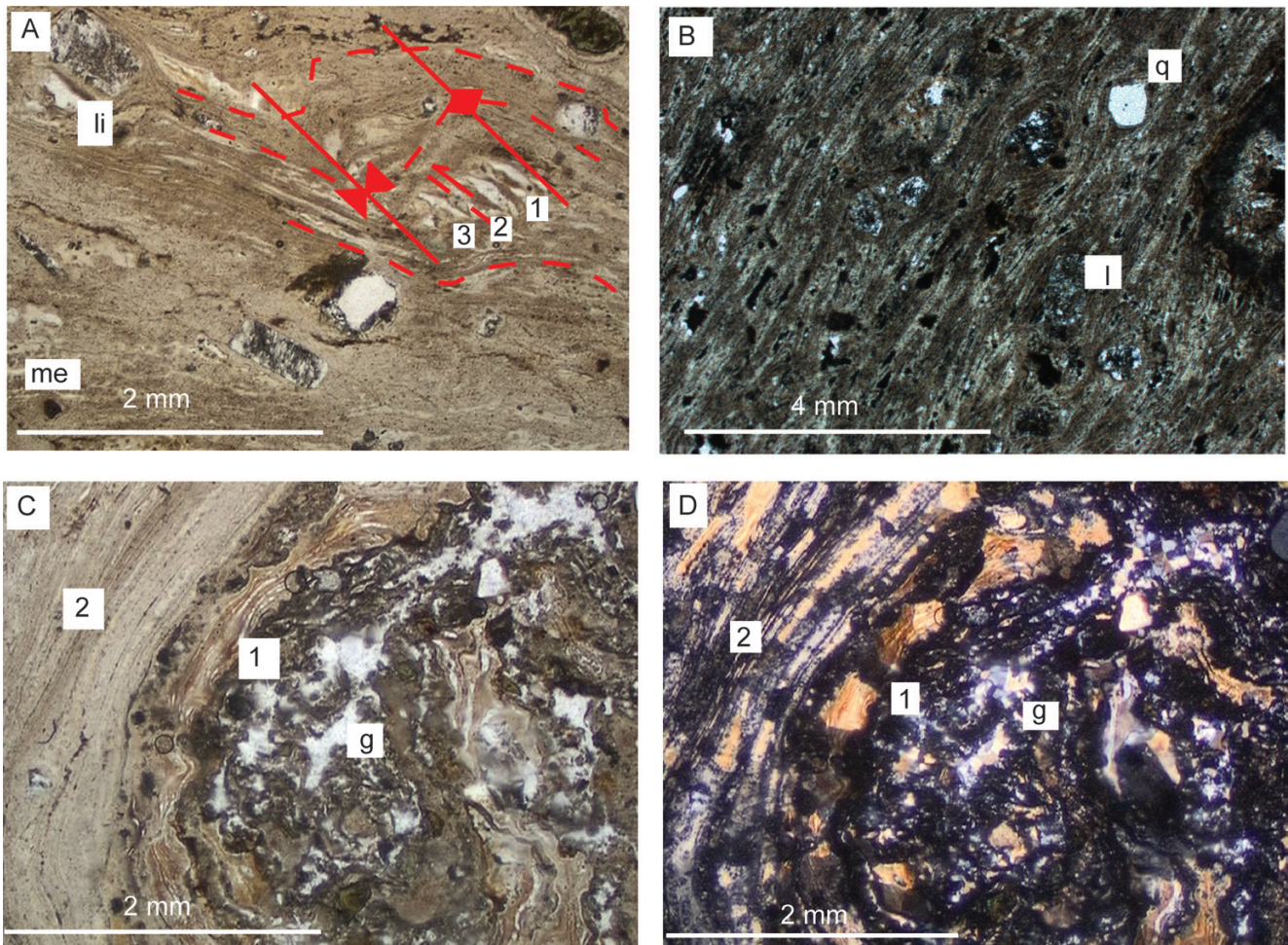


Figure S9: Petrographic characteristics of mLT lava-like. [A] Photomicrograph in PPL showing antiform-synform pair within mLT lava-like matrix (Log 7, 15 m height, **Logs A**). Vergence was from the right of the image, and produced micro-imbricate thrust slices (1= oldest, 3=youngest). [B] XP image of parataxitic 'banded' fabric with mineralogically different layers (leucocratic and melanocratic). Vitroclastic texture has been destroyed by agglutination and coalescence of glass shards. Parataxitic fabric is deflected around quartz crystals (q), and micro-granite lithic lapilli (l). [C] PPL image of the hinge region within a). Region 1 boudinaged quartz rich layers, are juxtaposed with quartz rich glass (g). Region 2 is much finer grained, and parataxitic like fabric terminations, can be seen in leucocratic layers. [D] XP image of [C] showing intense parataxitic region at 1 and 2. Undeformed glass shards (g) are evident in areas which were subjected to less strain.

‘eye like structures on rock surfaces’ normal to the transport direction. Fabric is frequently deformed around sub-circular to these oblate sheath folds which are  $\leq 7$  cm long, occur in clusters, and comprise a core and  $\leq 5$  concentric rings. The kinematics of the sheath folds suggests flow direction of fissure fed tuff was to the SSW. Substantial thicknesses of alternating mLTi and mLTe units, together with a mLT lava-like unit crop out  $\sim 30$  m SSW of the fissure (Log 16, height 720–790 m and log 18 height 0–318 m, **Logs B**). Lapilli of fissure-derived tuff are contained within the mLT lava-like exposure.

In hand specimen the tuff contains sporadic angular mafic lithic fragments ( $\leq 4$  mm diameter) and ubiquitous chloritised type III enclaves  $\leq 1$  cm diameter. Intense ‘rheomorphic’ matrix folding occurs around pumiceous fragments. Lithophysae are common throughout the outcrop. At Allt Coire Forsaidh rhyolitic fissure filled tuff is  $\sim 10$  m thick and crops out for 170 m along a faulted stream section. The rock is auto-brecciated and is pervaded by randomly orientated elutriation pipes, containing recrystallised glass, and angular quartz fragments. A strong sub-vertical fabric is frequently deformed around weathered in recesses, and auto-brecciated clasts of tuff. Direct contacts between the tuff and mLT lava-like are not evident. However, sub-horizontally flow-banded, vitrophyric, mLT lava-like (**Figure S10A**) crops out on the opposite stream bank  $\leq 5$  m from the tuff strongly suggesting the mLT-lava like was fed from the fissure.

The fissure fed tuffs are rhyolitic (**Figure S13**) and have extremely similar whole rock geochemistry to adjacent mLT lava-like deposits (**Figure S12**). Thin sections comprise  $\leq 95$  % devitrified glass together with abundant spherical spherules (0.5–4 mm diameter) of radiating crystals of quartz and alkali feldspar. Tuff matrix is frequently pervaded by perlitic cracks and contains type II and III mafic enclaves together with dendritic alkali feldspar crystallites and rare magnetite and pyrite. The extremely close proximity of mLT lava-like and mLTe to fissure fed tuffs, together with similar matrix chemistry suggests high-grade ignimbrites were fissure fed during very ‘hot’ eruptions in upward flaring multiple conduits (**Figure S10B–D**). These fissures frequently coincide in orientation with NNW trending dykes of the regional Paleogene swarm. The ubiquitous presence of mafic enclaves within all fissure fed tuff suggests basic magma pulses were incorporated into silicic chambers throughout eruptions. Field evidence further suggests that some fissures were ‘re-exploited’ by later NNW basic dykes of the regional swarm since they chill into, and are juxtaposed with, fissure fed tuff (log 11, **Logs B**, **Figure S10E**).

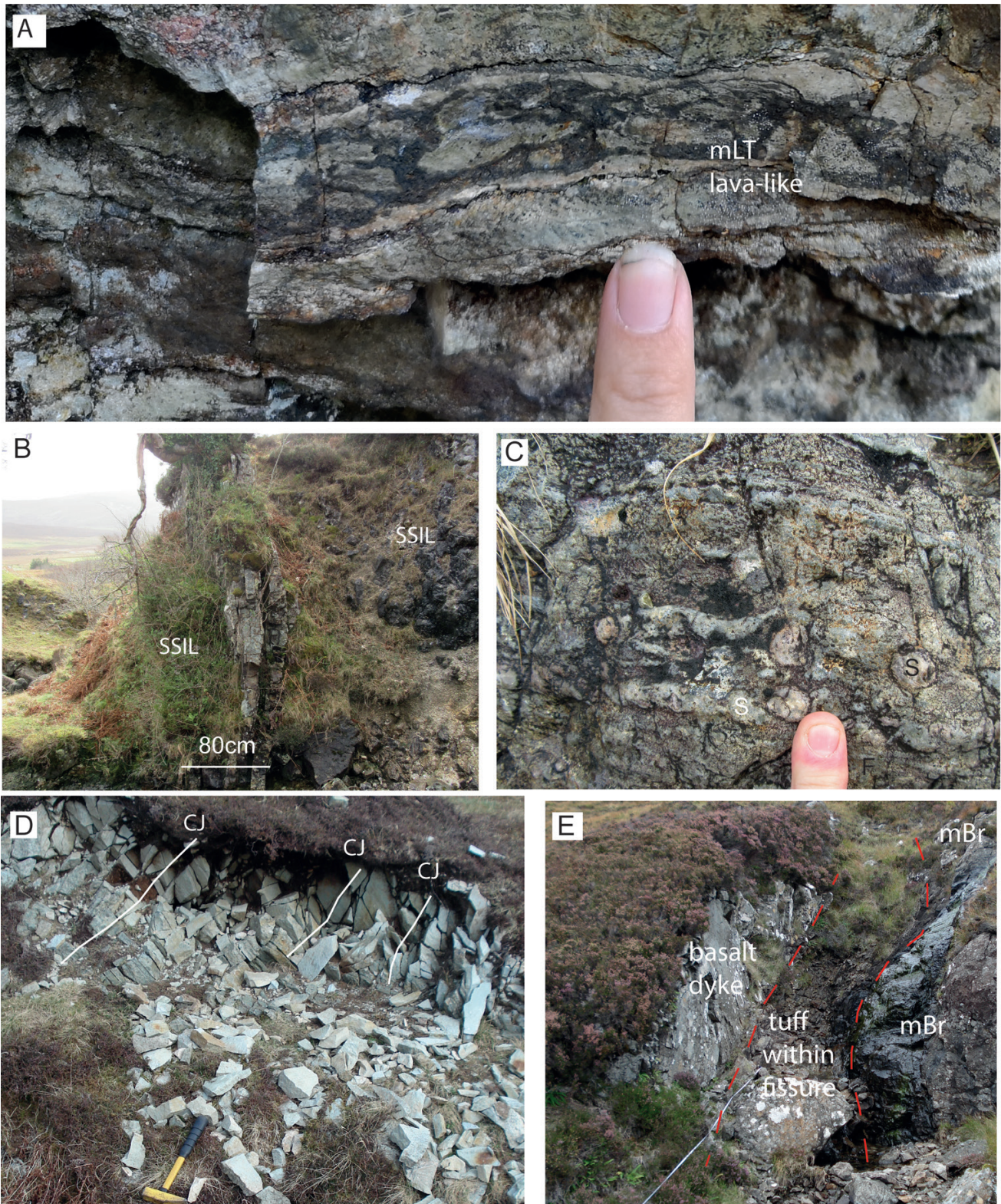


Figure S10: Field characteristics of tuff filling fissures and mLT lava-like in close proximity. [A] Spherulitic lava-like ignimbrite within 50m of tuff filling fissure on western bank of Allt Coire Forsaidh. [B] Silicic tuff filling a fissure (TFF) outside the inner ring fault at Allt a Choire. The fissure is NNW trending, sinuous, and cross cuts Cambro-Ordovician dolostone of the Strath Suardal Formation (SSF). [C] Spherulitic (S) rhyolitic tuff within the fissure at [B] separated by sub-parallel planar fabric, in places fabric is contorted around individual spherulites (NG 62154 23527). [D] Localised 5 m × 2 m mLT lava-like deposit filling a paleo-depression ~300 m from B and C at NG 61803 23119. Note the presence of cooling joints (CJ). [E] Fissure filled tuff juxtaposed with later basaltic dyke (trending NNW) and mBr (log 11, [Logs B](#)). Mafic magma has therefore exploited fissures previously exploited by silicic magma.

Table S3: Radiometric age determinations on Palaeogene rocks from the Kilchrist area. Ages in millions of years (Ma).

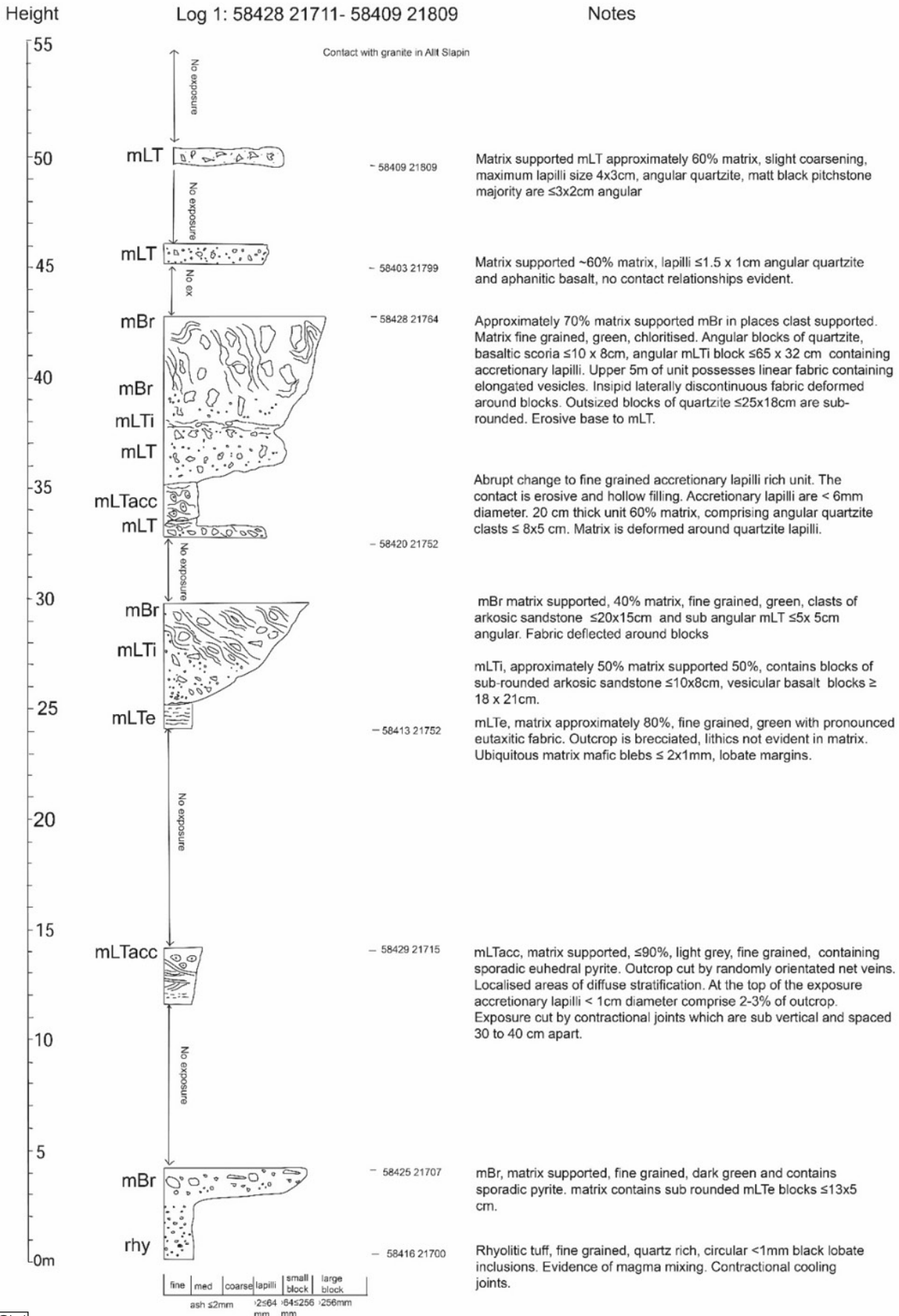
Eastern Red Hills Centre (ERH)	Age (Ma)	System
Silicic inclusions within mafic dyke, Ben Suardal (NG 63191 20477)	56.45 ± 0.19	U-Pb*
mLTi Allt nan Suidheachan (NG 59618 20783)	56.15 ± 0.19	U-Pb*
Beinn an Dubhaich Granite	55.89 ± 0.15	U-Pb†
Pitchstone dyke cutting Beinn na Caillich Granite	55.7 ± 0.10	U-Pb†

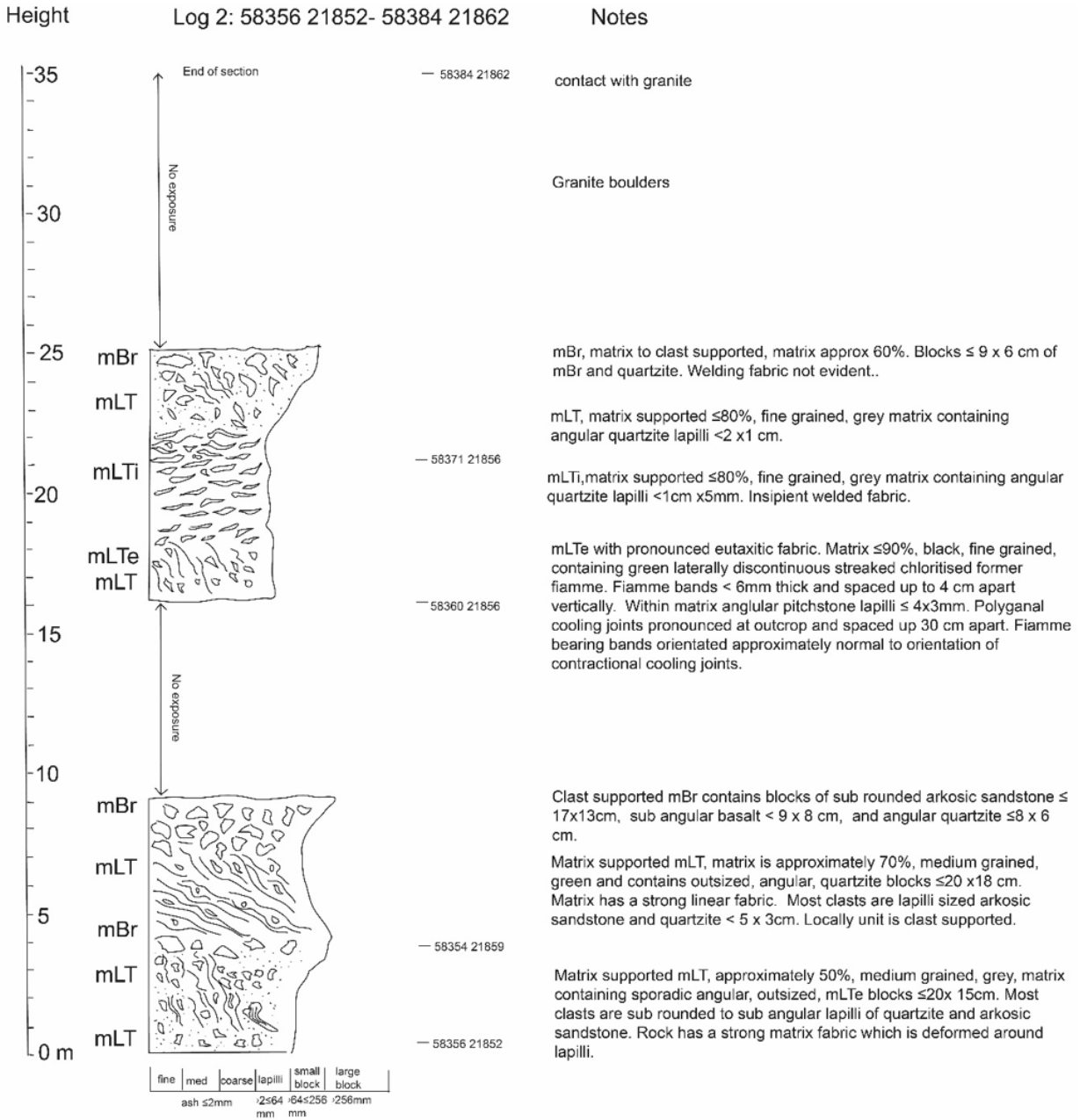
\* This study;

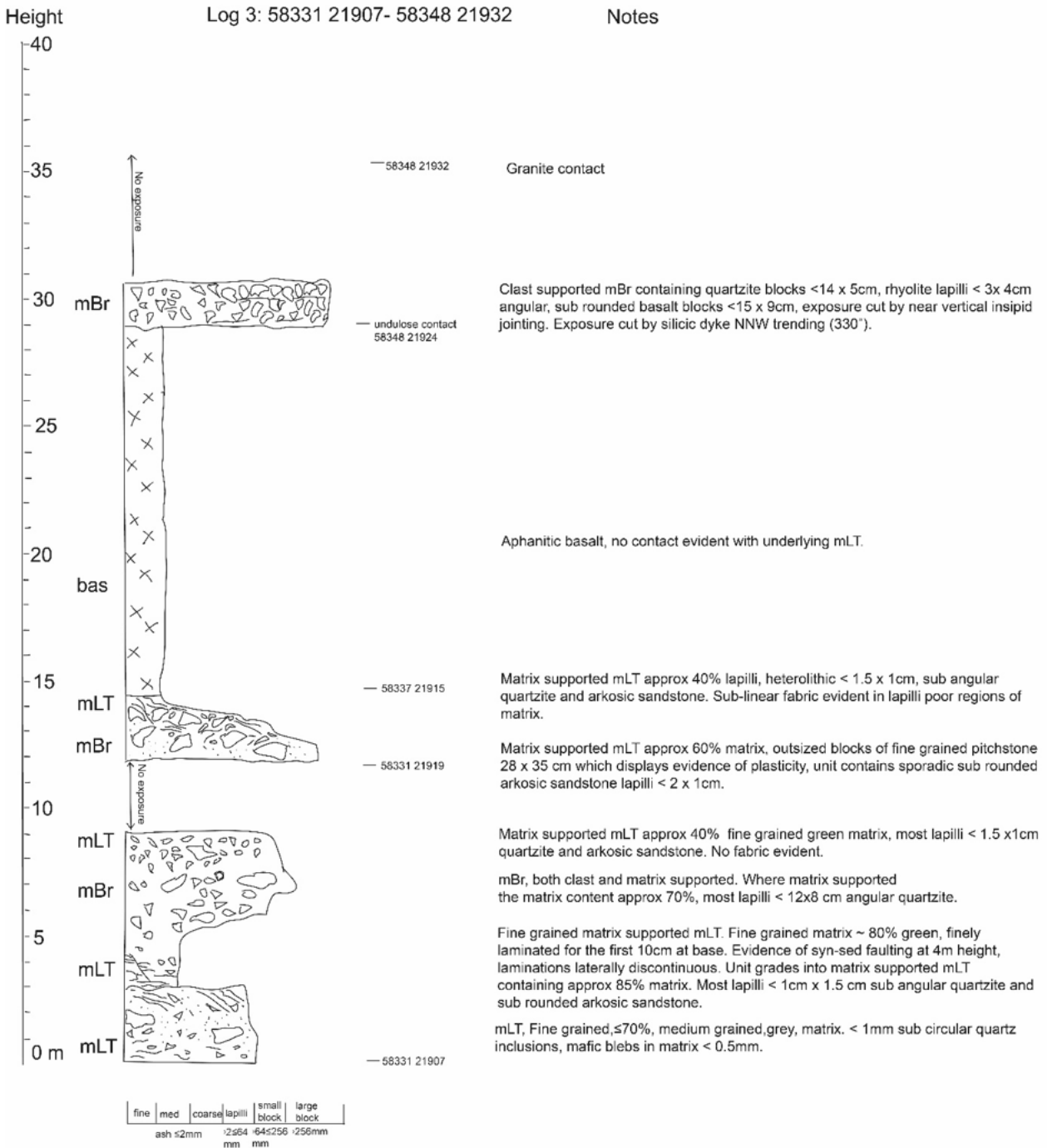
† Unpublished U-Pb analysis by M. A. Hamilton, Jack Slattery Geochronology Laboratory, Department of Geology, University of Toronto, in [Emeleus and Bell \[2005\]](#).

3 LOGS A

Logs 1–8 and 15 West of Beinn na Caillich Centre



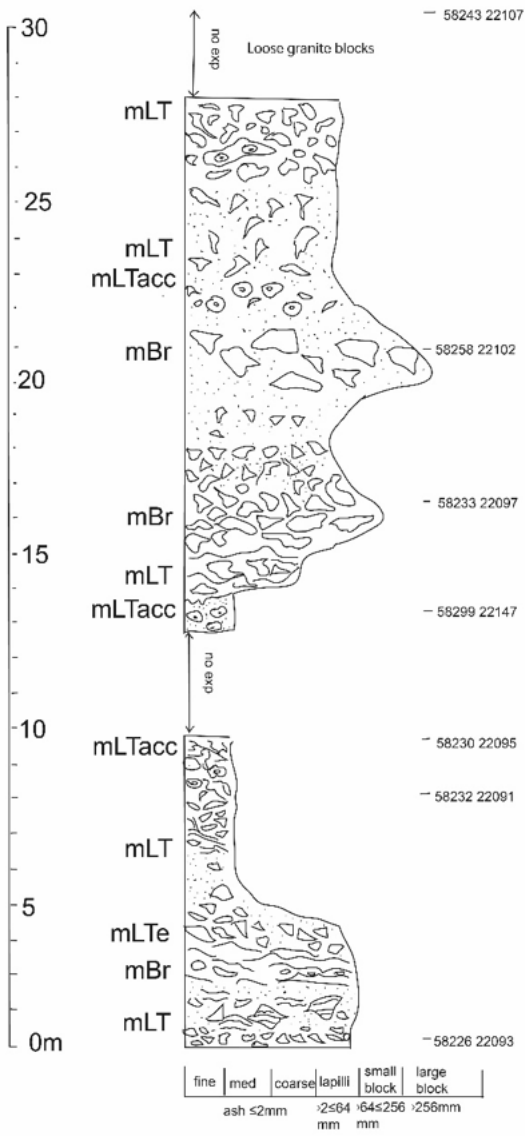




Height

Log 4 5822622093-5824322107

Notes



Contact with granite

Clast supported mLT contains oversized rhyolitic blocks <math>< 26 \times 15\text{ cm}</math> which contain accretionary lapilli. Majority of blocks are <math>< 26 \times 5\text{ cm}</math> of angular mLTe and sub rounded arkosic sandstone.

Matrix supported mLT comprising 60%, fine grained, green, matrix. Maximum block size 10 x 8 cm of mLTe. Most are <math>\le 5.5\text{ cm}</math> and sub-angular. Exposure pervaded by cooling joints which are spaced <math>\le 5\text{ cm}</math> apart.

mLT, matrix supported, <math>\le 70\%</math> matrix, fine grained, mid grey, which contains concentric accretionary lapilli <math>\le 5\text{ mm}</math> diameter. Majority of lapilli are sub-angular quartzite <math>< 1\text{ cm} \times 5\text{ mm}</math>.

Coarsening upwards matrix supported mBr, comprises 40%, fine grained matrix, and oversized sub-rounded blocks of arkosic sandstone <math>\le 31 \times 17\text{ cm}</math>. Most clasts of arkosic sandstone are lapilli and small block sized <math>< 8 \times 4\text{ cm}</math>.

mLT, clast supported, fining upwards. Angular mLTe lapilli <math>\le 6 \times 4\text{ cm}</math>. In places unit is matrix supported with up to 50% matrix. Cooling joints sporadically pervade the exposure and are sub-vertical.

Clast supported mBr containing basaltic scoria blocks <math>\le 22 \times 9\text{ cm}</math> with lobate margins. Also angular mLTe blocks <math>\le 9 \times 3\text{ cm}</math> majority are <math>> 6 \times 3\text{ cm}</math>.

Erosional contact with overlying mLT which is matrix supported (40% matrix), fine grained, green and contains bomb sized clasts of partially melted arkosic sandstone <math>\le 15 \times 12\text{ cm}</math>. Accretionary lapilli occur sporadically throughout different levels in unit with maximum diameter of 1.5cm.

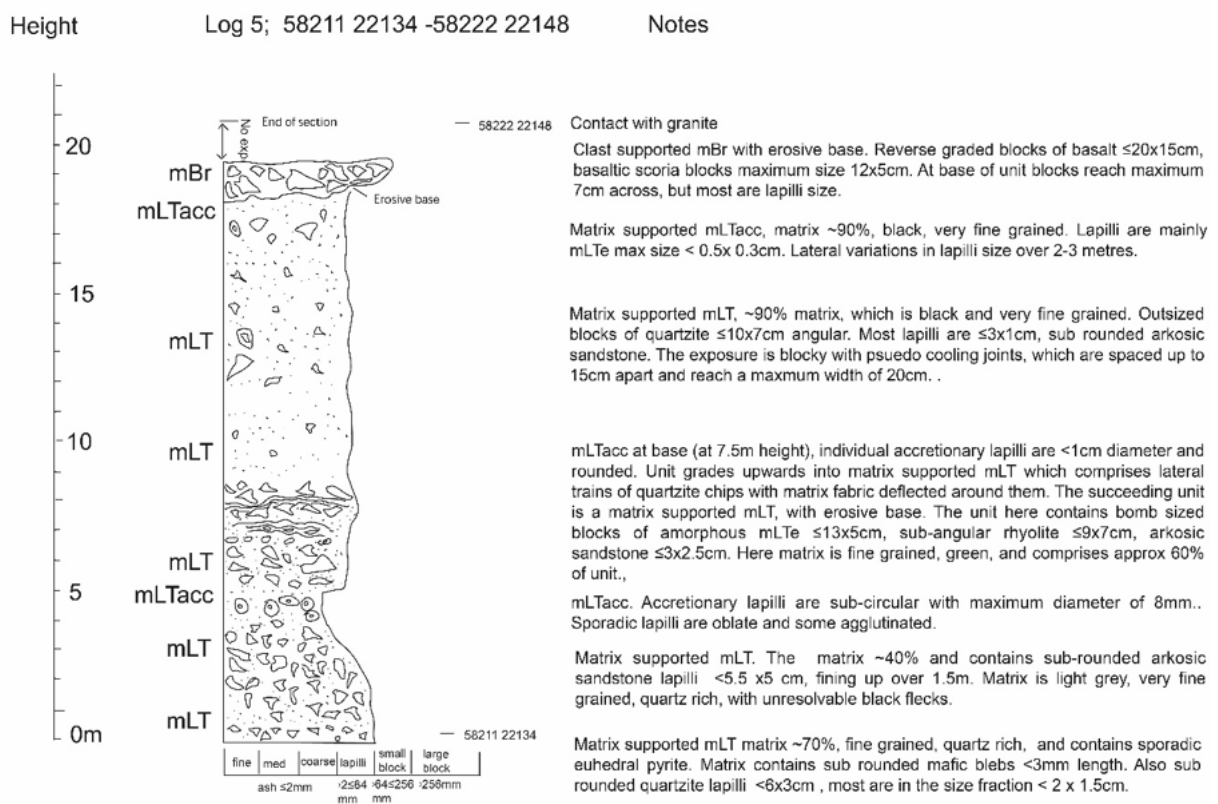
Matrix supported mLTacc, the accretionary lapilliacc comprise approximately 5% of outcrop and are oblate. Their maximum size is 1.4 cm x 5mm. Randomly orientated net veins pervade the exposure. The matrix comprises 40% and is fine grained green, insipient welded fabric is deflected around sub rounded arkosic sandstone lapilli which are <math>< 5 \times 4\text{ cm}</math>.

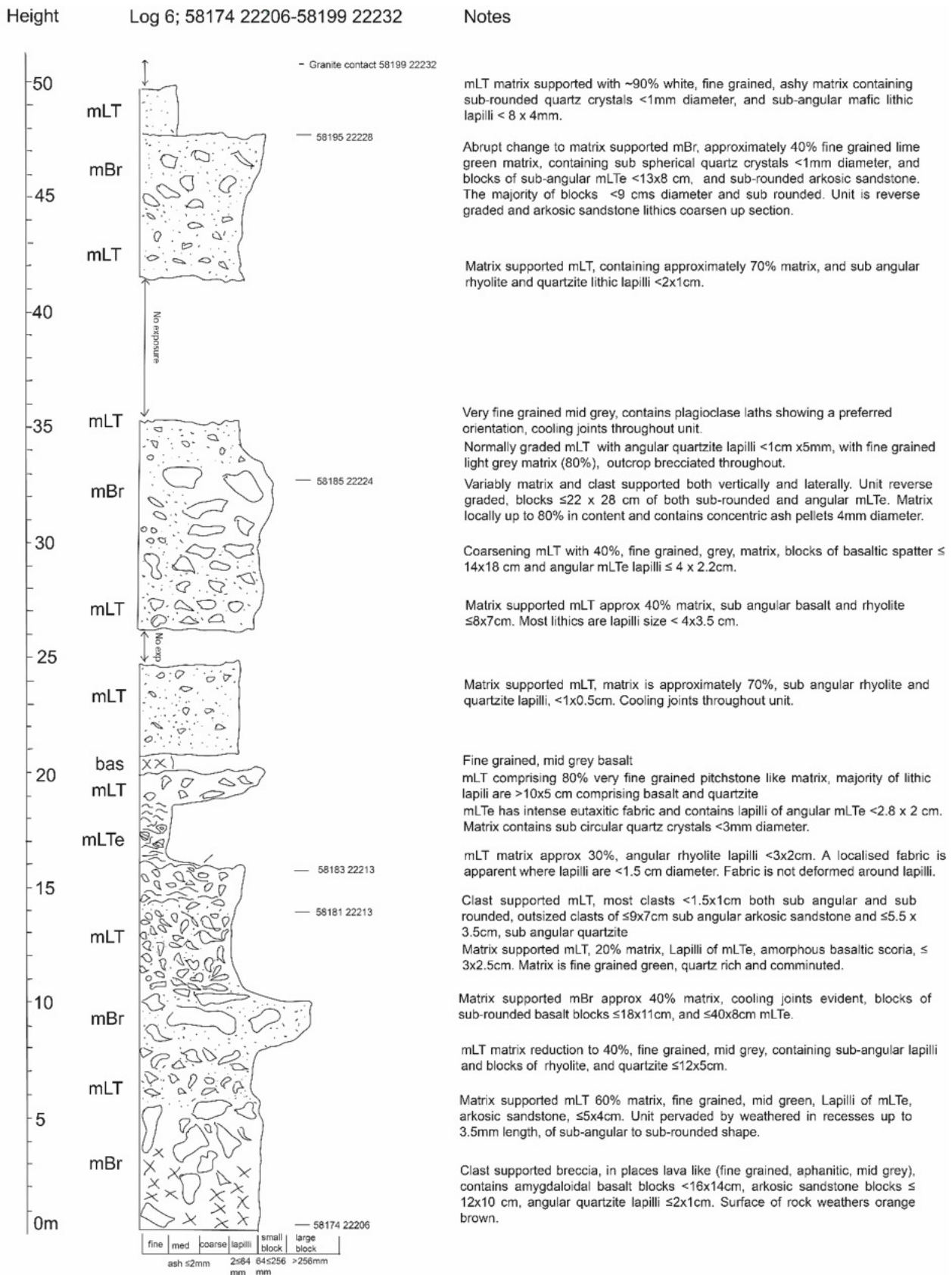
Matrix supported, mLT. Matrix comprises 80% and is very fine grained, green. The dominant lapilli type is quartzite <math>\le 4 \times 3\text{ cm}</math>.

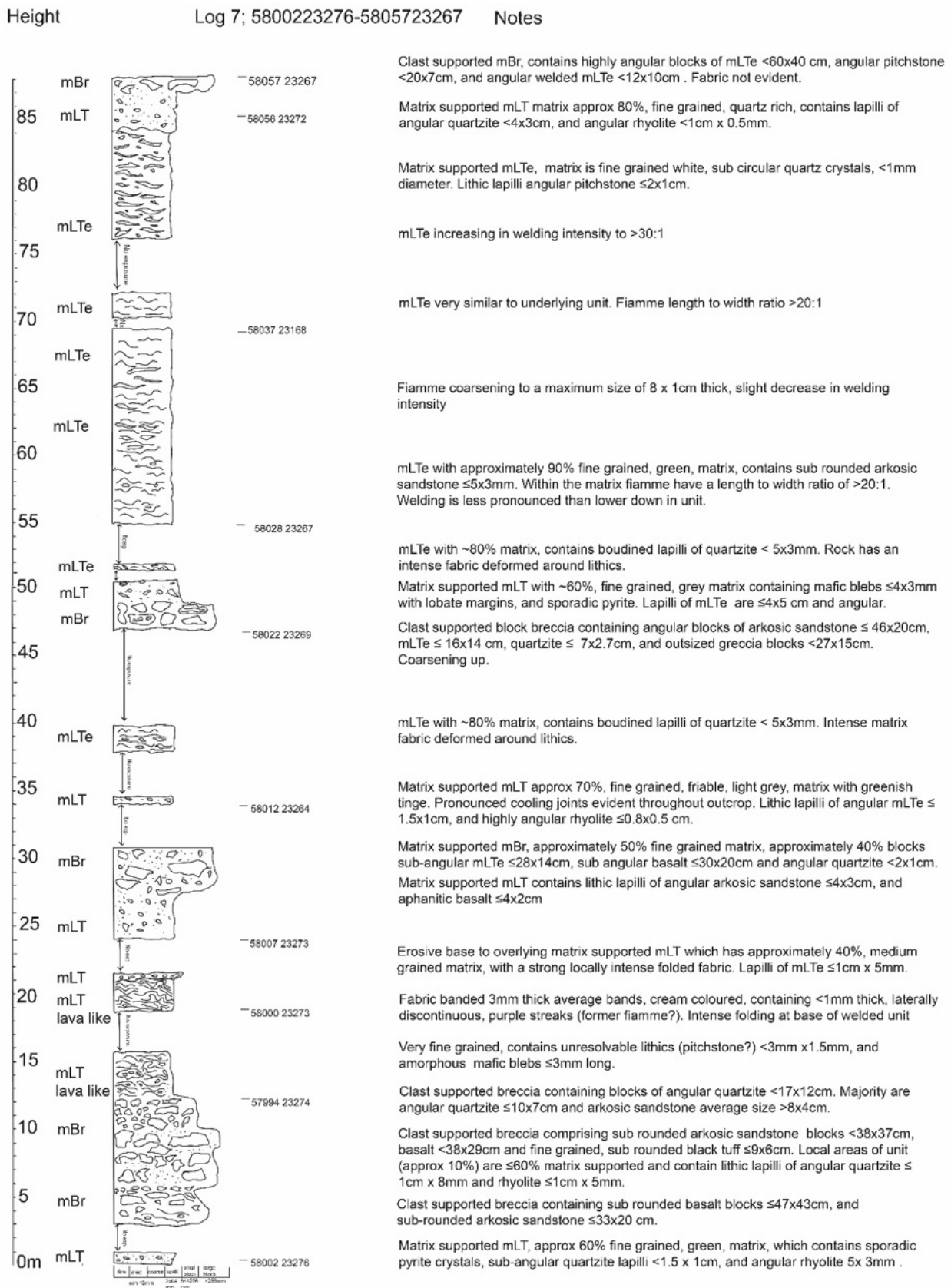
Matrix supported mLT, approx 30% fine grained green matrix, contains clasts of sub angular mLTe <math>\le 8 \times 5\text{ cm}</math>, also sub rounded arkosic sandstone <math>\le 1.5 \times 1\text{ cm}</math>. Evidence of mechanical fracturing of clasts. Cooling joints average spacing 8-10 cm apart.

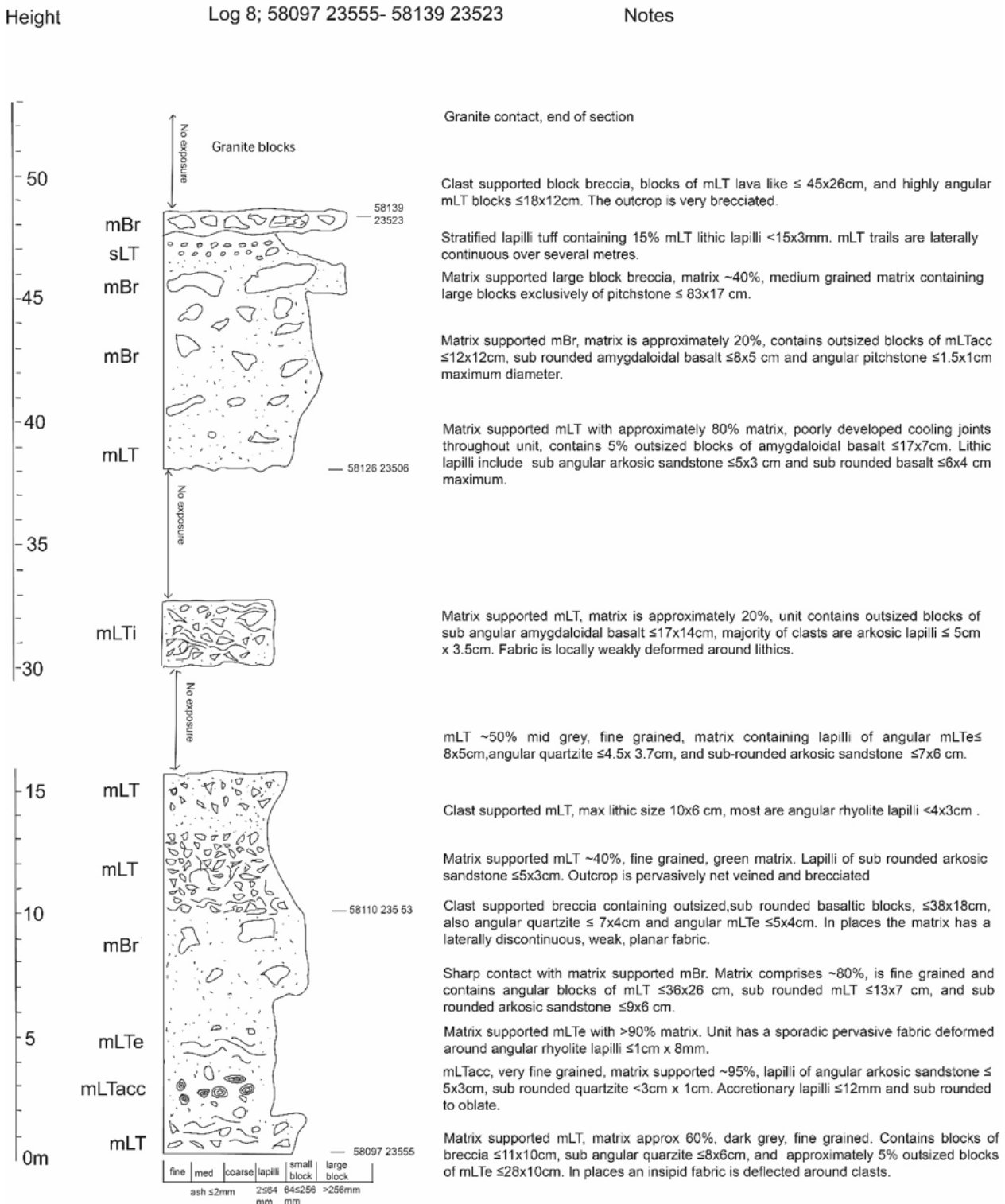
Matrix supported mBr with approximately 40% matrix. Contains blocks of mLTe <math>\le 12 \times 10\text{ cm}</math> sub rounded. Intense fabric but is not deflected around lithics.

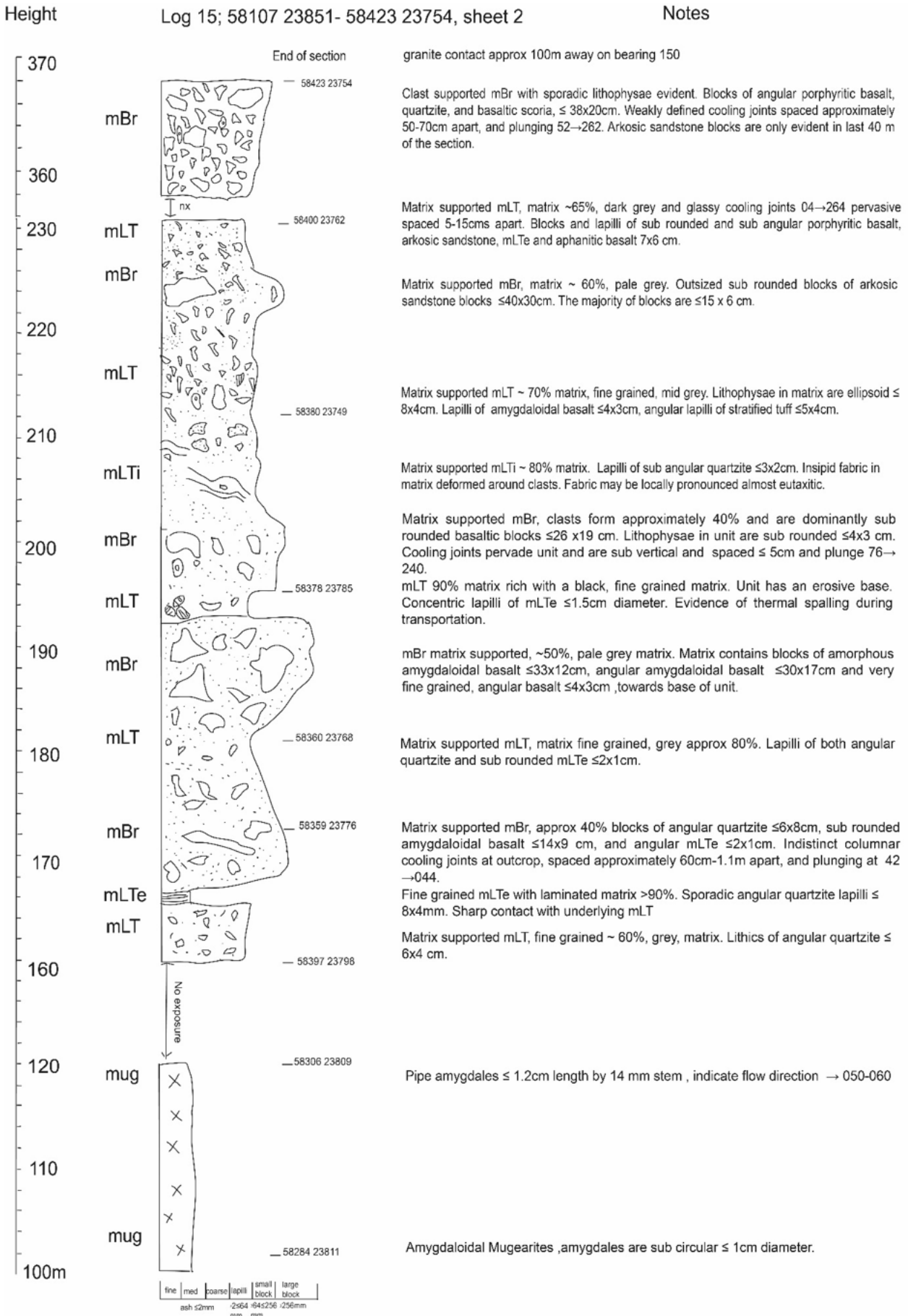
Clast supported heterolithic mLT. Contains angular rhyolitic lapilli <math>\le 4 \times 2\text{ cm}</math>, amygdaloidal basalt <math>\le 4 \times 3\text{ cm}</math> together with sub-angular, and sub-rounded arkosic sandstone <math>\le 6 \times 4\text{ cm}</math>.







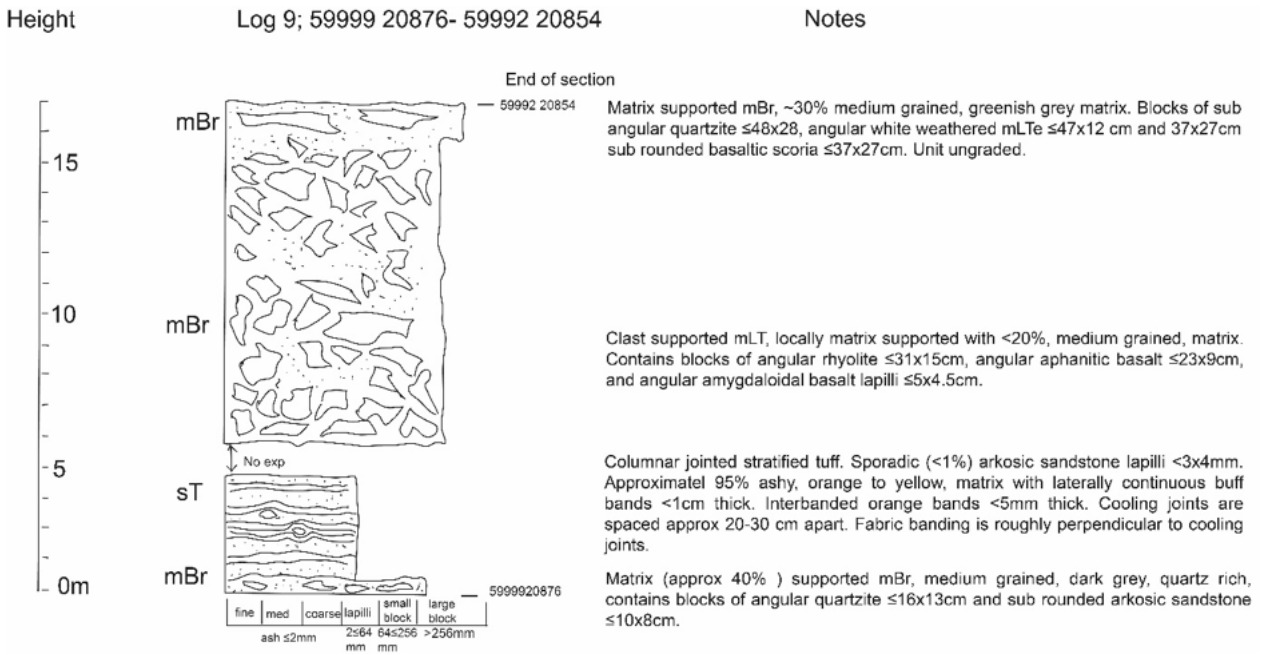






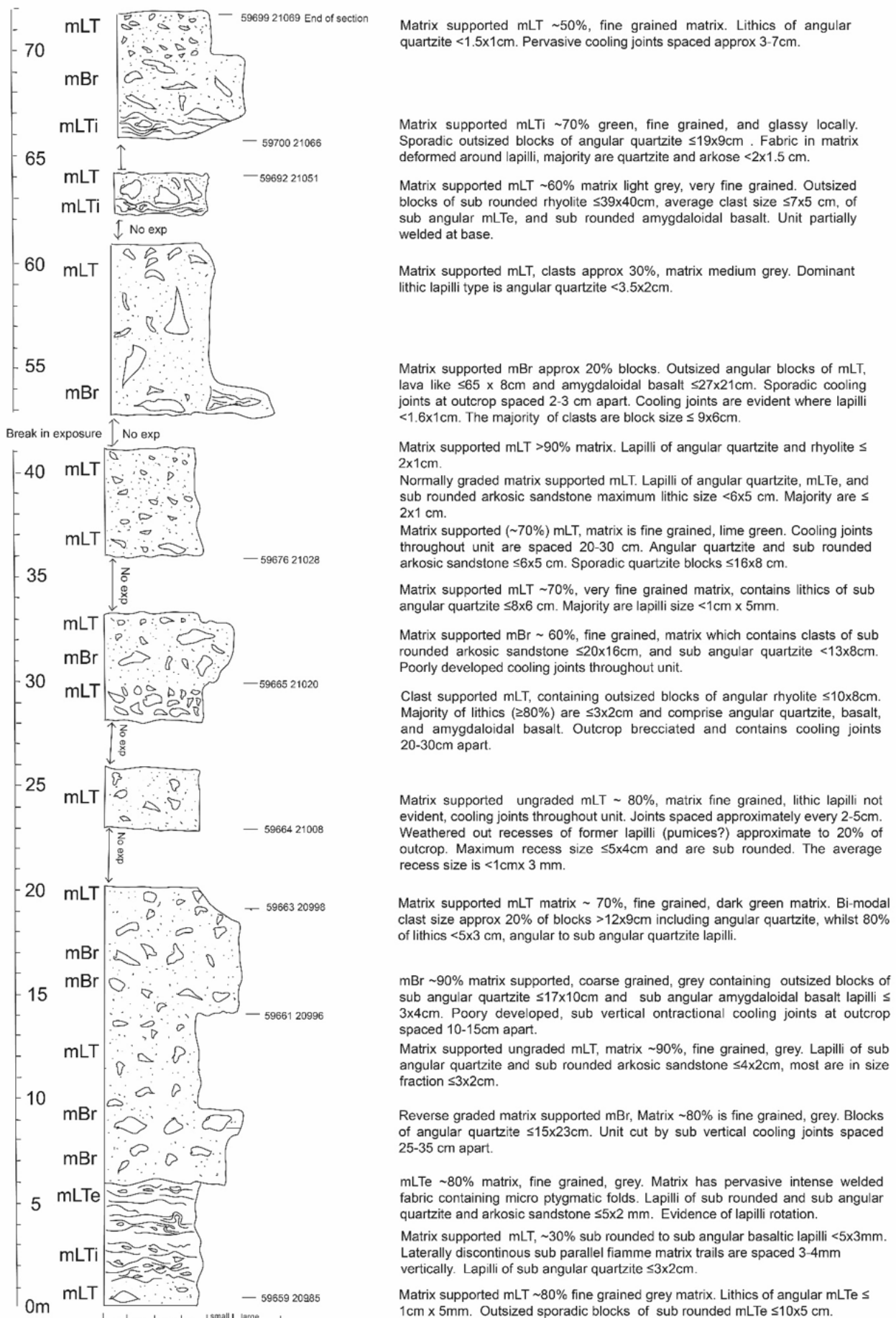
### 4 LOGS B

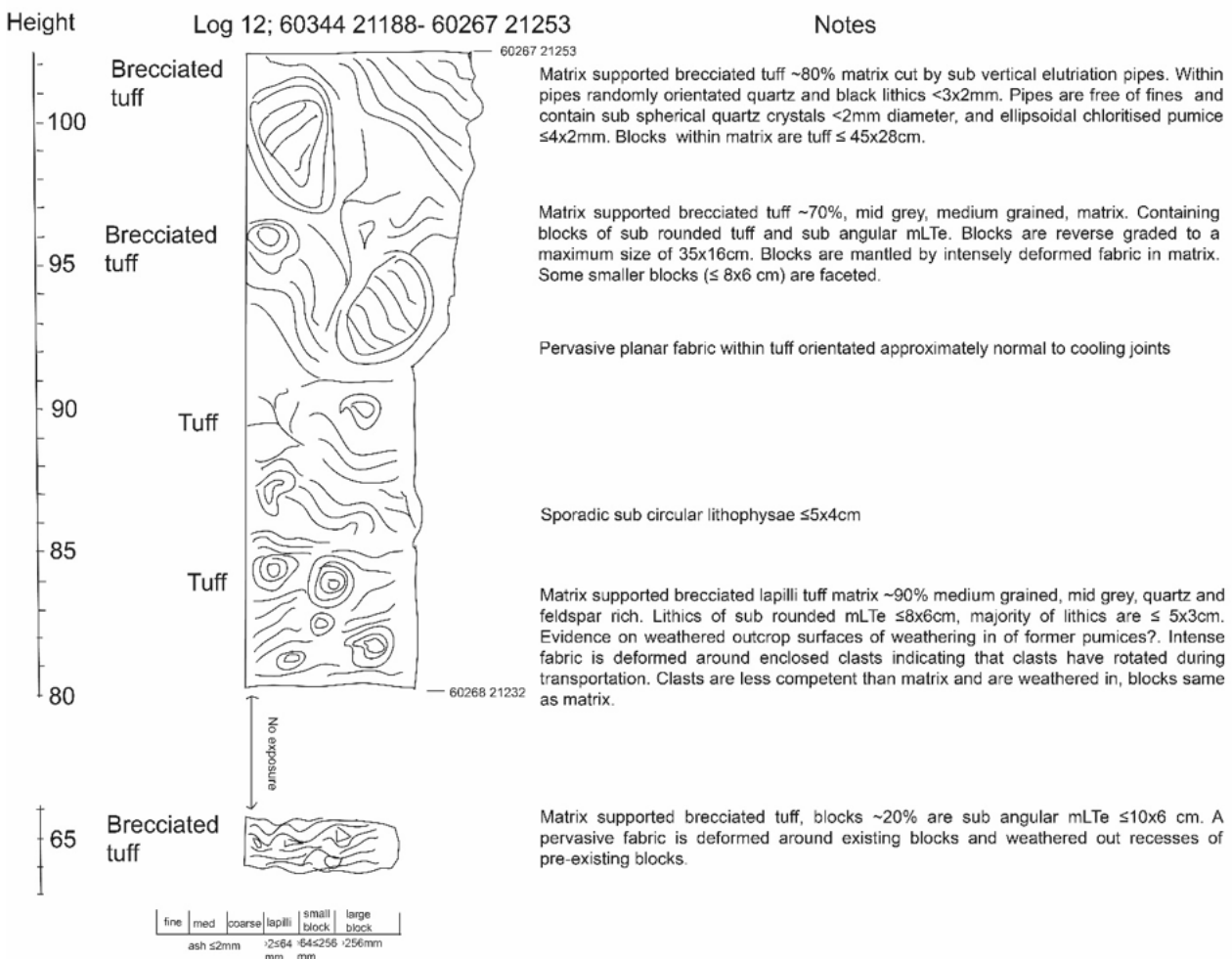
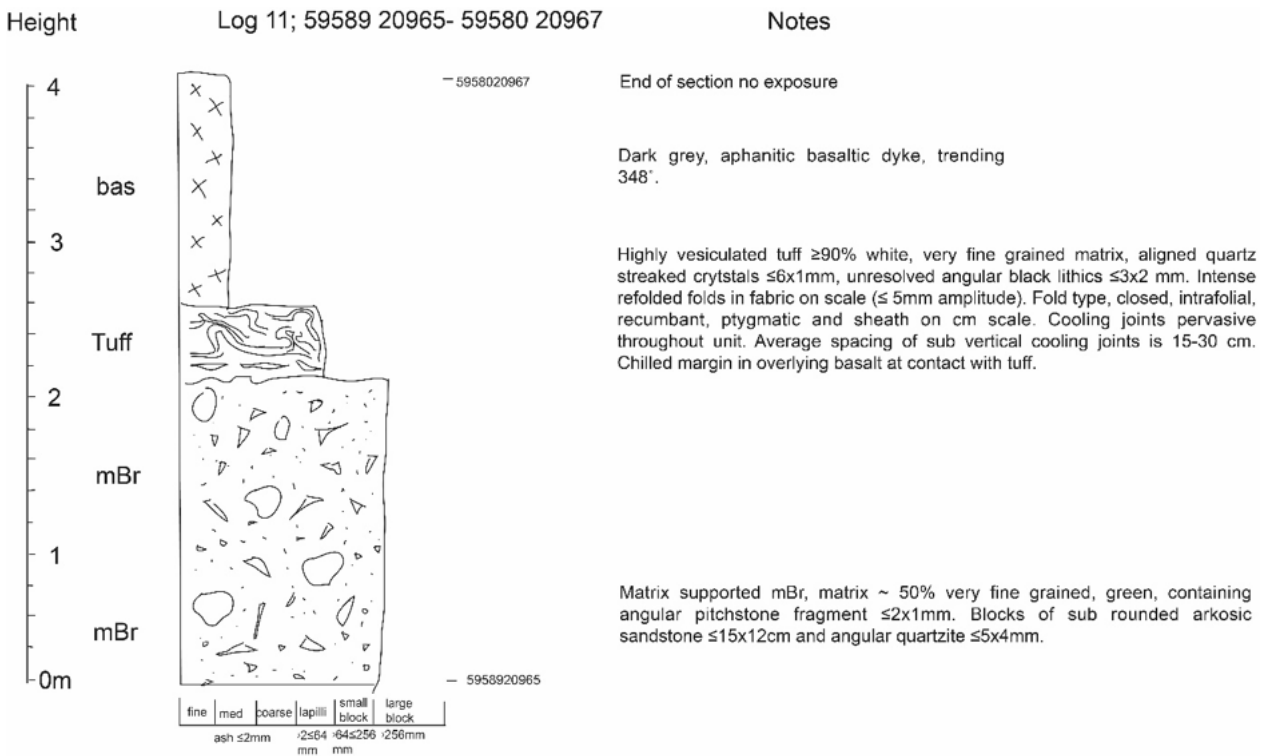
#### Kilchrist logs 9–14 and 16–18 South of Beinn na Caillich Centre

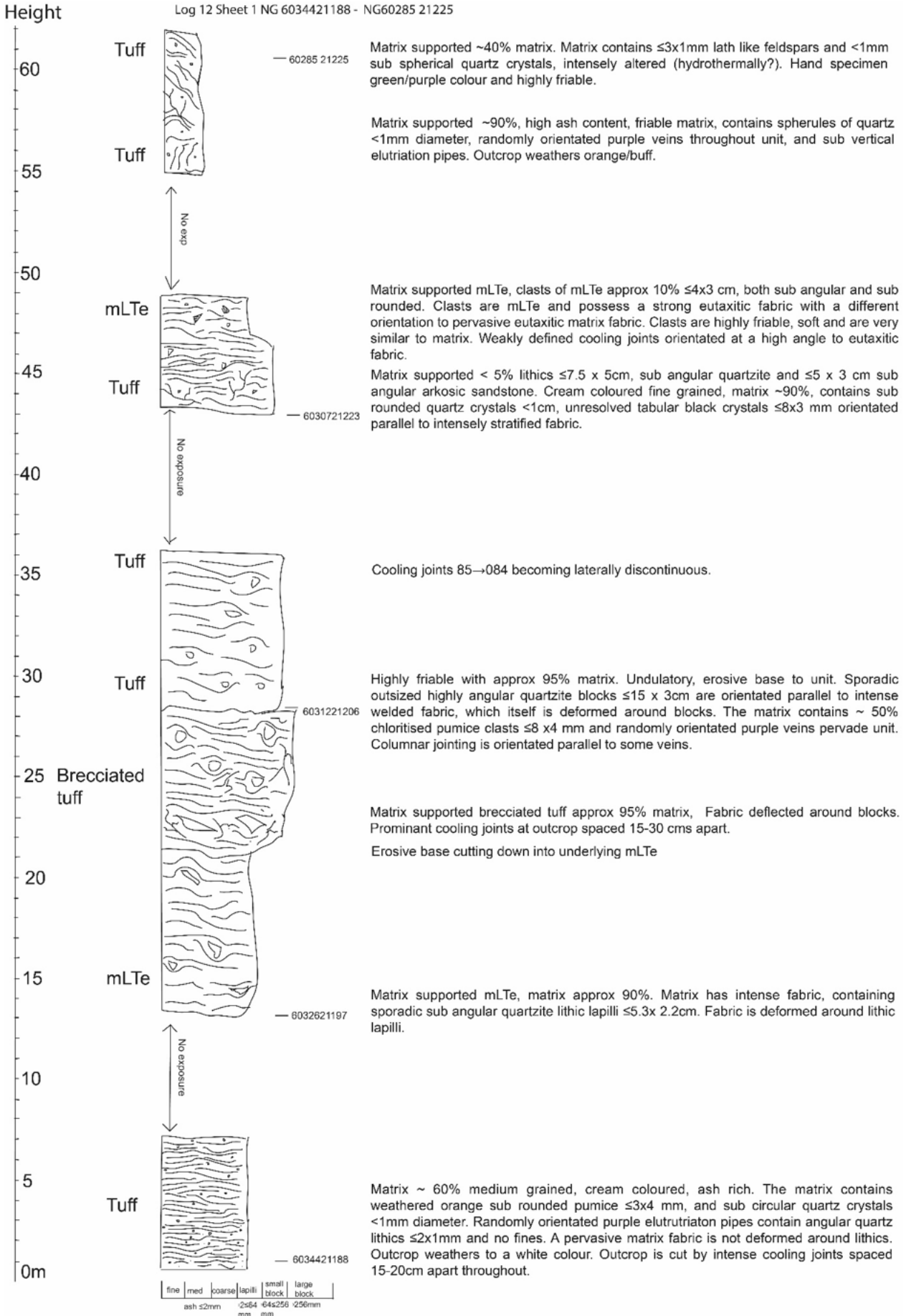


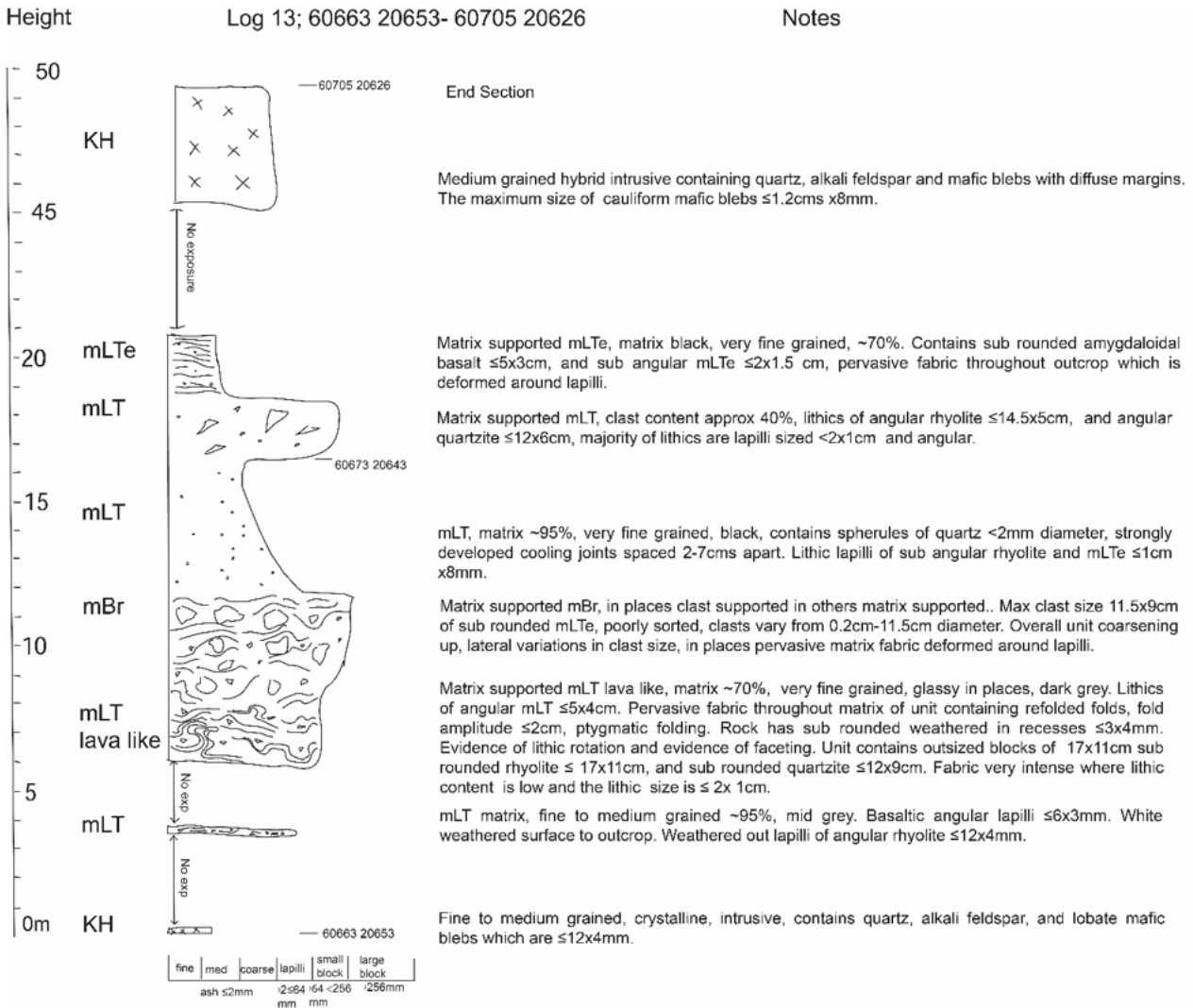
Height Log 10; 59659 20985-59669 21067

Notes





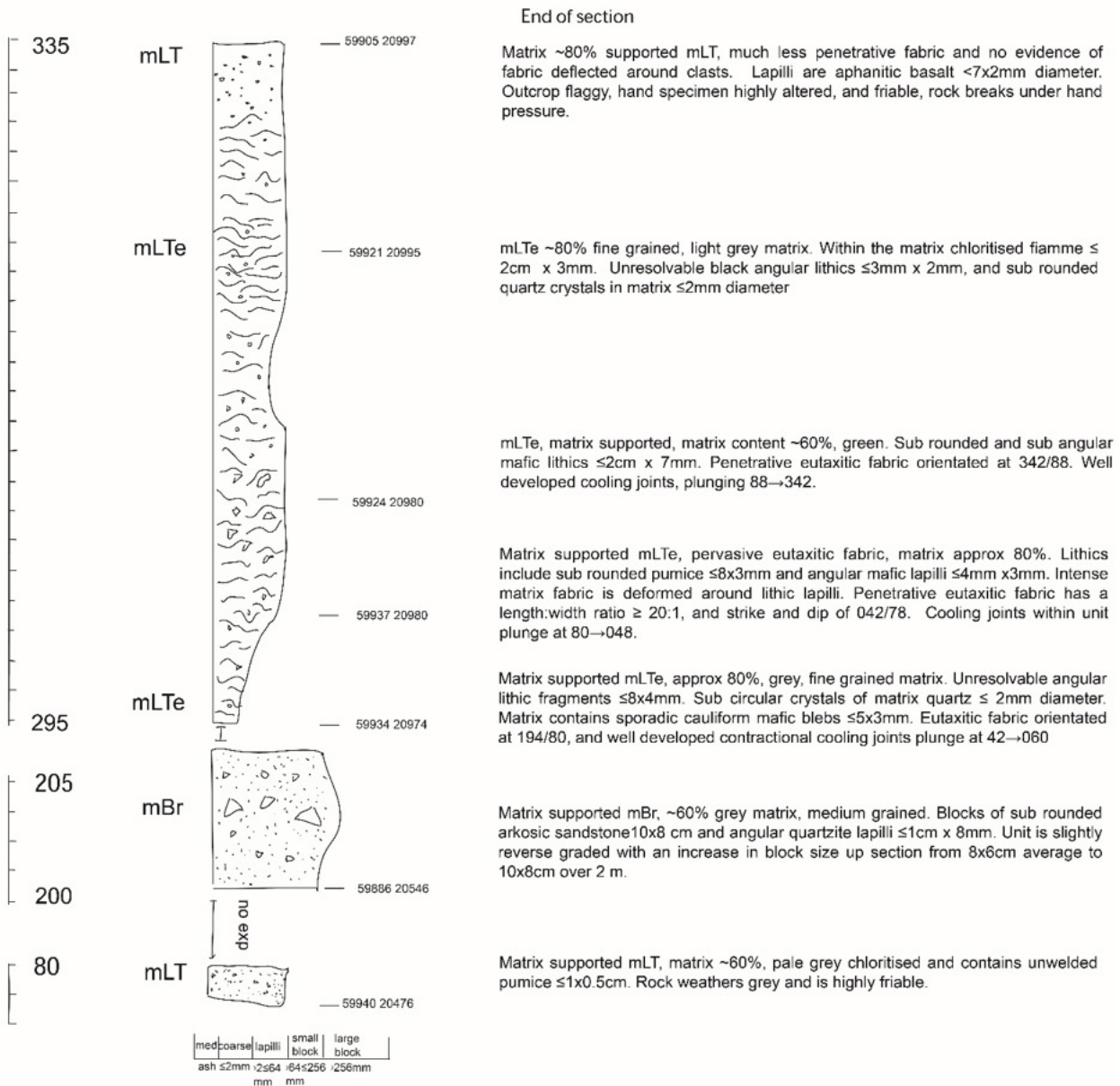


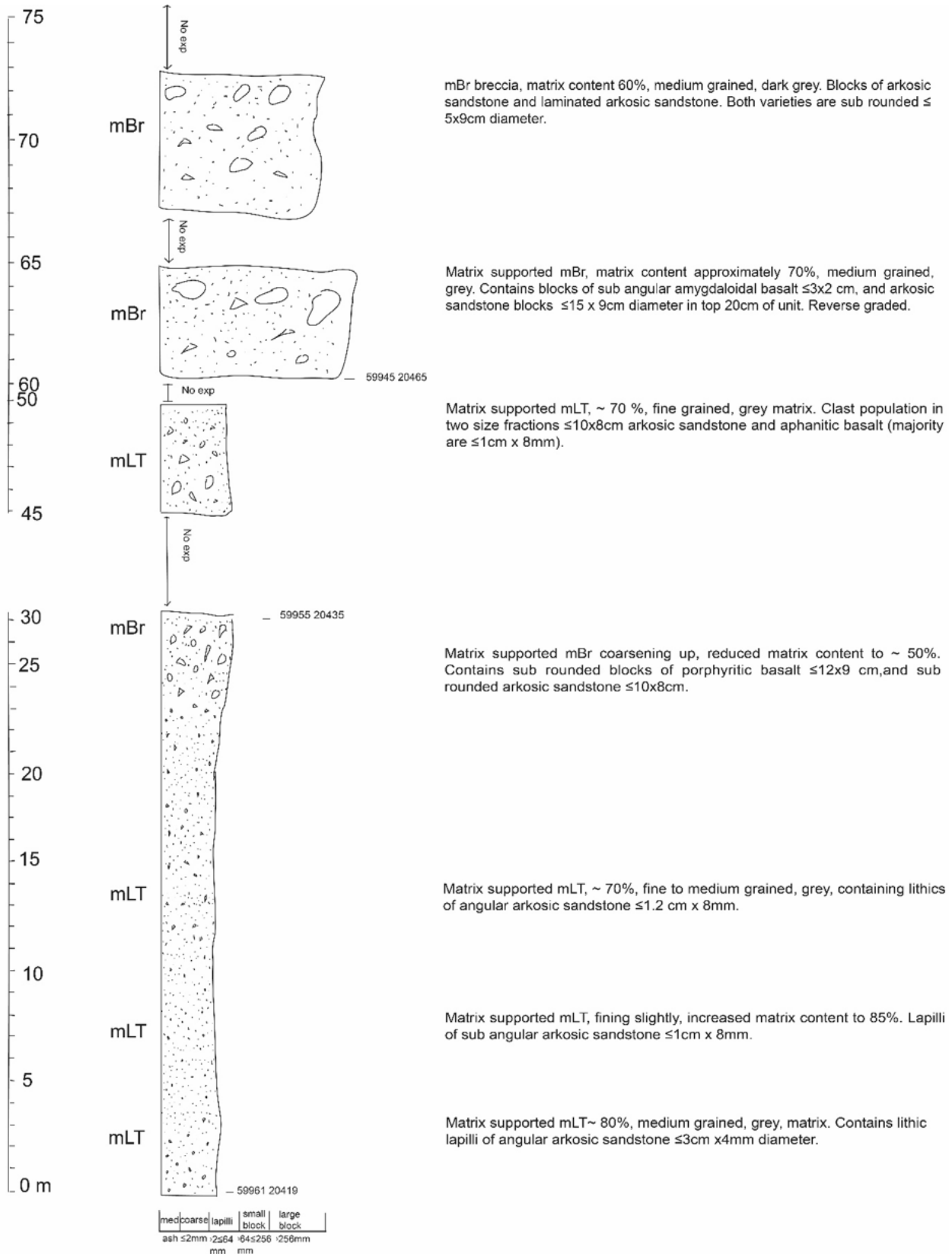


Height

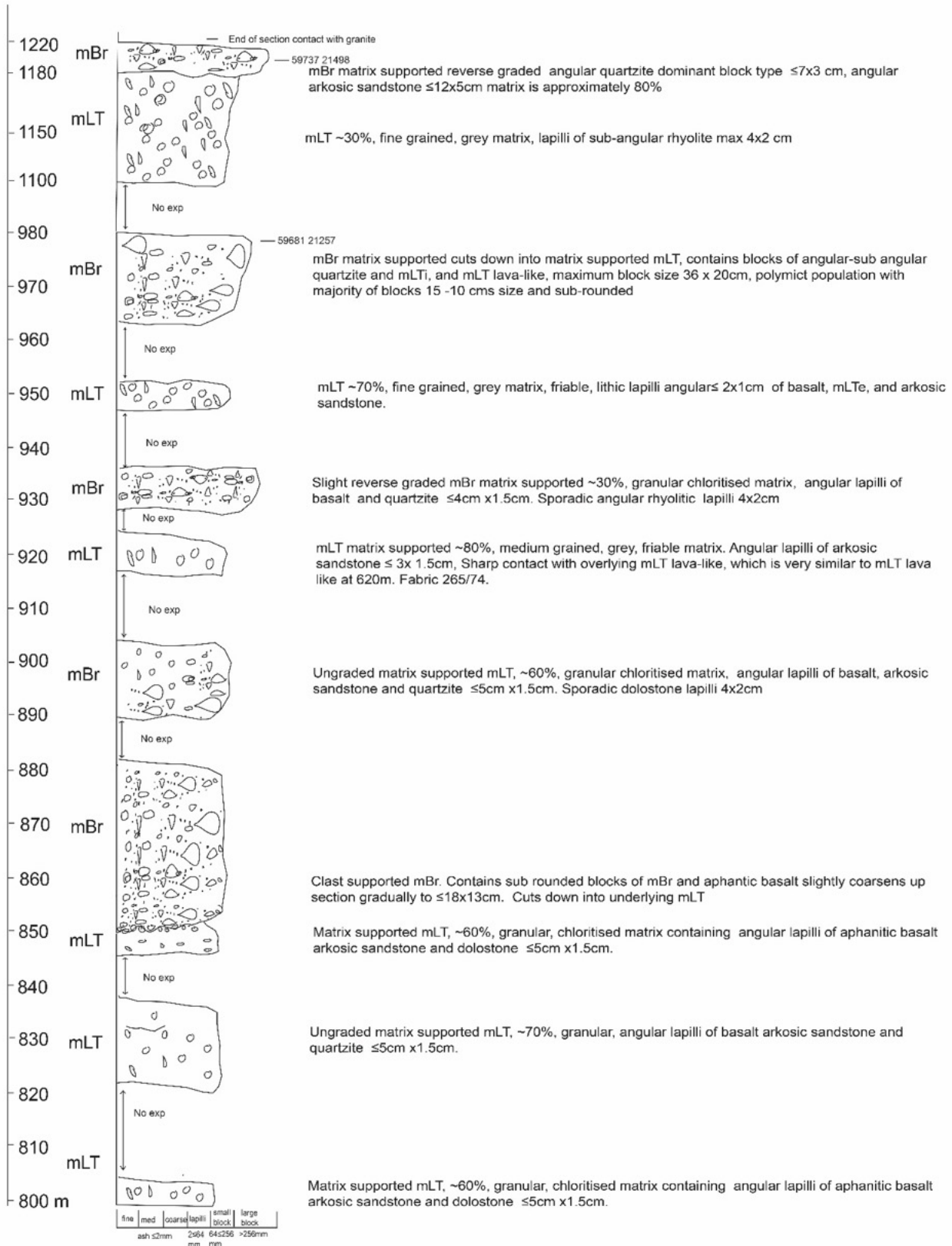
Log 14; 59961 20419 - 59905 20997, sheet 2

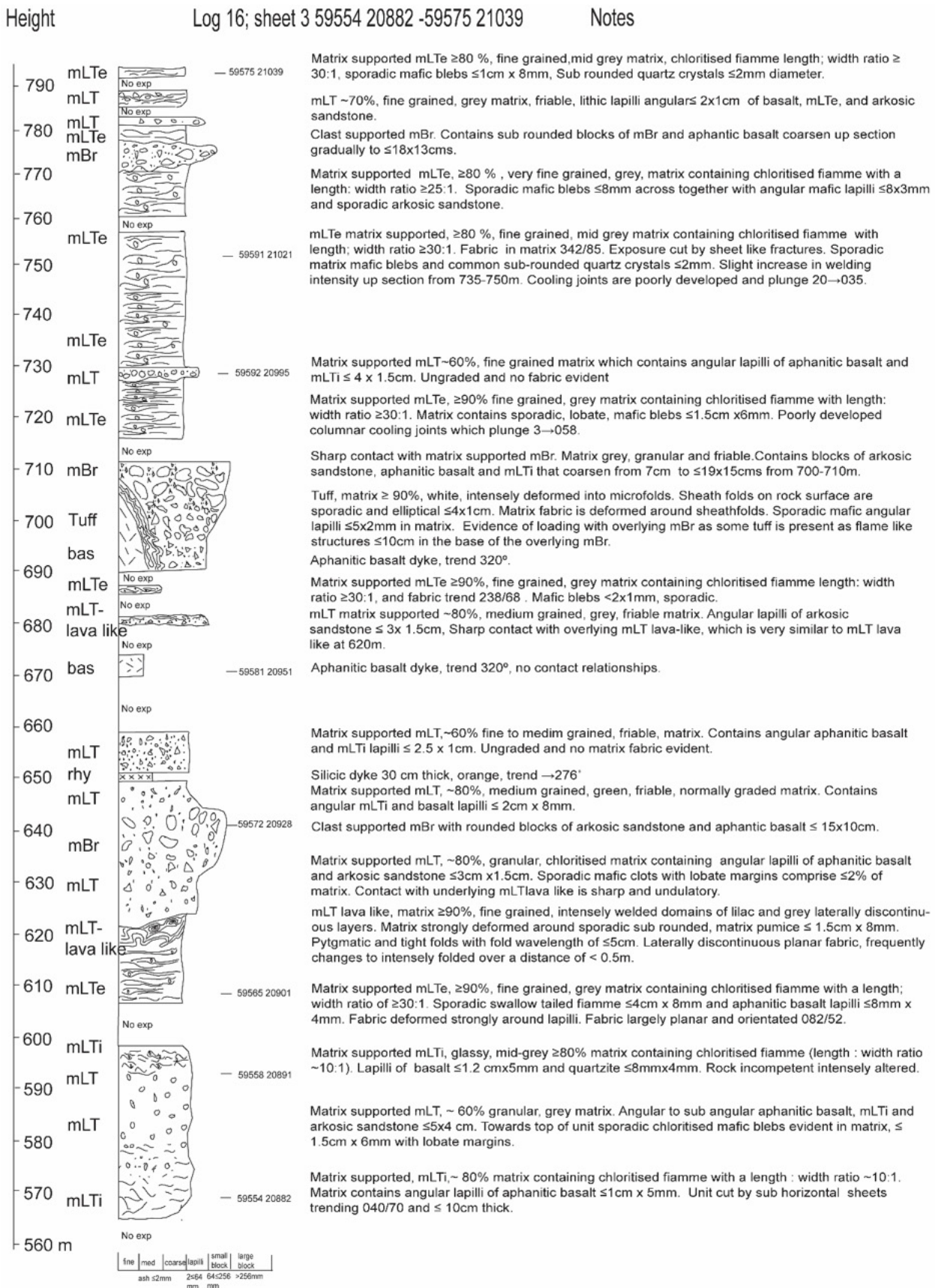
Notes

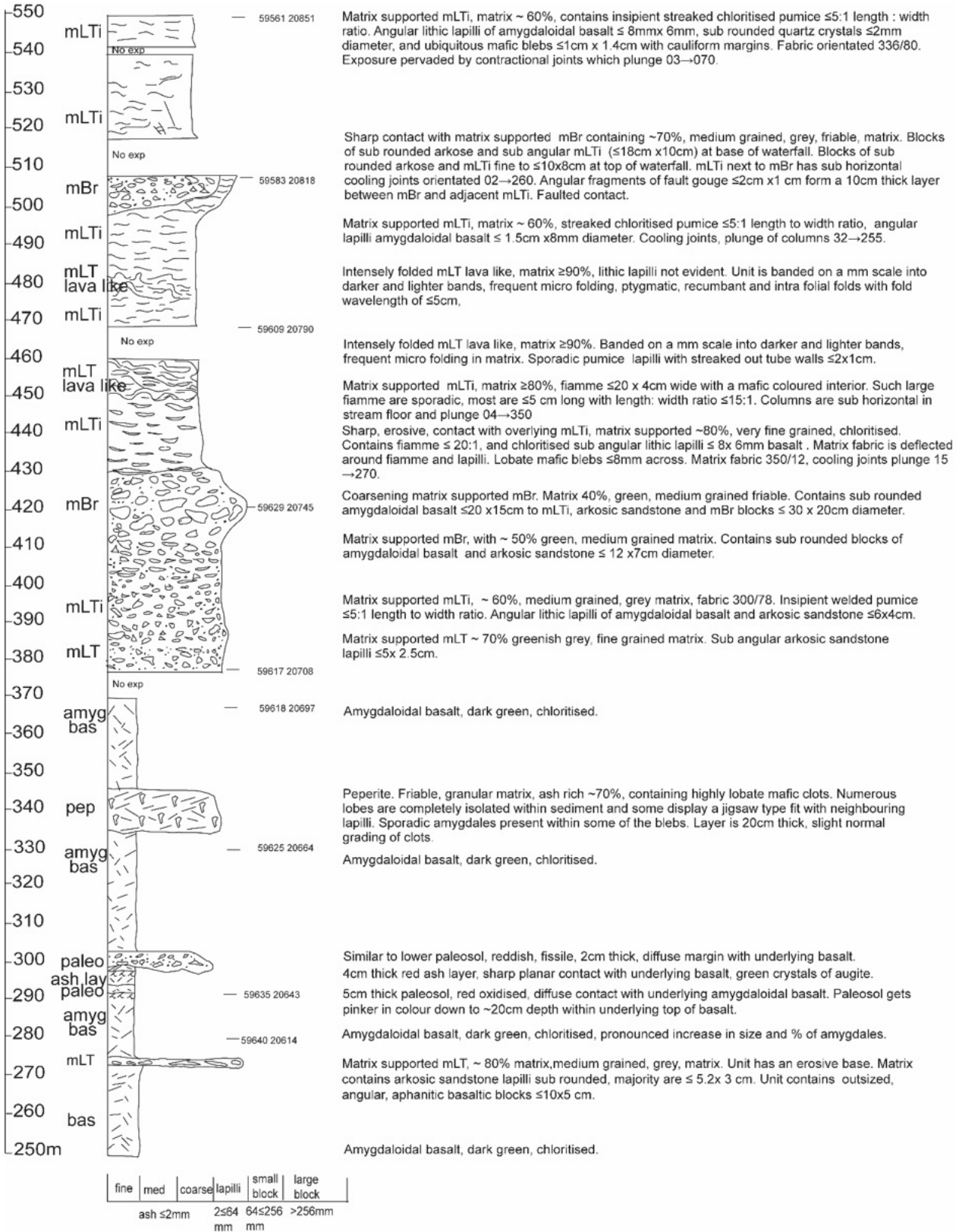


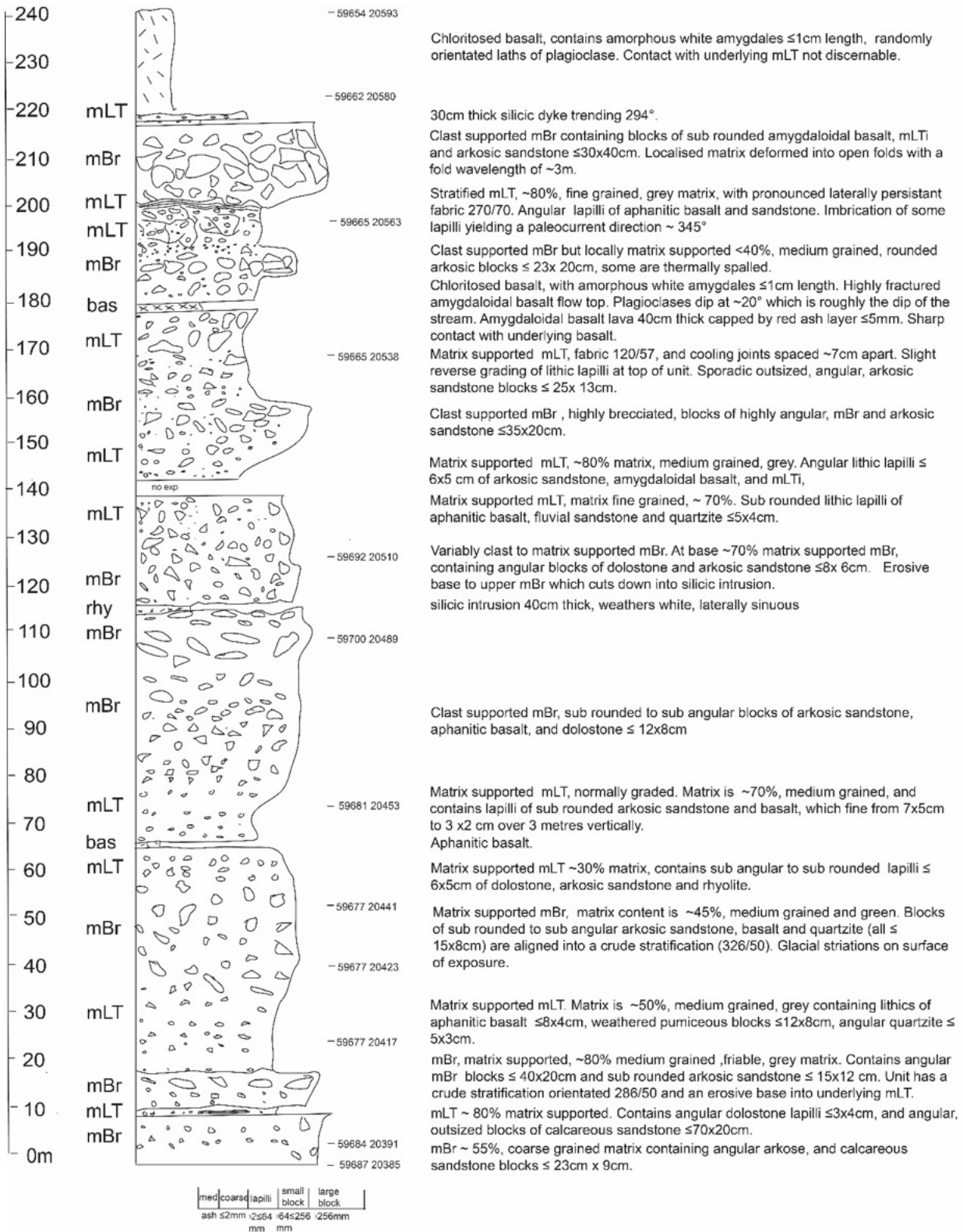


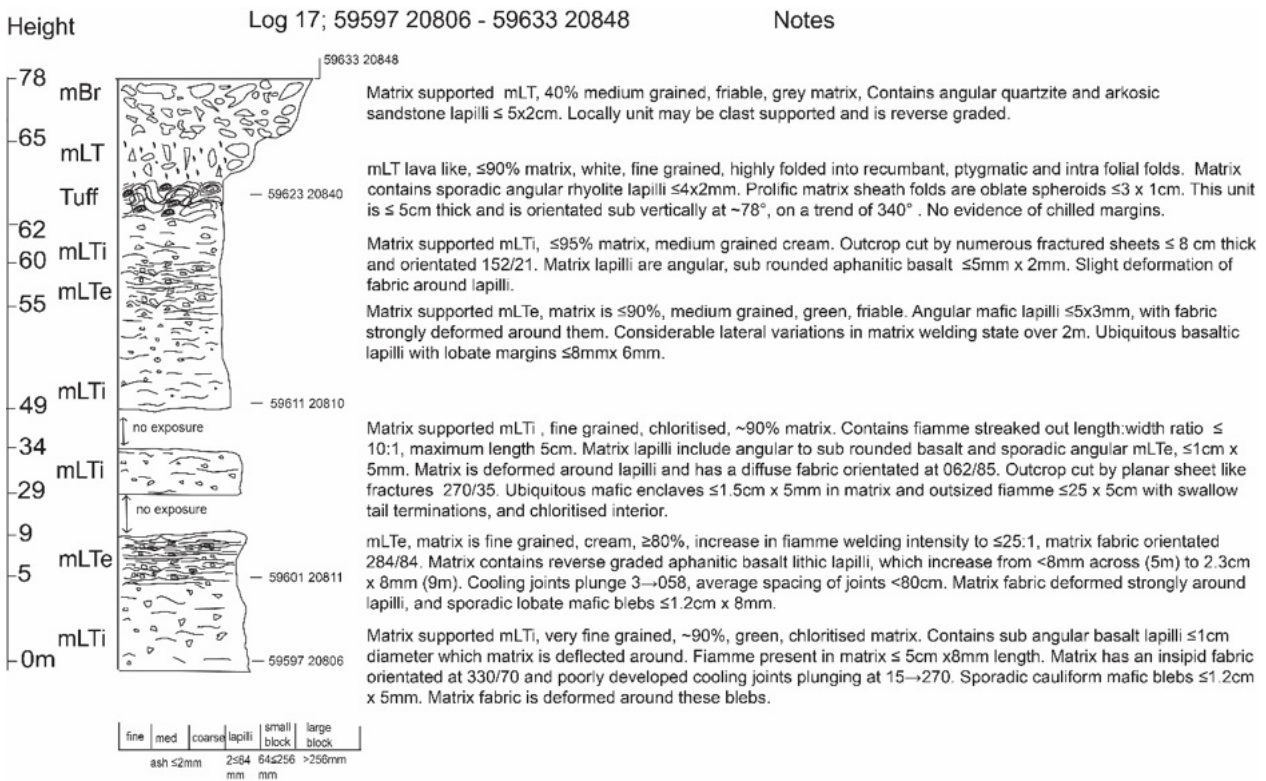
Height Log 16; sheet 4: 59575 21039- 5975021478 Notes

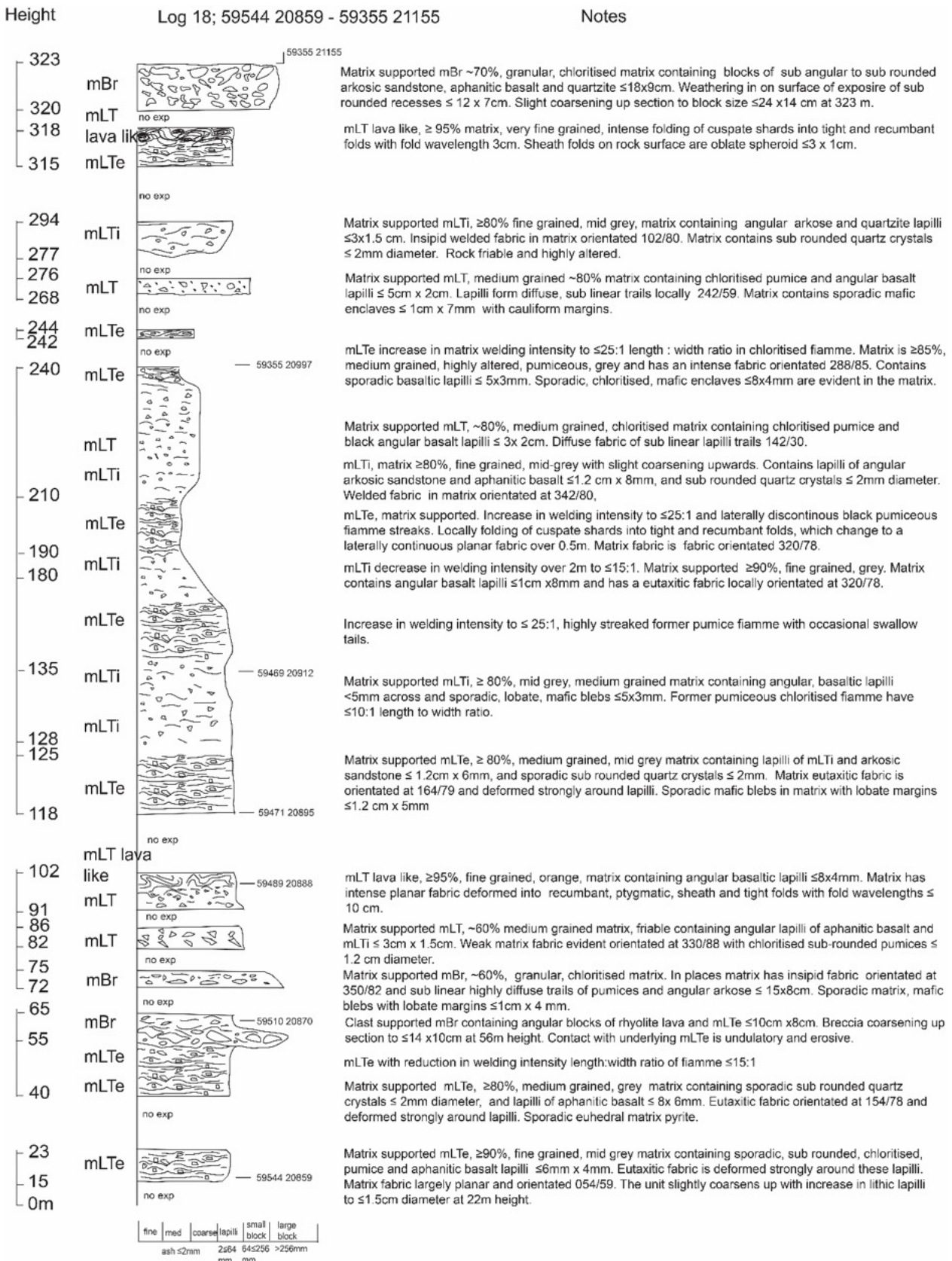












## 5 METHODOLOGY U/Pb ZIRCON DATING FOR ALLT NAN SUIDHEACHAN MLT1 (NIGL FACILITY, BRITISH GEOLOGICAL SURVEY, KEYWORTH, NOTTINGHAM, UK)

U/Pb dating of samples was conducted at the NIGL facility, British Geological Survey, Keyworth. Nottingham UK. Zircons were isolated using conventional mineral separation techniques. Prior to isotope dilution thermal ionization mass spectrometry (ID-TIMS) analyses zircons were subject to a modified version of the chemical abrasion technique (Mattinson, 2005). U-Pb ID-TIMS analyses herein utilized the EARTHTIME  $^{205}\text{Pb}$ - $^{233}\text{U}$ - $^{235}\text{U}$  (ET535) tracer solution. Measurements at the NERC Isotope Geosciences Laboratory were performed on a Thermo Triton TIMS. Pb analyses were measured in dynamic mode on a MassCom SEM detector and corrected for  $0.14 \pm 0.04$  ‰ mass fractionation. Linearity and dead-time corrections on the SEM were monitored using repeated analyses of NBS 981 and U500. Uranium was measured in static Faraday mode on  $10^{11}$  ohm resistors or for signal intensities  $<15$  mV, in dynamic mode on the SEM detector. Uranium was run as the oxide and corrected for isobaric interferences with an  $^{18}\text{O}/^{16}\text{O}$  composition of 0.00205 (IUPAC value and determined through direct measurement at NIGL). Single analysis U-Pb dates and uncertainties were calculated using the algorithms of [Schmitz and Schoene \[2007\]](#).

## 6 GEOCHEMICAL DATA

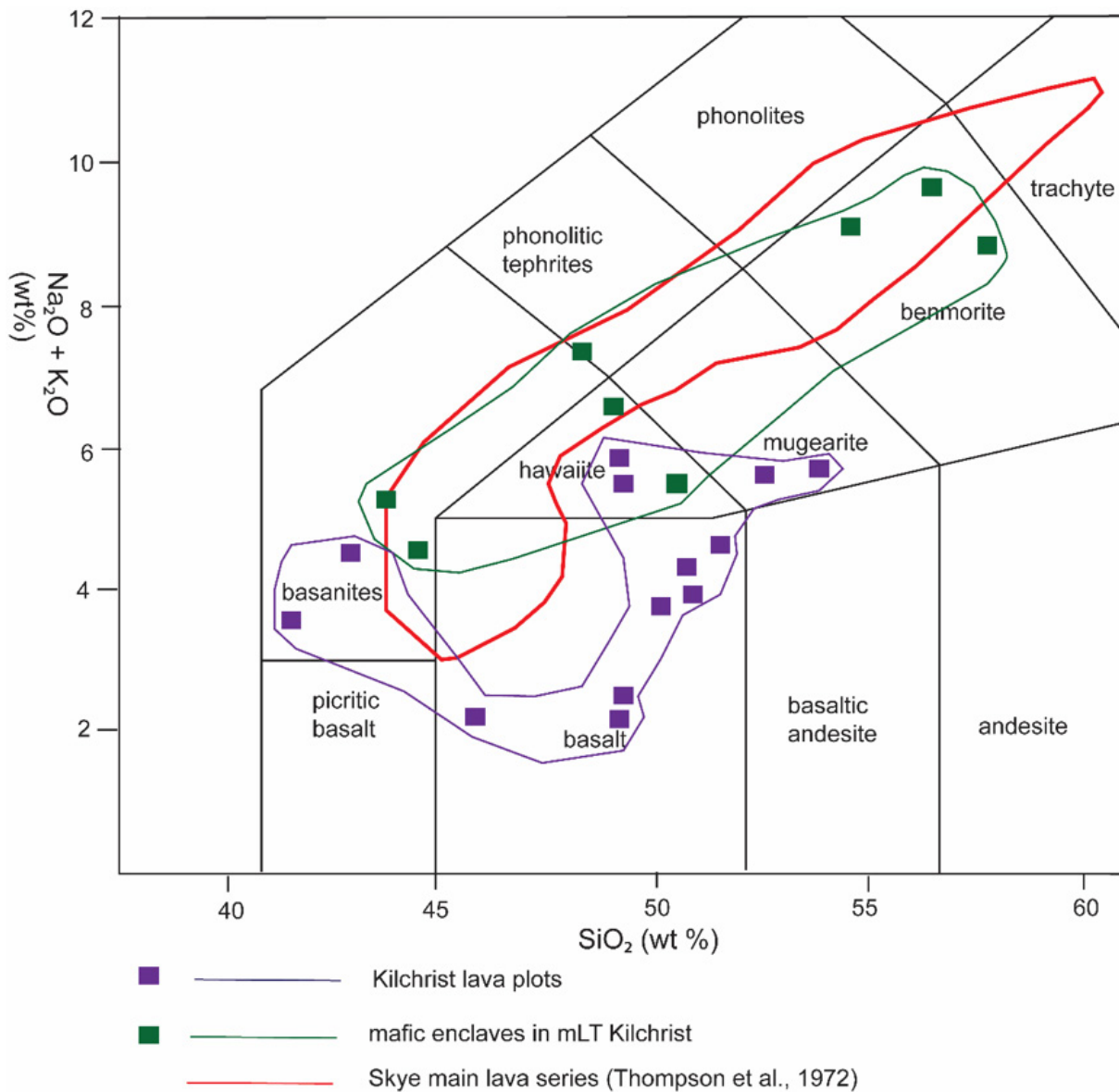


Figure S11: Total alkali versus silica diagram for Kilchrist basalts and mafic enclaves within mLT matrix. Modified from [Emeleus and Bell \[2005\]](#).

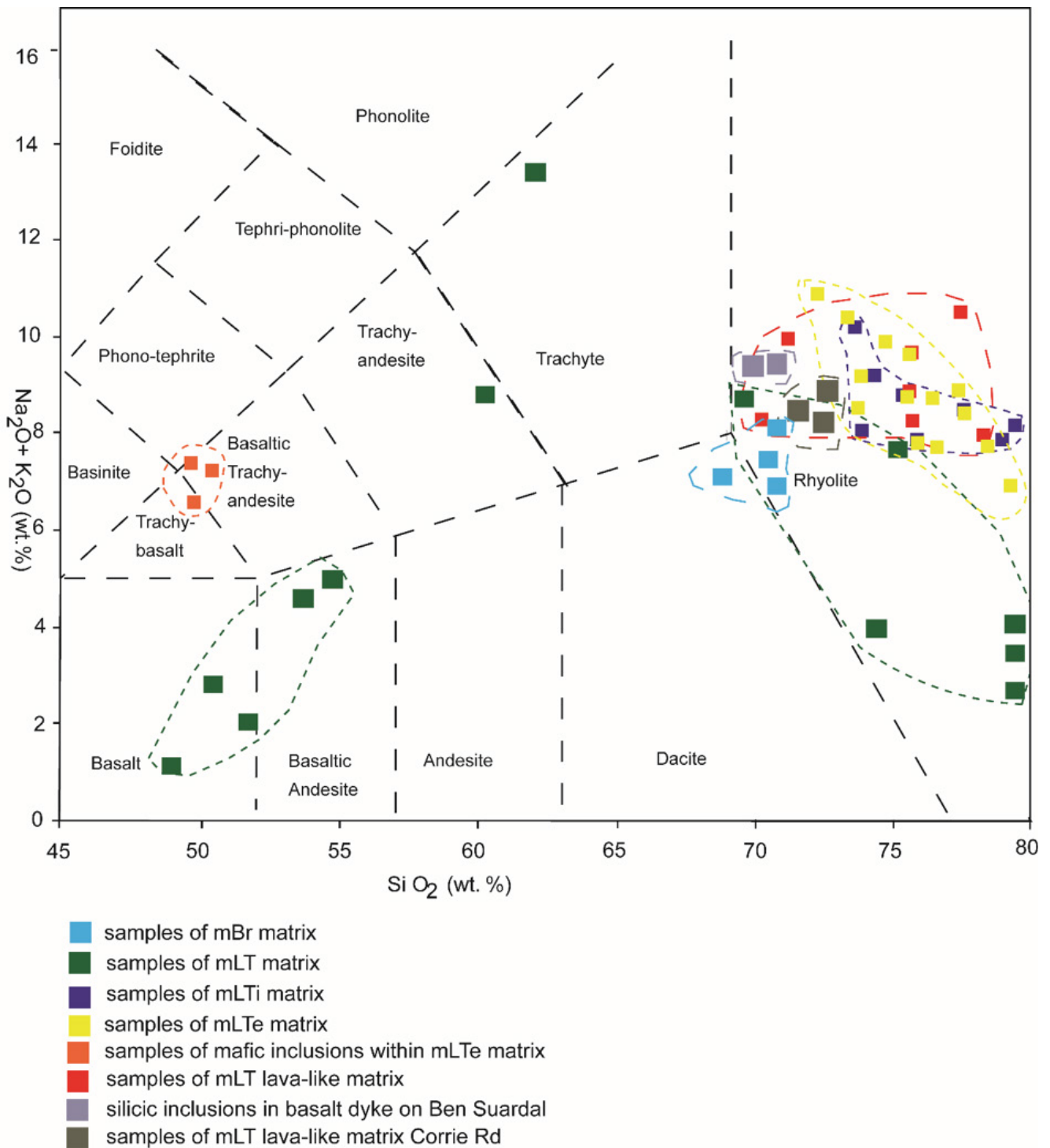


Figure S12: Compositional plots of representative mBr, mLT, mLTi, mLTe and mLT lava-like area matrix scans together with samples of mafic enclaves within mLTe matrix, and granitic xenoliths from within a basaltic dyke on Ben Suardal.

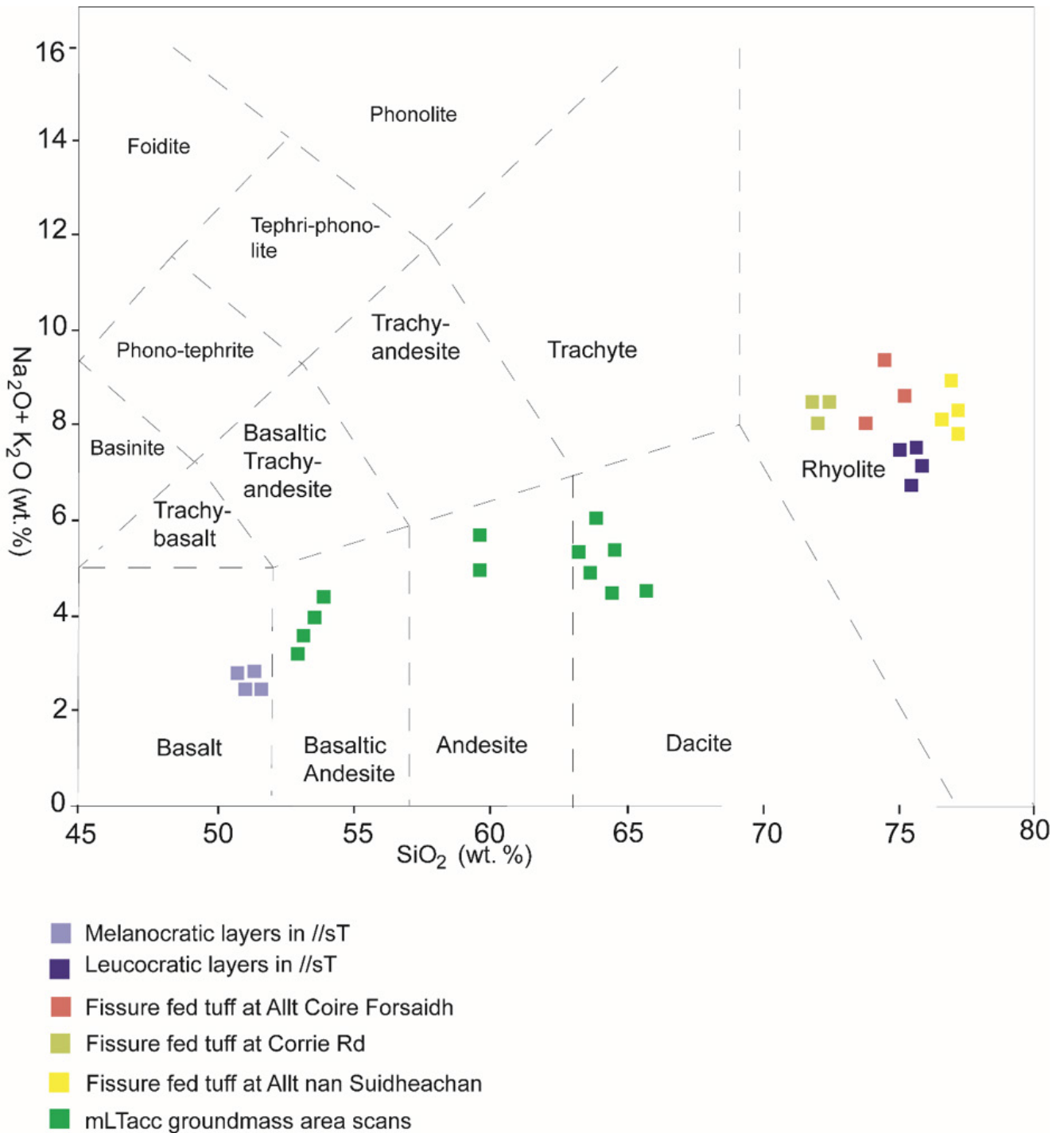


Figure S13: Compositional plots of representative fissure fed tuff, stratified tuff (//sT) and accretionary lapilli bearing massive lapilli tuff (mLTacc).

Table S4: CA-ID-TIMS data for analysed zircons.

Sample*	Compositional Parameters						
	Th/U <sup>†</sup>	<sup>206</sup> Pb* (×10 <sup>-13</sup> mol) <sup>‡</sup>	<sup>206</sup> Pb* (mol%) <sup>‡</sup>	Pb*/Pbc	Pbc (pg) <sup>‡</sup>	<sup>206</sup> Pb/ <sup>204</sup> Pb <sup>§</sup>	
SD-BS-01	z1	0.8	0.0262	90.00	2.9	0.24	180
	z2	0.85	0.0251	88.90	2.7	0.26	163
	z3	0.87	0.0436	92.50	4.1	0.29	243
	z4	0.87	0.0299	87.60	2.4	0.35	146
	z5	0.87	0.0327	90.50	3.2	0.28	190
SD-ANS-01	z1	0.99	0.1777	84.80	1.9	2.63	119
	z2	0.83	0.1758	85.30	1.9	2.52	123
	z4	0.85	0.0858	87.20	2.3	1.04	142

Sample*	Radiogenic Isotope Ratios								
	<sup>208</sup> Pb/ <sup>206</sup> Pb <sup>¶</sup>	<sup>207</sup> Pb/ <sup>206</sup> Pb <sup>¶</sup>	% err <sup>**</sup>	<sup>207</sup> Pb/ <sup>235</sup> U <sup>¶</sup>	% err <sup>**</sup>	<sup>206</sup> Pb/ <sup>238</sup> U	% err <sup>**</sup>	corr. coef.	
SD-BS-01	z1	0.261	0.04813	6	0.058388	6.4	0.008798	0.7	0.59
	z2	0.285	0.04939	6.7	0.060007	7.1	0.008812	0.7	0.6
	z3	0.282	0.04771	4.3	0.057659	4.6	0.008765	0.5	0.65
	z4	0.29	0.04897	7.5	0.05945	7.9	0.008805	0.7	0.69
	z5	0.286	0.04824	5.6	0.058331	6	0.008771	0.6	0.65
SD-ANS-01	z1	0.319	0.04758	9.2	0.057278	9.8	0.008731	0.6	0.93
	z2	0.268	0.04772	8.9	0.057368	9.5	0.008719	0.6	0.9
	z4	0.276	0.04791	7.6	0.057811	8.1	0.008751	0.6	0.88

Sample*	Isotopic Ages						
	<sup>207</sup> Pb/ <sup>206</sup> Pb <sup>⊛</sup>	± <sup>**</sup>	<sup>207</sup> Pb/ <sup>235</sup> U <sup>⊛</sup>	± <sup>**</sup>	<sup>206</sup> Pb/ <sup>238</sup> U <sup>⊛</sup>	± <sup>**</sup>	
SD-BS-01	z1	102.4	141.8	57.6	3.6	56.5	0.4
	z2	163.1	156.2	59.2	4.1	56.6	0.4
	z3	81.8	102.1	56.9	2.5	56.3	0.3
	z4	143.3	175	58.6	4.5	56.6	0.4
	z5	107.6	132.8	57.6	3.4	56.4	0.3
SD-ANS-01	z1	75.2	219.6	56.6	5.4	56.1	0.3
	z2	82.2	211.9	56.6	5.2	56	0.4
	z4	91.7	180.5	57.1	4.5	56.2	0.3

\* z1, z2 etc. are labels for fractions composed of single zircon grains or fragments; all fractions annealed and chemically abraded after [Mattinson \[2005\]](#).

<sup>†</sup> Model Th/U ratio calculated from radiogenic <sup>208</sup>Pb/<sup>206</sup>Pb ratio;

<sup>‡</sup> Pb\* and Pbc represent radiogenic and common Pb, respectively; mol % <sup>206</sup>Pb\* with respect to radiogenic, blank and initial common Pb.

<sup>§</sup> Measured ratio corrected for spike and fractionation only. Daly analyses, based on analysis of NBS-981 and NBS-982.

<sup>¶</sup> Corrected for fractionation, spike, and common Pb; up to 1 pg of common Pb was assumed to be procedural blank: <sup>206</sup>Pb/<sup>204</sup>Pb = 18.60 ± 0.80 %; <sup>207</sup>Pb/<sup>204</sup>Pb = 15.69 ± 0.32 %; <sup>208</sup>Pb/<sup>204</sup>Pb = 38.51 ± 0.74 % (all uncertainties 1-sigma). Excess over blank was assigned to initial common Pb.

\*\* Errors are 2-sigma, propagated using the algorithms of [Schmitz and Schoene \[2007\]](#).

⊛ Calculations are based on the decay constants of [Jaffey et al. \[1971\]](#).

Table S5: CO<sub>2</sub> flux calculations resulting from decarbonation reactions and direct melting of dolostone country rock.

Aerial extent of dolostone outcrop (pre-volcanic episode) is ~31 km <sup>2</sup> (Figure 2 main text)
Cumulative thickness of Strath Suardal Formation = 530 m
Ben Suardal Member (BSIL) ~170 m thick
Dark grey dolostone (SSIL) ~85 m thick. This unit is recorded as having up to three repetitions [BGS 2005]
Mid- dark grey dolostone Kilchrist Member (KiLI) ~35 m thick
Pale grey, well bedded, Lonachan Member (LonL) 140 m thick
Total thickness estimated to include 3× SSIL repetitions.
To convert volume of limestone (proxy for dolostone) in to mass (kg)
1 m <sup>3</sup> of limestone = 2711 kg
1000 m <sup>3</sup> (km <sup>3</sup> ) = 2711000 kg
Percentage estimates volume of dolostone assimilated during KVF episode and resultant CO <sub>2</sub> mass flux
30 % consumption: 31 000 000 m <sup>2</sup> × 159 m = 4.9 × 10 <sup>9</sup> m <sup>3</sup> = 4.9 × 10 <sup>6</sup> km <sup>3</sup>
50 % consumption: 31 000 000 m <sup>2</sup> × 265 m = 8.2 × 10 <sup>9</sup> m <sup>3</sup> = 8.2 × 10 <sup>6</sup> km <sup>3</sup>
80 % consumption: 31 000 000 m <sup>2</sup> × 424 m = 1.31 × 10 <sup>10</sup> m <sup>3</sup> = 1.33 × 10 <sup>7</sup> km <sup>3</sup>
Converted volume of dolostone to total mass
30 %: 4.9 × 10 <sup>6</sup> km <sup>3</sup> × 2711000 = 1.34 × 10 <sup>13</sup> kg
50 %: 8.2 × 10 <sup>6</sup> km <sup>3</sup> × 2711000 = 2.23 × 10 <sup>13</sup> kg
80 %: 1.33 × 10 <sup>7</sup> km <sup>3</sup> × 2711000 = 3.56 × 10 <sup>13</sup> kg
Range of calculated CO <sub>2</sub> flux measured in Giga tons (Gt) for different percentages of assimilated dolostone consumed during KVF producing eruptions. 1 kg of limestone produces 239 g CO <sub>2</sub> [Ganino et al. 2013]
30 %: 1.34 × 10 <sup>13</sup> kg × 0.239 = 3.19 × 10 <sup>12</sup> kg of CO <sub>2</sub> = (3.19 × 10 <sup>9</sup> mt) = 3.9 Gt
50 %: 2.23 × 10 <sup>13</sup> kg × 0.239 = 5.32 × 10 <sup>12</sup> kg of CO <sub>2</sub> = (5.32 × 10 <sup>9</sup> mt) = 5.32 Gt
80 %: 3.56 × 10 <sup>13</sup> kg × 0.239 = 8.52 × 10 <sup>12</sup> kg of CO <sub>2</sub> = (8.52 × 10 <sup>9</sup> mt) = 8.52 Gt

Table S6: CH<sub>4</sub> flux calculations resulting from contact metamorphism and dehydration of organic rich Lower Jurassic Shale

50 % of total thickness of Pabay Shales and Broadford Beds ~200 m Total area of above which surrounds composite sills and other intrusions = 18 km <sup>2</sup> (18 000 000 m <sup>2</sup> ), Total volume of shale = 18000000 × 200 = 3.6 × 10 <sup>9</sup> m <sup>3</sup> (Figure 2 main text)
Total volume of shale = m <sup>3</sup>
(100 %) 200 × 18000000 = 7.2 × 10 <sup>9</sup> m <sup>3</sup>
(80 %) 160 × 18000000 = 5.8 × 10 <sup>9</sup> m <sup>3</sup>
(50 %) 80 × 18000000 = 3.6 × 10 <sup>9</sup> m <sup>3</sup>
(30 %) 60 × 18000000 = 2.16 × 10 <sup>9</sup> m <sup>3</sup>
1 m <sup>3</sup> of shale = 2675 kg
1000 m <sup>3</sup> (km <sup>3</sup> ) = 2675000 kg
100 kg CH <sub>4</sub> = per kg m <sup>-3</sup>
Total mass of shale kg
(100 %) = (7 × 10 <sup>9</sup> m <sup>3</sup> ) × 2675000 = 1.93 × 10 <sup>16</sup> kg
(80 %) = (5.6 × 10 <sup>9</sup> m <sup>3</sup> ) × 2675000 = 1.54 × 10 <sup>16</sup> kg
(50 %) = (3.5 × 10 <sup>9</sup> m <sup>3</sup> ) × 2675000 = 9.33 × 10 <sup>15</sup> kg
(30 %) = (2.1 × 10 <sup>9</sup> m <sup>3</sup> ) × 2675000 = 5.78 × 10 <sup>15</sup> kg
130 CH <sub>4</sub> (kg) driven off per kg m <sup>-3</sup> .
(100 %) = (1.93 × 10 <sup>16</sup> kg) / 130 = 1.48 × 10 <sup>14</sup> kg
(80 %) = (1.54 × 10 <sup>16</sup> kg) / 130 = 1.19 × 10 <sup>14</sup> kg
(50 %) = (9.33 × 10 <sup>15</sup> kg) / 130 = 7.41 × 10 <sup>13</sup> kg
(30 %) = (5.78 × 10 <sup>15</sup> kg) / 130 = 4.44 × 10 <sup>13</sup> kg
As Gt (1Kg = 1.0 × 10 <sup>-12</sup> Gt) – CH <sub>4</sub> driven off one side of intrusive sheet following contact metamorphism and dehydration
(100 %) = 1.48 × 10 <sup>14</sup> kg = 148 Gt
(80 %) = 1.19 × 10 <sup>14</sup> kg = 119 Gt
(50 %) = 9.32 × 10 <sup>13</sup> kg = 74.1 Gt
(30 %) = 5.62 × 10 <sup>13</sup> kg = 44.4 Gt
CH <sub>4</sub> driven off both sides of intrusive sheet following contact metamorphism and dehydration
(100 %) = 296 Gt
(80 %) = 237 Gt
(50 %) = 148 Gt
(30 %) = 88.9 Gt

## 7 ADDITIONAL TEXT ON PALEOCENE GEOLOGY OF SKYE

The Cuillin Central Complex has been sub-divided, in age of emplacement from oldest to youngest, into the Cuillin Centre, the Srath na Creitheach Centre, the Western Red Hills (WRH) Centre, and the Eastern Red Hills (ERH) Centre [Emeleus and Bell 2005]. The Cuillin Centre is typically gabbroic, and comprises plutonic bodies, with minor intrusions including arcuate 'cone-sheets'. Pegmatitic veins in Cuillin Centre gabbro have been dated at  $58.91 \pm 0.08$  Ma [Hamilton et al. 1998]. The Coire Uaigneach Granite [ $59.3 \pm 0.7$  Ma, Dickin 1981], crops out adjacent to the SE Cullin Centre margin. The Srath na Creitheach Centre comprises granitic intrusions and volcanoclastic rocks. The Western Red Hills Centre typically comprises granitic plutons and mixed magma intrusions, with the Loch Ainort Granite having been dated at  $58.58 \pm 0.13$  Ma [Chambers and Pringle 2001]. The Eastern Red Hills Centre typically comprises granitic intrusions, although gabbroic units are also present [Bell 1966; 1976; Emeleus and Bell 2005]. The Eastern Red Hills Centre has been sub-divided into two suites: 1) the older Outer Granite comprising granite intrusions forming the hills of Glas Beinn Mhor, Beinn na Cro, Beinn an Dubhaich, and east of Beinn na Caillich to Creag Strollamus, together with the Beinn na Cro and Broadford gabbros and; 2) the younger Inner Granite comprising the granite intrusions forming Beinn na Caillich, Beinn Dearg Mhor and Beinn Dearg Bheag (Figure 2). The Beinn an Dubhaich Granite has been dated at  $55.89 \pm 0.15$  Ma [M. A. Hamilton, in Emeleus and Bell 2005], whilst a pitchstone dyke cross-cutting the Beinn na Caillich Granite has been dated at  $55.7 \pm 0.1$  Ma [M. A. Hamilton, in Emeleus and Bell 2005]. Emplacement of the Beinn an Dubhaich Granite formed a well-developed contact aureole in surrounding Cambro-Ordovician country rock [Holness 1992].

### COPYRIGHT NOTICE

© The Author(s) 2022. This article is distributed under the terms of the [Creative Commons Attribution 4.0 International License](https://creativecommons.org/licenses/by/4.0/), which permits unrestricted use, distribution, and reproduction in any medium, provided you give appropriate credit to the original author(s) and the source, provide a link to the Creative Commons license, and indicate if changes were made.

### REFERENCES

- Andrews, G. D. M. and M. J. Branney (2011). "Emplacement and rheomorphic deformation of a large, lava-like rhyolitic ignimbrite: Grey's Landing, southern Idaho". *Geological Society of America Bulletin* 123(3–4), pages 725–743. ISSN: 1943-2674. DOI: [10.1130/b30167.1](https://doi.org/10.1130/b30167.1).
- Bell, B. R., I. T. Williamson, F. E. Head, and D. W. Jolley (1996). "On the origin of a reddened interflow bed within the Palaeocene lava field of north Skye". *Scottish Journal of Geology* 32(2), pages 117–126. DOI: [10.1144/sjg32020117](https://doi.org/10.1144/sjg32020117).
- Bell, B. R. and J. W. Harris (1986). *An excursion guide to the geology of the Isle of Skye*. Geological Society of Glasgow. ISBN: 0902892088.
- Bell, B. R. and I. T. Williamson (1994). "Picritic basalts from the Palaeocene lava field of west-central Skye, Scotland: evidence for parental magma compositions". *Mineralogical Magazine* 58(392), pages 347–356. DOI: [10.1180/minmag.1994.058.392.01](https://doi.org/10.1180/minmag.1994.058.392.01).
- Bell, J. D. (1966). "XIII.—Granites and Associated Rocks of the Eastern Part of the Western Redhills Complex, Isle of Skye". *Transactions of the Royal Society of Edinburgh* 66(13), pages 307–343. ISSN: 2053-5945. DOI: [10.1017/s0080456800023632](https://doi.org/10.1017/s0080456800023632).
- (1976). "The Tertiary intrusive complex on the Isle of Skye". *Proceedings of the Geologists' Association* 87(3), pages 247–271. DOI: [10.1016/s0016-7878\(76\)80001-6](https://doi.org/10.1016/s0016-7878(76)80001-6).
- Bierwith, P. N. (1982). "Experimental welding of volcanic ash". Master's thesis. Monash University.
- Branney, M. J. and P. Kokelaar (1992). "A reappraisal of ignimbrite emplacement: progressive aggradation and changes from particulate to non-particulate flow during emplacement of high-grade ignimbrite". *Bulletin of Volcanology* 54(6), pages 504–520. ISSN: 1432-0819. DOI: [10.1007/bf00301396](https://doi.org/10.1007/bf00301396).
- (2002). "Pyroclastic Density Currents and the Sedimentation of Ignimbrites". 27(1). DOI: [10.1144/gsl.mem.2003.027](https://doi.org/10.1144/gsl.mem.2003.027).
- Breitkreuz, C. (2013). "Spherulites and lithophysae—200 years of investigation on high-temperature crystallization domains in silica-rich volcanic rocks". *Bulletin of Volcanology* 75(4). DOI: [10.1007/s00445-013-0705-6](https://doi.org/10.1007/s00445-013-0705-6).
- British Geological Survey (BGS) (2005). *Skye Central Complex, Scotland, Bedrock*. 1:25000 British Geology Series. Keyworth, Nottingham, British Geological Survey.
- Brown, D. J. and B. R. Bell (2007). "How do you grade peperites?" *Journal of Volcanology and Geothermal Research* 159(4), pages 409–420. ISSN: 0377-0273. DOI: [10.1016/j.jvolgeores.2006.08.008](https://doi.org/10.1016/j.jvolgeores.2006.08.008).
- (2013). "The emplacement of a large, chemically zoned, rheomorphic, lava-like ignimbrite: the Sgurr of Eigg Pitchstone, NW Scotland". *Journal of the Geological Society* 170(5), pages 753–767. ISSN: 2041-479X. DOI: [10.1144/jgs2012-147](https://doi.org/10.1144/jgs2012-147).
- Brown, R. J., M. J. Branney, C. Maher, and P. Davila-Harris (2010). "Origin of accretionary lapilli within ground-hugging density currents: Evidence from pyroclastic couplets on Tenerife". *Geological Society of America Bulletin* 122(1–2), pages 305–320. DOI: [10.1130/b26449.1](https://doi.org/10.1130/b26449.1).
- Chambers, L. M. and M. S. Pringle (2001). "Age and duration of activity at the Isle of Mull Tertiary igneous centre, Scotland, and confirmation of the existence of subchrons during Anomaly 26r". *Earth and Planetary Science Letters* 193(3–4), pages 333–345. DOI: [10.1016/s0012-821x\(01\)00499-x](https://doi.org/10.1016/s0012-821x(01)00499-x).
- Dickin, A. P. (1981). "Isotope Geochemistry of Tertiary Igneous Rocks from the Isle of Skye, N.W. Scotland". *Journal of Petrology* 22(2), pages 155–189. DOI: [10.1093/petrology/22.2.155](https://doi.org/10.1093/petrology/22.2.155).
- Duffield, W. A. and G. B. Dalrymple (1990). "The Taylor Creek Rhyolite of New Mexico: a rapidly emplaced field of lava domes and flows". *Bulletin of Volcanology* 52(6), pages 475–487. DOI: [10.1007/bf00268927](https://doi.org/10.1007/bf00268927).

- Eichelberger, J. C. (1980). “Vesiculation of mafic magma during replenishment of silicic magma reservoirs”. *Nature* 288(5790), pages 446–450. ISSN: 1476-4687. DOI: [10.1038/288446a0](https://doi.org/10.1038/288446a0).
- Emeleus, C. H., E. A. Allwright, A. C. Kerr, and I. T. Williamson (1996). “Red tuffs in the Palaeocene lava successions of the Inner Hebrides”. *Scottish Journal of Geology* 32(1), pages 83–89. DOI: [10.1144/sjg32010083](https://doi.org/10.1144/sjg32010083).
- Emeleus, C. H. and B. R. Bell (2005). *The Palaeogene volcanic districts of Scotland*. Volume 3. British Geological Survey Nottingham.
- Folch, A. and J. Martí (1998). “The generation of overpressure in felsic magma chambers by replenishment”. *Earth and Planetary Science Letters* 163(1–4), pages 301–314. DOI: [10.1016/S0012-821X\(98\)00196-4](https://doi.org/10.1016/S0012-821X(98)00196-4).
- Freundt, A. (1999). “Formation of high-grade ignimbrites Part II. A pyroclastic suspension current model with implications also for low-grade ignimbrites”. *Bulletin of Volcanology* 60(7), pages 545–567. DOI: [10.1007/s004450050251](https://doi.org/10.1007/s004450050251).
- Ganino, C., N. T. Arndt, C. Chauvel, A. Jean, and C. Athurion (2013). “Melting of carbonate wall rocks and formation of the heterogeneous aureole of the Panzhihua intrusion, China”. *Geoscience Frontiers* 4(5), pages 535–546. ISSN: 1674-9871. DOI: [10.1016/j.gsf.2013.01.012](https://doi.org/10.1016/j.gsf.2013.01.012).
- Hamilton, M. A., D. G. Pearson, R. N. Thompson, S. P. Kelley, and C. H. Emeleus (1998). “Rapid eruption of Skye lavas inferred from precise U–Pb and Ar–Ar dating of the Rum and Cuillin plutonic complexes”. *Nature* 394(6690), pages 260–263. ISSN: 1476-4687. DOI: [10.1038/28361](https://doi.org/10.1038/28361).
- Holness, M. B. (1992). “Metamorphism and Fluid Infiltration of the Calc-silicate Aureole of the Beinn an Dubhaich Granite, Skye”. *Journal of Petrology* 33(6), pages 1261–1293. DOI: [10.1093/petrology/33.6.1261](https://doi.org/10.1093/petrology/33.6.1261).
- Jaffey, A. H., K. F. Flynn, L. E. Glendenin, W. C. Bentley, and A. M. Essling (1971). “Precision Measurement of Half-Lives and Specific Activities of <sup>235</sup>U and <sup>238</sup>U”. *Physical Review C* 4(5), pages 1889–1906. DOI: [10.1103/physrevc.4.1889](https://doi.org/10.1103/physrevc.4.1889).
- Lofgren, G. (1974). “An experimental study of plagioclase crystal morphology isothermal crystallization”. *American Journal of Science* 274(3), pages 243–273. DOI: [10.2475/ajs.274.3.243](https://doi.org/10.2475/ajs.274.3.243).
- Mattinson, J. M. (2005). “Zircon U–Pb chemical abrasion (“CA-TIMS”) method: Combined annealing and multi-step partial dissolution analysis for improved precision and accuracy of zircon ages”. *Chemical Geology* 220(1–2), pages 47–66. DOI: [10.1016/j.chemgeo.2005.03.011](https://doi.org/10.1016/j.chemgeo.2005.03.011).
- Moore, J. G. and D. L. Peck (1962). “Accretionary Lapilli in Volcanic Rocks of the Western Continental United States”. *The Journal of Geology* 70(2), pages 182–193. DOI: [10.1086/626807](https://doi.org/10.1086/626807).
- Pioli, L. and M. Rosi (2005). “Rheomorphic structures in a high-grade ignimbrite: the Nuraxi tuff, Sulcis volcanic district (SW Sardinia, Italy)”. *Journal of Volcanology and Geothermal Research* 142(1–2), pages 11–28. DOI: [10.1016/j.jvolgeores.2004.10.011](https://doi.org/10.1016/j.jvolgeores.2004.10.011).
- Riehle, J. R. (1973). “Calculated Compaction Profiles of Rhyolitic Ash-Flow Tuffs”. *Geological Society of America Bulletin* 84(7), page 2193. DOI: [10.1130/0016-7606\(1973\)84<2193:ccpora>2.0.co;2](https://doi.org/10.1130/0016-7606(1973)84<2193:ccpora>2.0.co;2).
- Riehle, J. R., T. F. Miller, and R. A. Bailey (1995). “Cooling, degassing and compaction of rhyolitic ash flow tuffs: a computational model”. *Bulletin of Volcanology* 57(5), pages 319–336. DOI: [10.1007/bf00301291](https://doi.org/10.1007/bf00301291).
- Ross, C. S. and R. L. Smith (1961). *Ash-flow tuffs: Their origin, geologic relations, and identification*. DOI: [10.3133/pp366](https://doi.org/10.3133/pp366). Professional Paper 366.
- Russell, J., D. Giordano, and D. Dingwell (2003). “High-temperature limits on viscosity of non-Arrhenian silicate melts”. *American Mineralogist* 88(8–9), pages 1390–1394. ISSN: 0003-004X. DOI: [10.2138/am-2003-8-924](https://doi.org/10.2138/am-2003-8-924).
- Schmitz, M. D. and B. Schoene (2007). “Derivation of isotope ratios, errors, and error correlations for U–Pb geochronology using <sup>205</sup>Pb–<sup>235</sup>U–(<sup>233</sup>U)–spiked isotope dilution thermal ionization mass spectrometric data”. *Geochemistry, Geophysics, Geosystems* 8(8). ISSN: 1525-2027. DOI: [10.1029/2006gc001492](https://doi.org/10.1029/2006gc001492).
- Smith, S., A. Billi, and G. di Toro (2010). “Principal Slip Zones in Carbonate: Microstructural Characterization and Implications for the Seismic Cycle”. *EGU General Assembly Conference Abstracts*. EGU General Assembly Conference Abstracts, page 8722.
- Sparks, S. R. J., H. Sigurdsson, and L. Wilson (1977). “Magma mixing: a mechanism for triggering acid explosive eruptions”. *Nature* 267(5609), pages 315–318. ISSN: 1476-4687. DOI: [10.1038/267315a0](https://doi.org/10.1038/267315a0).
- Thordarson, T. (2004). “Accretionary-lapilli-bearing pyroclastic rocks at ODP Leg 192 Site 1184: a record of subaerial phreatomagmatic eruptions on the Ontong Java Plateau”. *Geological Society, London, Special Publications* 229(1), pages 275–306. DOI: [10.1144/gsl.sp.2004.229.01.16](https://doi.org/10.1144/gsl.sp.2004.229.01.16).
- Troll, V. R., C. H. Donaldson, and C. H. Emeleus (2004). “Pre-eruptive magma mixing in ash-flow deposits of the Tertiary Rum Igneous Centre, Scotland”. *Contributions to Mineralogy and Petrology* 147(6), pages 722–739. ISSN: 1432-0967. DOI: [10.1007/s00410-004-0584-0](https://doi.org/10.1007/s00410-004-0584-0).
- White, J. D. L., J. McPhie, and I. Skilling (2000). “Peperite: a useful genetic term”. *Bulletin of Volcanology* 62(1), pages 65–66. ISSN: 1432-0819. DOI: [10.1007/s004450050293](https://doi.org/10.1007/s004450050293).
- Wilson, C. J. N. and G. P. L. Walker (1985). “The Taupo eruption, New Zealand I. General aspects”. *Philosophical Transactions of the Royal Society of London. Series A, Mathematical and Physical Sciences* 314(1529), pages 199–228. DOI: [10.1098/rsta.1985.0019](https://doi.org/10.1098/rsta.1985.0019).